UNIVERSITÀ DEL PIEMONTE ORIENTALE

Department of Translational Medicine

PHD PROGRAM IN BIOTECHNOLOGIES FOR HUMAN HEALTH

XXVII cycle
Academic years 2011-2014

PhD THESIS

Inhibition of Diacylglycerol kinase alpha restores TCR-induced diacylglycerol signaling and restimulation-induced cell death in XLP1 T lymphocytes

Supervisor:
Prof. Gianluca Baldanzi

Co-supervisor:
Prof. Andrea Graziani

PhD Coordinator:
Prof. Claudio Santoro

PhD Student:
Valeria Malacarne

Table of Contents

During my PhD fellowship, I focused on the role of Diacylglycerol kinase alpha (DGKα) in defining the cell morphology [1] and in modulating the signal transduction in both T lymphocytes and epithelial cells. Also, I contributed to the characterization of the antitumoral activities of ICOS on transformed epithelial cells [2].

In this thesis I reported my main PhD project, which was a part of an international collaboration aimed to understand the role of DGKα in the modulation of TCR-induced diacylglycerol signaling and in the pathogenesis of X-linked lymphoproliferative disease 1 (XLP1). The following units contributed in the data presented in this thesis: i) Dr. A.L. Snow (USUSH, Bethesda) for studies on XLP1-derived T lymphocytes, ii) Dr. K.E. Nichols, MD (St. Jude Children's Research Hospital, Memphis) for animal model of XLP1 and iii) Dr. I. Rubio (CMB, Jena) who hosted me to carry out the morphological studies on the immunological synapse.

Project summary

X-linked lymphoproliferative disease (XLP1) is a rare primary immunodeficiency associated with an unconstrained, life-threatening expansion of CD8+ T cells following Epstein-Barr virus (EBV) infection. XLP1 is caused by mutations in SAP, an adaptor protein that mediates signaling through the SLAM family receptors. SAP-deficient cells exhibit impaired T cell receptor (TCR) restimulation-induced cell death (RICD), a key physiological process in maintaining lymphocyte homeostasis. We previously showed that SAP has a critical role in TCR-induced inhibition of diacylglycerol kinase alpha (DGKα), which phosphorylates diacylglycerol (DAG) to phosphatidic acid, acting as a major regulator of T cell signaling. Here, we show that in SAP-deficient Jurkat cells, DGKα activity impairs immune synapse (IS) formation, MTOC reorientation and affects the integrity of DAG gradient. By taking advantage of confocal live-cell imaging, we found that RNAi-mediated silencing or pharmacological inhibition of DGKα in SAP-deficient cells rescues both immune synapse formation and MTOC repositioning, and the subsequent DAG accumulation at the IS. Inhibition/silencing of DGKα was also sufficient to restore PKCθ and RasGRP1 recruitment at the immune synapse, as well as ERK1/2 activation and IL-2 production/IL-2 receptor membrane exposure in SAP knockdown primary T cells. Notably, DGKα blockade specifically reestablished RICD in both SAP-silenced cells and XLP1 patients' T cells by restoring RSK-mediated induction and phosphorylation of the pro-apoptotic genes Nur77 and Nor1.

Furthermore, *in vivo* inhibition of DGKα prevented aberrant CD8+ T cell expansion, TNFα and IFNγ production as well as tissue infiltration in Lymphocytic Choriomeningitis Virus-infected SAP KO mice, a mouse model of XLP1.

Altogether, these data demonstrates that DGKα inhibition, by increasing localized DAG signaling at the IS, restores RICD in SAP deficient cells. *In vivo*, this limits the CD8+ T cell expansion and tissue damage that characterize XLP1.

Collectively, these data highlight the key role for the SAP-mediated DGKα inhibition in regulating T lymphocyte homeostasis and highlight DGKα as an attractive therapeutic target in XLP1 patients.

Abbreviations

AICD	Activation-induced cell death
APC	Antigen Presenting Cell
cSMAC	Central supramolecular activation complex
CTLs	Cytotoxic T lymphocytes
DAG	Diacylglycerol
DCs	Dendritic cells
DGKs	Diacylglycerol kinases
dSMAC	Distal supramolecular activation complex
EBV	Epstein-Barr virus
FIM	Fulminant infectious mononucleosis
GAPDH	Glyceraldehyde-3-phosphate dehydrogenase
GAPs	GTPase activating proteins
GEF	Guanine nucleotide exchange factor
HLH	Hemophagocytic lymphohistiocytosis
HSC	Hematopoietic stem cell
IL	Interleukin
INF	Interferon
IS	Immunological synapse
ITAMs	Immunoreceptor tyrosine-based activation motifs
LCMV	Lymphocytic Choriomeningitis Virus
MTOC	Microtubule-organizing center
NTB-A	NK, T, and B cell Antigen (Ly108 in mice)
PA	Phosphatidic acid
PKC	Protein kinase C
PMA	Phorbol myristate acetate - DAG functional analogue
pSMAC	Periferal supramolecular activation complex
RasGRP1	RAS guanyl-releasing protein 1
RICD	Restimulation-induced cell death
RSK	p90 ribosomal protein S6 kinase
SAP	SLAM-associated protein
SEE	Staphylococcal enterotoxin E
SHP-1	SH2 domain-containing phosphatase 1
SLAM	Signaling lymphocyte activation molecule
TCR	T cell receptor
XLP1	X-linked lymphoproliferative syndrome

Introduction

1. TCR signaling and T cell activation

T cells are key effectors of the adaptive immune response, playing a central role in clearing pathogens' infection.

Activation of T cells occurs upon ligation of T cell receptors (TCRs) with peptides processed and exposed by antigen-presenting cells (APCs) for CD8+ and CD4+ T cells on class I or class II MHC molecules, respectively [3, 4].

This interaction is necessary but not sufficient to fully establish lymphocyte's activation: indeed, the concomitant triggering of several accessory molecules on the surface of T cell as well on APC is required. The engagement of the TCR by specific antigens, along with stimulation by co-stimulatory receptors such as CD28, CD2, CD4 and CD8, leads to a cascade of signaling events that culminate in T cell activation, which causes the proliferation and differentiation of T cells coupled with their acquisition of effector functions [5]. Conversely, stimulation via the TCR alone, while partially activates intracellular signaling pathways, is not sufficient to induce effector functions such as cytokines production and proliferation [6]. Notably, engagement of TCR in the absence of co-stimulation results in a weak and transient activation of both Ras and PKCθ, which drives T cells into anergy, a hypo-responsive status characterized by the inability to produce IL-2 and proliferate [7, 8].

TCR is multi-molecular complex composed of separate antigen binding and signal-transduction subunits. The unique, clonotypic α and β chains are responsible for the recognition of the antigen, while the invariant subunits of the CD3 (heterodimers γ-ε/ ε-δ and homodimer ζ-ζ) drive the signal transduction upon antigen recognition [5, 9]. On the invariant CD3 subunits, immunoreceptor tyrosine-based activation motifs (ITAMs) play a major role in branching out signals from TCR [5]. Indeed, TCR has no intrinsic enzymatic activity and, to initiate the signaling, activation of Src kinase family member (SFKs), and in particular of LCK, is required. LCK is recruited to the cytoplasmatic domain of the TCR co-receptors CD4 and CD8, which serve to drive LCK in close proximity of its substrates ITAMs (**Figure 1**).

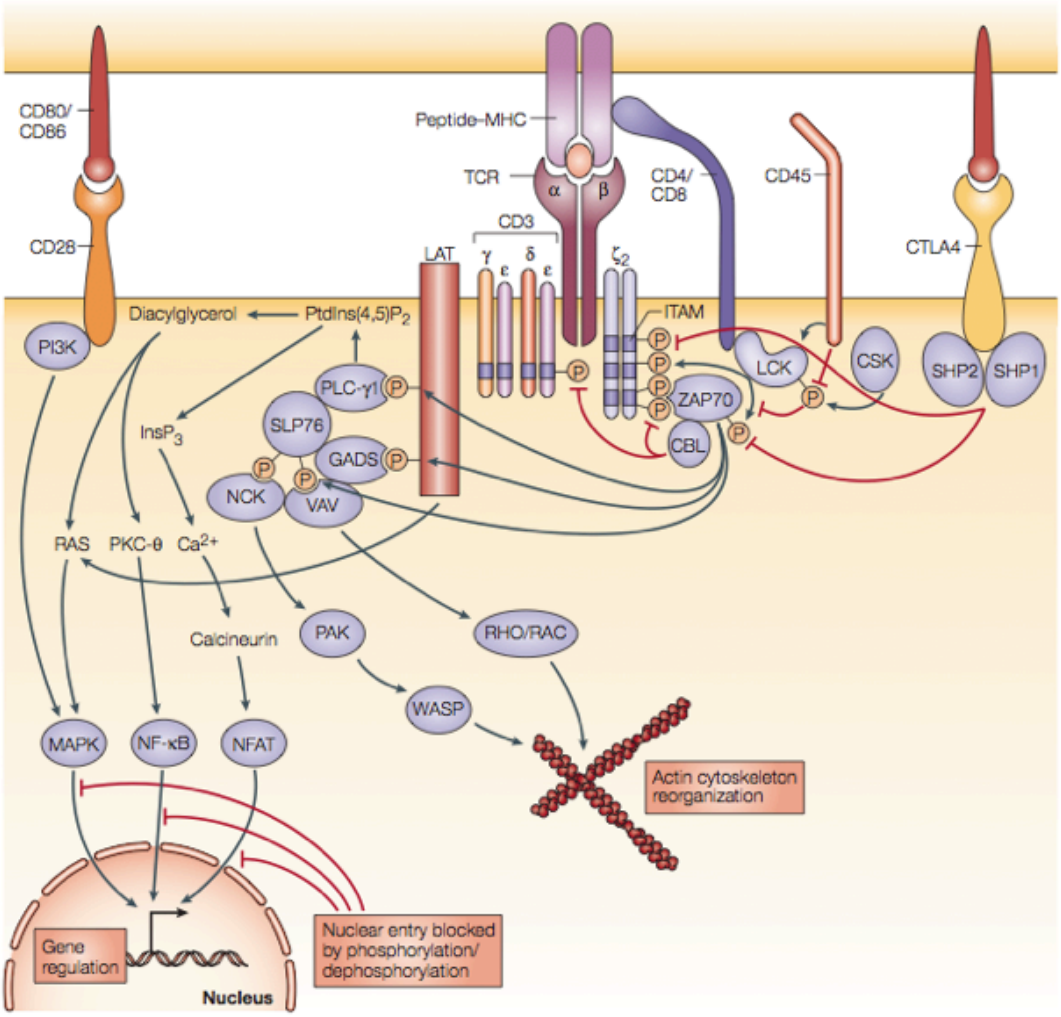

Figure 1. **Signals controlling the TRC-mediated T-cell function**. (Baniyash et al., 2004)

For conveying the signal, at least two ITAMs must be phosphorylated by LCK. The double phosphorylation leads to the recruitment and activation of zeta chain-associated protein kinase 70 kDa (ZAP-70) through its tandem SH2 domains [10, 11].

Subsequently, active ZAP-70 phosphorylates the membrane-bound linker for activation in T cells (LAT) and the SH2-domain-containing leukocyte protein of 76 kDa (SLP-76) [12, 13], which serve as scaffolds to recruit many other adaptor and effector molecules, including growth factor receptor-bound protein 2 (Grb2), phospholipase C gamma (PLCγ) and phosphatidyl-inositol 3-kinase (PI3K) [14] (**Figure 1**). LAT and SLP-76 have a central role in nucleating the signal complexes, and ultimately serve as a platform to recruit many other effector molecules: among them, Itk. Itk is the

prominent and best characterized member of the Tec family in T cells. Through its PH domain, Itk is recruited to the membrane via the phosphatidylinositol 3-kinase (PI3K) lipid product phosphatidylinositol-3,4,5-trisphosphate (PIP3), in close proximity to LCK, which phosphorylates Itk in its activation loop [15]. Once activated, Itk interacts with and phosphorylates the phospholipase C gamma 1 (PLCγ1) (**Figure 1**). PLCγ1 hydrolyzes phosphatidylinositol-4,5-bisphosphate (PIP2) producing the second messengers inositol-1,4,5-trisphosphate (IP3) and diacylglycerol (DAG). IP3 generation results in release of Ca^{2+} from intracellular stores [16].

Calcium release is an important trigger for transcriptional activation in the nucleus [17, 18] (**Figure 1**). For instance, sustained calcium elevation is critical for the activation of the IL-2 promoter by the calcineurin/NFAT pathway [17, 18].

Besides the calcium flux, the TCR triggering induces the production of DAG, which leads to the activation of two major pathways involving PKCθ and Ras (**Figure 1**). T cells express multiple functionally distinct PKC isoforms that can be classified into the classical PKCs (α, β1, β2, and γ), which are regulated by calcium, diacylglycerol, and phospholipids; novel PKCs (δ, ε, η, and θ), which are regulated by diacylglycerol and phospholipids; and atypical PKCs (ζ and λ), which lack calcium or diacylglycerol-binding domains [19]. It was previously thought that among the available PKCs, only the θ isoform is recruited to the site of TCR engagement [20-22]; however, recently Quann et al. showed that also PKCε and PKCη, but not the δ isoform, are recruited at the IS and are necessary, in turn, to recruit PKCθ [23]. Once recruited, PKCθ regulates a number of critical pathways, i.e. NF-κB activation, which leads to the activation of genes involved in the function, survival, and homeostasis of T cells.

The second major signaling pathway regulated by DAG is mediated by Ras. Ras cycles between a GTP-associated active state (Ras-GTP) and GDP-bound inactive state (Ras-GDP). The activation state of Ras is defined by the balance of two regulators of the process: in the one hand, guanine nucleotide exchange factor (GEFs) promotes the Ras GTP-bound state by enhancing exchange of GDP with GTP. On the other hand, GTPase activating proteins (GAPs) promote the inactive GDP-bound state of Ras by increasing the rate of GTP hydrolysis [24].

In T cells, two families of Ras GEFs are expressed: Son of sevenless (which consist of SOS1 and SOS2), and Ras guanine nucleotide-releasing proteins (four proteins which include RasGRP1 to RasGRP4). While SOS proteins are ubiquitously expressed, RasGRPs, and particularly RasGRP1, have a major role in T cells [24]. Upon TCR stimulation, DAG recruits RasGRP1 to the membrane, where it can activate Ras [22, 25]. However, RasGRP1 can also be activated in a way that depends

only indirectly from DAG: indeed, DAG can activate PKCθ, which in turns phosphorylates RasGRP1 on T184, thus enhancing its GEF activity [26, 27]. The other major GEF of Ras is SOS. SOS is constitutively bound to the adapter protein GRB2, and upon TCR stimulation, the GRB2 SH2 domain is recruited to and binds phosphorylated tyrosines on LAT, thereby bringing SOS into the proximal signaling complex where it can facilitate the localized activation of Ras [12]. The significance of these two modes of Ras activation was unclear until it was shown that RasGRP1-dependent RasGTP production catalyzes SOS activity, resulting in a positive feedback loop and robust TCR-induced Ras activation [27]. This explains why RasGRP1 plays a more dominant role in antigen receptor-stimulated Ras activation [24]. Ras is then responsible for the activation of multiple effector pathways, including the extracellular signal-regulated kinase (ERK), as well as linkage to Rho GTPases [28, 29]. ERK1/2 belongs to the mitogen-activated protein kinases (MAPKs), a family of serine/threonine kinases that mediates intracellular signal transduction in response to different physiological stimuli and stressing conditions. MAPKs are activated by a cascade involving a MAP3K (Raf-1) and a MAP2K (MEK-1 or MEK-2) [29, 30]. Once activated, ERK plays an essential role in the expression of the activator protein 1 (AP- 1) transcription factor c-Fos, as well as c-myc [30]. Beside its role in modulating proliferation and differentiation, ERK1/2 was shown to have also pro-apoptotic effects, especially in thymocytes during negative selection triggered by high affinity TCR ligands [31]. Particularly, it has been shown that the ERK1/2-MAPK pathway mediates these pro-apoptotic functions by phosphorylating Nur77, an orphan nuclear receptor whose expression and phosphorylation are strongly induced after TCR-triggering. This phosphorylation is mediated by both ERK2, which phosphorylates Nur77 at threonine 142 [32] and p90 ribosomal protein S6 kinase 2 (RSK2), a serine/threonine kinase that acts as downstream effector of the MEK1/2-ERK1/2 MAPK cascade [33, 34]. RSK2 is known to phosphorylate Nur77 at serine 351, both *in vitro* and *in vivo* [33, 34]. Also, it has been demonstrated that phosphorylation of Nur77 on this specific residue mediates its translocation from the nucleus to the mitochondria, where activates the intrinsic apoptotic pathway by interacting with Bcl-2 [34, 35]. Besides MAPK cascade, also PKCs were shown to be responsible for the Nur77 mitochondrial targeting, as their inhibition prevented the association with Bcl-2 and apoptosis in thymocytes induced by the combination of PKC agonist with calcium ionophore [36].

2. The immunological synapse

The immunological synapse (IS) refers to a contact between the T cell and the APC that results in a well-defined organization of the membrane proteins [37, 38]. In 1998, Kupfer was the first to show that the IS formed at the T cell : APC interface consists of two rings according to the spatial-segregation of distinct molecules. Because of its typical double-ring structure, the IS organization is known as "bull's eye" [38]. Specifically, the IS is divided in peripheral supramolecular activation complex (pSMAC) and central supramolecular activation complex (cSMAC). Lymphocyte function-associated antigen-1 (LFA-1, also known as $\alpha_L\beta 2$), which interacts with ICAM [39], localizes to the pSMAC of the immunological synapse during T-cell activation, and is believed to be the most important integrin that is involved in conjugate formation. In addition, the $\alpha_4\beta_1$-integrin (also known as VLA4) binds to vascular cell-adhesion molecule-1 (VCAM1) to facilitate the extravasation, as well as to extracellular matrix components, such as fibronectin. Similar to LFA-1, α4β1-integrin accumulates at the pSMAC and can function as a co-stimulatory molecule for T-cell activation [40].

On the other hand, the activated TCR diffuses in the cSMAC, in the center of the IS. Outside the pSMAC is another domain named distal supramolecular activation complex (dSMAC), a CD45-enriched region characterized by active actin movement, thereby recently associated to the lamellipodia of epithelial cells [41] (**Figure 2**).

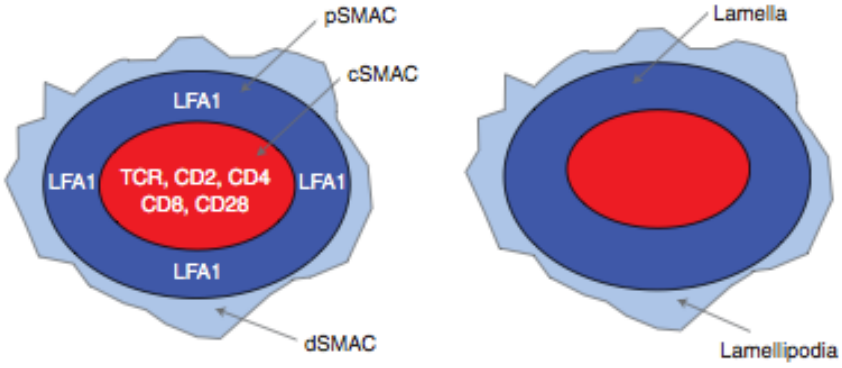

Figure 2. **Structure of the immunological synapse**. The basic structure of the "bull's eye" immunological synapse with SMACs is shown (left). Given the active membrane movement and enrichment in actin, pSMAC and dSMAC are associated with lamellae and lamellipodia, respectively (right) (Dustin et al., 2010)

Although mature IS formation is observed with B cells, artificial bilayers, or tumor cells, this does not apply with dendritic cells (DCs). Indeed, even if DCs are capable to strongly induce T cell

activation, they form multifocal ISs rather then cSMAC and pSMAC structures [38]. Therefore, the function of the d-, p- and cSMAC is still debated. It was first thought that the cSMAC serves to convey the signal at the center of the synapse, allowing the recognition of low-affinity ligands for the TCR [37, 38]. Nevertheless, further studies showed that strong peptides tended to result in less phosphotyrosine staining at the cSMAC, whereas weak peptides showed more signals at the cSMAC [42]. Based on these observations, and given the enrichment of the cSMAC in lysobisphosphatidic acid [43], a marker of multivesicular bodies, it was suggested that the cSMAC ultimately might serve as a specific compartment to facilitate the TCR internalization/degradation [44, 45]. Furthermore, it has been proposed that the role of the pSMAC might be to contain the release of the cytolytic granule contents to bystander cells, thus preventing their non-specific cytolysis [46]. However, appears to be clear that the ultimate function of the IS is to provide signals to and from the T cell, during the phase of priming and the ultimate effector function, respectively [41]. The process of IS formation is extremely fast – it takes approximately 2-3 minutes [47] (**Figure 3**).

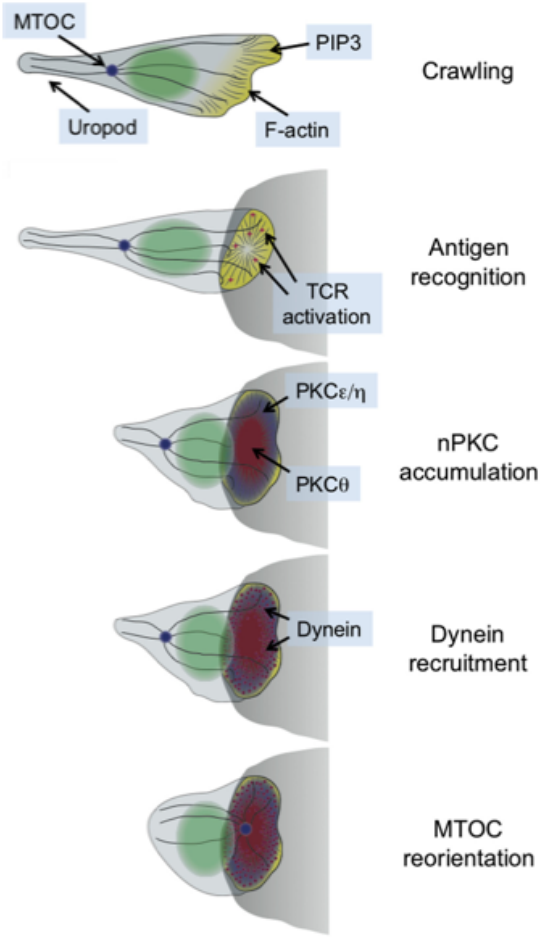

Figure 3. **Schematic diagram showing the transition between migratory and synaptic polarity that occurs upon antigen recognition by T cells**. (Huse, 2012)

First, the circulating T cells extend a leading edge searching for the antigen. Once encountered the antigen, they stop to form stable contacts with the APC, and the leading edge spreads in a lamellipodium, which literally embraces the APC. During this process, an extensive remodeling of the actin takes place, which can be easily followed by visualizing actin accumulation between the T and the APC cells [47] (**Figure 3**). As a direct consequence, the TCR complex is activated and PLCγ generates the lipid DAG, which accumulates in a polarized manner at the IS [48]. DAG acts as a second messenger by recruiting and activating the nPKCs PKCε and PKCη and, finally, PKCθ. [23, 49] (**Figure 3**). All these three proteins are required – with some redundancy between PKCε and PKCη [23]. The final step of IS formation is the reorientation of the microtubule-organizing center (MTOC) (**Figure 3**). The key player of this process is dynein, a "microtubule motor" that drives the MTOC toward the APC. It has been proposed that microtubules directly link to the integrin-rich pSMAC and to the cortical actin cytoskeleton, thus giving the force required to reposition the MTOC just behind the nucleus [50] (**Figure 3**).

Also, the IS formation and the repositioning of the MTOC are key events during the cytotoxic T lymphocytes (CTLs) killing of a cognate target cells. Cytotoxic granules (containing perforin + granzymes) move along microtubules and then cluster around the MTOC, juxtaposed to the plasma membrane. Then the granule's content is released between the CTL and the target cell, where perforin and granzymes cooperate to induce a rapid death of the target cell by apoptosis [51].

In this highly controlled process of synapse formation, the generation and preservation of a stable gradient of DAG at the IS plays a central role. Recently, this mechanism has been clarified in details by the work of Huse's group. Diacylglycerol kinase alpha (DGKα), by consuming the DAG to phosphatidic acid (PA), limits the diffusion of DAG and therefore determines the polarity of the cell. DGKα-deficient T cells exhibit an uncontrolled accumulation of DAG at the IS, and the repositioning of the MTOC is impaired, as a result of the mis-orientation of the cell. Moreover, they found that DGKα localizes at the pSMAC in a PI3K-dependent mechanism, while is excluded from the cSMAC, suggesting a role for DGKα in constraining the area of DAG accumulation at the cSMAC. Hence, DGKα acts as a negative regulator of signal initiated from the TCR, thus originating a polarized and fine-tuned DAG gradient [52].

3. SAP and X-linked lymphoproliferative disease

3.1. The SLAM/SAP signaling pathway

The activation of the immune cells depends on the integration of multiple signals, originating from multiple receptor and co-receptors on the cell surface. There is accumulating evidence that the signaling lymphocytic activation molecule (SLAM) family of receptors plays important roles in immunity [53, 54].

The SLAM-family is composed by a group of transmembrane receptors that include SLAM (CD150), 2B4 (CD244), Ly-9 (CD229), natural killer, T- and B-cell antigen (NTB-A) or Ly108 (in the mouse) (SLAMF6), CD84, and CD2-like receptor activating cytotoxic cells (CRACC; CD319) [53, 54]. They all share an extracellular region that contains two immunoglobulin-like domains: one variable (V)-like domain and one constant 2 (C2)-like domain. In the cytoplasmic segment multiple tyrosine-based motifs were found. The only exception is Ly-9, which has two tandem repeats of the basic V-like and C2-like organization [53, 54]. With the exception of 2B4, which interacts with CD48 on the surface of other hematopoietic cells, all the others SLAM receptors are self-ligands, so they can be triggered in homotypic (all) or heterotypic (2B4) interaction. For example, NTB-A is triggered by another NTB-A located on the APC cell surface [53].

SLAM receptors transduce the signal through SLAM-associated protein (SAP) family of adaptor proteins. This family includes three members: SAP (gene name SH2D1A), which is expressed in T, NK and NK-T cells, EAT-2 (SH2D1B1), which is found in NK cells, DCs and macrophages, and ERT (SH2D1B2), which is expressed only in murine NK cells. Among them, I will focus on SAP protein, since mutations on its gene are responsible for the X-linked lymphoproliferative disease (XLP1), which will be the topic of the next section of this thesis.

The SAP (SH2D1A) gene is located on the X chromosome and encodes for a 128 amino acid protein, which is composed almost entirely by a Src homology 2 (SH2) domain. Its SH2 domain binds immunoreceptor tyrosine-based switch motifs (ITSMs) on the cytoplasmic domain of the SLAM-related receptors [55-59].

Because of the “adaptor” nature of the SAP protein, it was first thought that SAP promoted cell activation through an anti-inhibitory mechanism, by blocking the interaction of SLAM family receptors with SH2 domain containing phosphatase such as SHP-1, SHP-2 and SHIP-1 [54, 59]. However, SAP itself was later found to have a crucial role in signal transduction.

One of the best-characterized functions of SAP is the association with the Src-related tyrosin kinase Fyn, through an arginine (R78) located within the SAP SH2 domain [60-62]. This specific residue binds to the Src homology 3 (SH3) region of Fyn. Because the residue involved in SAP-Fyn interaction (R78) is distinct from the one involved in its association with SLAM (R32), SAP can simultaneously associate with SLAM and Fyn to form a trimolecular complex [60-63], which appears to be critical for some functions of SAP. For instance, it has been shown that SAP/Fyn-mediated pathway enhances PKCθ/NF-κB activation and TH2 differentiation [64] (**Figure 6**).

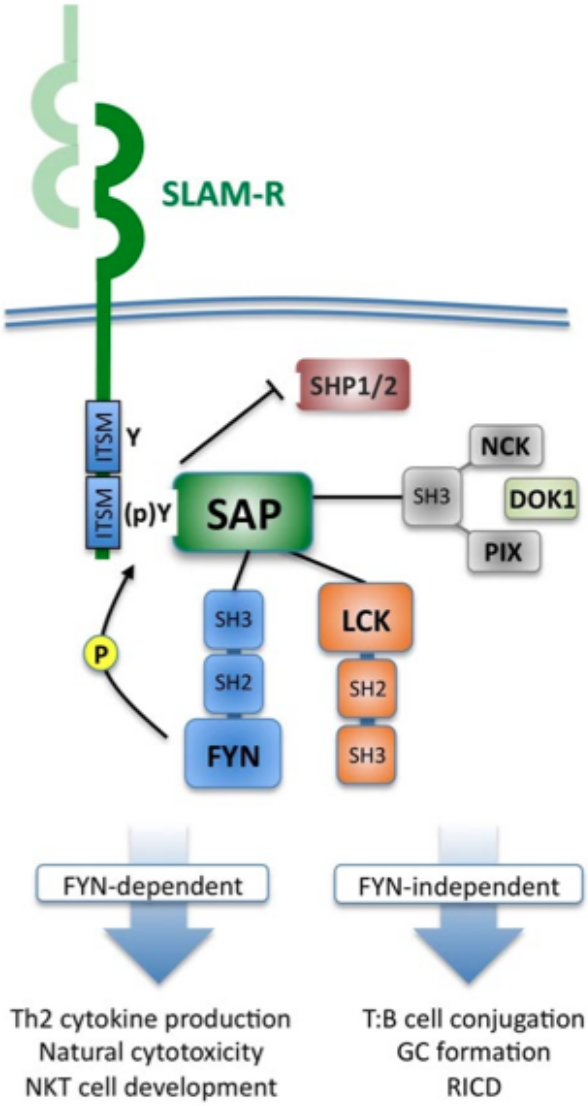

Figure 6. **SLAM/SAP signaling pathway** (Filipovich et al., 2010)

In addition to the binding of Fyn, the R78-based motif of SAP can interact also with other SH3 domain-containing proteins, such as PAK-interacting exchange factor (β-PIX), the adaptor Nck and PCKθ [65-67]. Moreover, SAP was recently found to directly associate with the phosphorylated CD3ζ chain, contributing to the activation of Erk, Akt and PLCγ1 pathways [68].

Depending on the cell type, state of activation, and specific SLAM family member engaged, multiple mechanisms exist for recruitment of other downstream proteins. Is important to note that SAP may either acts as a competitor or as an adaptor to recruit Src kinases, and these two processes may not be mutually exclusive [63].

In the following chapter, I will specifically focus on the role of SLAM and SAP in XLP1 disease, where studies with both genetic murine models and cells from XLP1 patients contributed to clarify this complex scenario.

3.2. X-linked lymphoproliferative disease (XLP1) and cellular defects

X-liked lymphoproliferative disease type 1 (XLP1) is a rare primary immunodeficiency that affects both innate and adaptive immunity of male patients. David Purtilo originally reported it in 1975, describing a big American family – the Duncan kindred - in which, out of 18 boys, 6 died for a lymphoproliferative disease [69]. For this reason, XLP1 is also known as "Duncan's disease" or "Purtilo syndrome". XLP1 is caused by mutations on SH2D1A (SAP) gene, which is located on the long arm of the chromosome X (Xq25). So far, more than 70 mutations resulting in XLP1 have been reported to the Human Gene Mutation Database (HGMD), which are gross deletions, nonsense, missense, small insertion/deletion and splice-site mutations [70]. Even in patients with the same mutations, and within the same family, there are no well-defined correspondences in most of the cases between genotype and clinical phenotype. A certain grade of correlation with an Epstein-Barr virus (EBV) infection was initially reported, and it is still considered to be the ultimate cause for the development of at least the acute clinical manifestations in XLP1. However, some patients develop the disease even without prior EBV exposure.

XLP1 affects 1 to 3 million boys worldwide and most commonly arises during the childhood or early adolescence. The main clinical feature of XLP1 is represented by a fulminant infectious mononucleosis (often triggered by EBV) and followed by hemophagocytic lymphohistiocytosis (HLH) [71]; the latter is responsible alone for more than 80% of mortality before receiving stem cell transplantation [72]. In the individuals who survived these initial episodes or who are not

infected by EBV, other lymphoproliferative manifestations such as malignant lymphomas and lymphoid vasculitis, dysgammaglobulinemias - including hypo/hyper-gammaglobulinemias - or syndromes related to common variable immunodeficiency (CVID) are observed [73]. While healthy individuals are able to orchestrate an efficient immune response to EBV, XLP1 patients exhibit a deregulated response, characterized by an excessive accumulation of CD8 and CD4 T cells, NK cells and macrophages, unable to mount a response to EBV, and a consequent accumulation of EBV+ B lymphocytes.

At present, allogeneic hematopoietic stem cell (HSC) transplantation remains the only curative option for XLP1 [70, 72, 74]. Improved chemotherapy regimes for lymphoma and immunosuppressive protocols to treat HLH (including rituximab) may reduce the mortality rate for XLP1 patients and allow stabilization before HSC transplant, but due to the rarity of the cases the debate on the right procedure to be used is still open.

However, despite of the new improved regimens of conditioning, HSC transplantation still displays high mortality in the mismatched and/or unrelated donor setting [74]. Therefore, recently a first study was carried out on mice models of XLP1 to investigate the possibility to perform gene therapy on XLP1 patients. In 2013, Rivat and colleagues transduced murine SAP -/- HSC with lentiviral vectors containing either SAP or reporter gene before transplantation into irradiated recipients. They found that NKT-cell development was significantly higher and NK-cell cytotoxicity restored to wild-type levels in mice receiving the SAP vector compared to control mice. Moreover, in SAP-transduced mice, they observed a significant increase in the basal immunoglobulin levels, and a nearly normal response to the immunization with NP-CGG, including germinal center formation [75]. This study provides proof of concept that SAP gene transfer into HSCs can correct the multiple immune defects seen in XLP1.

XLP1 patients have a great number of cellular defects that are implicated in the phenotype, and to find an effective cure for at least one of them might be a successful approach for the patients to safely reach the time of the transplant.

For instance, they exhibit impaired NK- and CD8- mediated killing of EBV-infected B cell targets, whereas cytotoxicity against non- EBV-infected cells appears normal, highlighting the specificity of this phenotype [76-80]. Specifically, SAP deficient CTLs from XLP1 patients display a defective polarization of 2B4 and of the lytic machinery, while exist divergences on the effect of SAP mutations on proliferation and production of interleukin 2 (IL-2), IL-4, and IFNγ [76-78]. In NK cells from XLP1 patients, 2B4 and NTB-A were found to associate to CD48 (their ligand on EBV+ target

cells) in an inhibitory fashion: in cells lacking SAP, the two SLAM receptors associate to the phosphatase SHP-1 [79, 80]. As result, in both cell types impairment in cytolytic function leads to the accumulation of virus-infected B cells as well as the persistence of reactive inflammatory cells, responsible for the exaggerated responses seen in XLP1.

XLP1 patients also have impaired NKT cells development; NKT cells differ from other lymphocytes because they are select by lipid antigens presented on other DP tymocytes, express invariant TCR, and rapidly secrete high levels of cytokine following stimulation [81]. Strikingly, in the absence of SAP, the development of NKT cells is severely impaired both in mice and humans (a process SLAM and Ly108-mediated) [82, 83].

Another major defect in XLP1 patients is the hypo-gammaglobulinemia, i.e. the defect in the production of Ab directed against the antigen. Surprisingly, despite some papers detected SAP in B cells, several other were not able to confirm these observations, and is now accepted that B cell do not express SAP [84]. Thus, the primary role of SAP during Ab responses occurs in CD4+ T cells carrying out their "helper" role for B cells [84]. Indeed, it has been demonstrated that SAP has a role in the development of T_{FH} cells. CD4+ T cells isolated from XLP1 patients showed defective IL-10 production *in vitro* [85]. Qi and colleagues provided an important insight into the mechanism of defective CD4+ T cell help in the absence of SAP. Using two-photon imaging, they demonstrated that SAP-deficient CD4+ T cells were unable to form stable and prolonged interactions with B cells in the germinal center, while, in contrast, SAP was not required for interaction between T cells and DCs [86].

Finally, loss of SAP has been implicated in a defect of restimulation-induced cell death (RICD), which is responsible for the uncontrolled and life-threatening accumulation of antigen-specific CD8+ T cells post EBV infection. This defect will be reviewed in the following section.

3.2.1 T cell homeostasis and RICD

In normal subjects, EBV infection of B cells leads to a massive proliferation of CD8+ cytotoxic T cells (CTLs) that exert their cytotoxic function clearing the infection. As foreign antigens are successfully eliminated, an intrinsic pathway of apoptosis triggered by cytokine withdrawal causes a major contraction phase of the T cell response, leading to the clearance of all but the small fraction of T lymphocytes that became memory T cells. At the peak of the immune response, when

antigen and IL-2 are still abundant, restimulation through the TCR also deletes effector T cells (**Figure 7**).

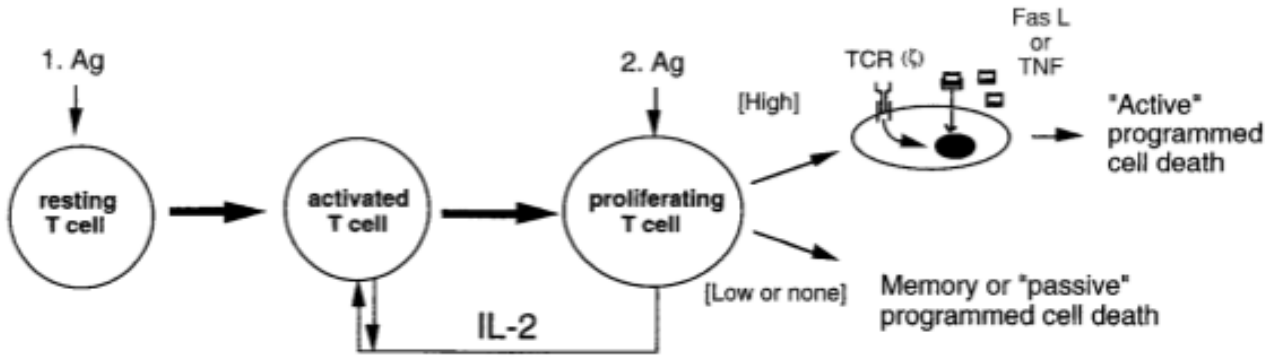

Figure 7. **Conceptual scheme of the two major apoptosis mechanisms, active and passive apoptosis, that serve as propriocidal feedback controls on the expansion of T cells during and after an immune response** (Lenardo, 2003)

This auto-regulatory program of restimulation-induced cell death (RICD) constitutes a negative feedback mechanism to impair over-lymphoproliferation and to maintain T cells homeostasis [87], and is mediated by the induction of multiple cellular pathways, including both death receptor signals (e.g., FAS-FASL) as well as pro-apoptotic Bcl-2 family proteins targeting the mitochondria (e.g., BIM) [88, 89].

Because of SAP deficiency, T lymphocytes of XLP1 patients fail in sensing the second restimulation through the TCR. Thus, these cells became resistant to RICD and accumulate, leading to development of the disease [90, 91]. Chen et al. described in 2007 a survival advantage of SAP KO murine CD8+ T cells 48 hours upon the first TCR stimulation of freshly isolated T lymphocytes, which they identified as AICD defect induced by p73, a protein involved in the mitochondrial cell death pathway [92].

In contrast to AICD, susceptibility to RICD depends on prolonged exposure to IL-2 (termed “propriocidal regulation”), upregulation of Fas and, importantly, a strong second restimulation of the TCR [93-95]. In 2009, Andrew Snow in Lenardo’s lab explored the role of SAP and SLAM in this process for the first time [90]. He showed that T cells from individuals with XLP1, as well as T cells in which SAP expression was reduced with iRNA, are specifically resistant to apoptosis mediated by TCR restimulation – RICD – and both SAP and NTB-A are required for the apoptosis [90]. Importantly, SAP/NTB-A signaling augmented the strength of the proximal TCR signal to achieve

the threshold required for RICD, since restimulation with a stronger stimulus such as phorbol ester (PMA) and ionomycin, reagents that bypass early TCR signaling events, triggered equivalent apoptosis in control and XLP1 patient T cells [90]. Once the threshold has been reached, RICD is specifically mediated by the expression of a number of pro-apoptotic molecules, i.e. FASL and BIM, which is lost in T lymphocytes from XLP1 patients [90].

Recently, Katz et al. in Snow's lab showed that LCK, but surprisingly not Fyn, is recruited to NTB-A through SAP and mediate RICD through a FASL/BIM dependent pathway [96].

4. The Diacylglycerol kinases

4.1. The Diacylglycerol kinases family

The Diacylglycerol kinases (DGKs) are a large family of enzymes that catalyze the conversion of diacylglycerol (DAG) to phosphatidic acid (PA). Ten mammalian isozymes have been identified so far, classified in five subtypes according to their primary structure (**Figure 4**).

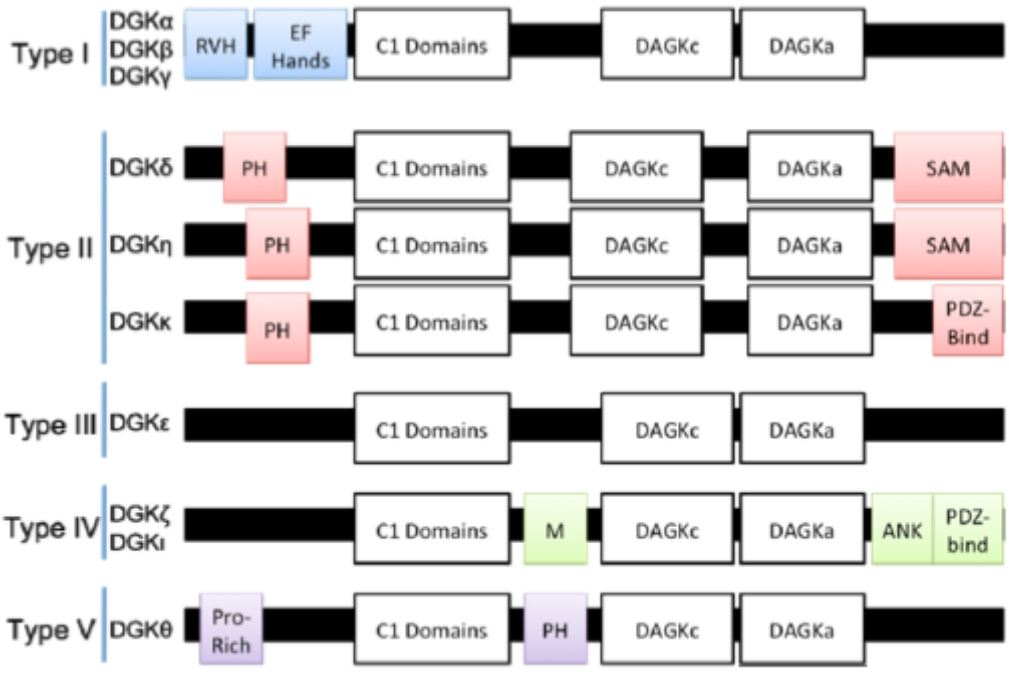

Figure 4. **The Diacylglycerol kinases family.** The five subtypes of Diacylglycerol kinases isoforms. All share the C1 domains and a catalytic domain. RVH: recoverin homology domain. PH: pleckstrin homology domain. SAM: sterile α motif. M: MARCKS homology domain. ANK, ankyrin repeat domain; PDZ-bind, PDZ-binding domain (Joshi et al., 2013).

All of them share at least two characteristic C1 (PKC-like) domains and a catalytic ATP-binding domain, while differ in other sub-specific domains [97]. Interestingly, the C1 domains do not show in all the DGK family members high affinity for DAG/phorbol esters binding; indeed, the disruption of the C1 domain does not affect the enzymatic activity of DGKα [98]. Instead, some reports indicate that the C1 domain of DGKγ, θ and ζ serves to mediate the membrane translocation [99-102].

Besides the differences in terms of structural features, each DGK shows a unique subcellular localization, which reflects their non-redundant function within the cells.

Moreover, most of the DGK isoforms are expressed in multiple tissues. Particularly, DGKα, DGKδ, and DGKζ are the most abundant isoforms expressed in lymphocyte-rich tissue. While DGKα, DGKδ, and DGKζ are all expressed in T cells, the function of DGKδ remains largely unknown [103, 104].

DGKα, together with β and γ isoforms, belongs to the class I of DGKs (**Figure 4)**. They contain calcium-binding EF-hand motifs and a recoverin homology domain (RVH). The EF-hand domains bind to calcium and the lack of these motifs causes the activation of class I DGKs, indicating that in absence of calcium EF-hand domains exert an auto-inhibitory effect on the enzymatic activity [105]. The RVH domain is homologous to the N-terminus of the recoverin family of neuronal calcium sensors and deletion of this domain causes the loss of calcium-dependent activation of these enzymes [106]. The other prominent member of DGK family expressed in T lymphocytes is DGKζ, which belongs to the class for of DGKs (**Figure 4)**. DGKζ has a MARCKS (myristoylated alanine-rich C kinase substrate) phosphorylation site domain (PSD), which functions as a nuclear localization signal and is phosphorylated by conventional PKC isoforms [107]. Also, it has four ankyrin repeats and carboxy terminal PDZ-binding domains [108].

Specifically, in this thesis I will discuss the role of DGKα as a negative regulator of apoptosis during the restimulation-induced cell death (RICD) in primary T cells. This work provides a proof of concept for the therapy of the life-threatening expansion of T cells in XLP1 disease.

4.2. Regulation of Diacylglycerol kinase alpha in T lymphocytes

As previously reported, DGKα is particularly abundant in T lymphocytes; therefore, this cell type represented over the past years the most suitable and interesting system to study DGKα physiological functions. In T cells, DGKα is regulated by calcium. Strikingly, $Ca2^{+}$ induces DGKα

translocation to the plasma membrane, rather then its activation, which is augmented only in a low extent [109].

Besides calcium, DGKα is regulated by the cytokine IL-2. Indeed the enzyme, which locates in the cytosol and nuclei of resting cells, translocates outside the nucleus in response to IL-2 binding. IL-2 also mediates the activation of the enzyme, which in turns promotes the IL-2-induced T cells proliferation by inducing G1 to S transition [110, 111]. Nevertheless, it has been shown that those effects are $Ca2^{+}$-independent, suggesting the existence of a different regulatory mechanism for DGKα activation [112]. In 2003, Merida's group demonstrated that DGKα is activated upon TCR engagement in a PI3K-dependent, calcium-independent manner. The lipid product of active PI3K, PIP3, directly activates and mediates DGKα translocation to the plasma membrane [102].

It has been demonstrated, in non-hematopoietic cells, that DGKα is positively regulated by Src phosphorylation on Tyr335, located at the hinge between the second C1 domain and the catalytic domain in the human sequence [113, 114]. Similarly, in T lymphocytes DGKα is phosphorylated on the same residue by the Src kinase family member LCK [115]. This phosphorylation leads to kinase activation and translocation to the plasma membrane, where it can negatively modulates DAG-dependent signals derived from TCR [115].

Recently, our research group also identified the adaptor protein SAP as a novel regulator of DGKα [116]. Upon TCR/CD28 or TCR/SLAM co-stimulation, DGKα exits from the nucleus and its catalytic activity is suppressed in a PLCγ1-dependent manner [116]. The knockdown of SAP results in a rescue of DGKα activity and impairs its exit from the nucleus upon TCR co-stimulation [116]. However, SAP and DGKα do not directly interact, and the mechanism by which SAP inhibits DGKα in normal T cells still has to be clarified.

4.3 Diacylglycerol kinases as negative regulators of T cell signaling

Engagement of the TCR by peptides presented on APCs trigger a signaling cascade that culminates in T cells activation. One of the early events is the activation of PLCγ, which in turn is responsible for DAG generation and, ultimately, calcium flux. DAG-dependent proteins, i.e. PKCs, RasGRP1 and PKD, represent the central hub of the TCR response.

Consistent with their catalytic activity, both DGKα and DGKζ have a crucial role in T cells by metabolizing DAG and therefore terminating the DAG-activated signaling cascade. It has been showed by Merida's group that in T cells stimulated with anti-CD3, DGKα rapidly translocates to

the plasma membrane, where metabolizes DAG into PA [117]. Importantly, overexpression of DGKα drastically reduces the expression of CD69, a well-known marker of T cells activation, demonstrating for the first time that DGKα acts as an integral component of the TCR-induced signaling cascade [117]. The same group then went on demonstrating that DGKα-mediated consumption of DAG culminates in RasGRP1 release from the plasma membrane and consequently terminates the RasGRP1-regulated signals [118, 119]. Consistently, DGKα activity controls DAG-mediated membrane localization of RasGRP1, ERK activation and IL-2 production upon TCR engagement [8, 117, 118, 120]. Similarly, it has been shown that DGKζ knockout T cells produce less PA after TCR stimulation compared to the wild type counterpart [121]. In addition, DGKζ-deficient T cells were found to be hyper-responsive to TCR stimulation, displaying an increased activation of MEK, ERK and high levels of the activation markers CD69 and CD25 [121]. Moreover, it has been demonstrated that DGKζ plays a pivotal role in determinating the threshold of T cells activation, acting as a modulator of the analog/digital signaling [122].

In 2006, two distinct groups simultaneously reported a critical role of DGKα and DGKζ in defining the activation status versus the induction of anergy upon TCR stimulation [8, 123]. They found high expression levels of both DGK isoforms in anergic cells, which are characterized by a state of antigen unresponsiveness induced by (TCR) stimulation in the absence of a co-stimulatory signal [8, 123] (**Figure 5**).

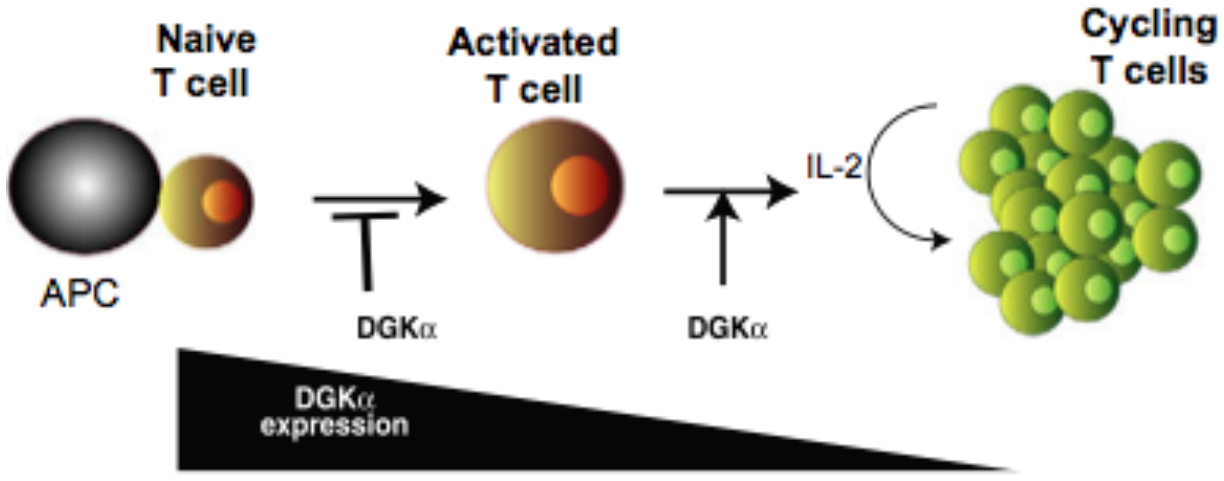

Figure 5. **DGKα expression levels in non-activated versus cycling T cells** (Merida et al., 2009)

Anergy is associated with DGKα overexpression, which ultimately leads to defective RasGRP1 translocation to the plasma membrane [8]. Accordingly, T cells from DGKα and DGKζ KO mice proliferate and produce IL-2, even under anergic conditions [8, 123].

Collectively, these data have provided evidences that DGKα and ζ, by metabolizing DAG, are key enzymes in the induction of the anergy state, which is controlled by signal strength, co-stimulatory signals and differentiation status of the cells.

As mentioned before, in order to have a functional immune synapse, is essential to form a sharp gradient of DAG in the contact zone between the T cell and the APC. DGKs have a pivotal role in the formation of a functional IS, where a fine regulation of DAG production is absolutely required. For instance, localized DAG synthesis causes reorientation of the MTOC towards the IS, which is required for transduction of the TCR signal [124]. In this context, inhibition of DGKs disrupts DAG-localized accumulation and impairs MTOC reorientation [124].

A first study in 2011 showed that although both DGKα and ζ localize at the IS upon TRC/CD28 engagement, DGKζ appears to play a dominant role in both DAG consumption and PA production at the IS [125]. However, a recent work from Huse's group elegantly demonstrates that DGKα, but not DGKζ, localizes at the periphery of the IS, where is required for optimal MTOC polarization toward the APC by constraining the area in which DAG accumulated at the IS [52]. This process of DGKα compartmentalization is PI3K-dependent [52].

Collectively, these evidences suggest that DGKα and ζ share overlapping and complementary roles in T cell signaling, acting as negative regulators of TCR signaling by terminating DAG-dependent pathways and inducing anergy. However, although no direct comparison of the relative contribution of the two DGK isoforms in the regulation of the signaling has been performed yet, the ζ isoform appears to be the more crucially involved in controlling the TCR-driven signaling, while DGKα seems to have a key role in driving the IS assembling.

Material and Methods

Cells culture and reagents

Blood samples were obtained with informed consent under protocols approved by the Institutional Review Board at Cincinnati Children's Hospital Medical Center or according to the declaration of Helsinki. Peripheral blood mononuclear cells (PBMCs) were isolated from healthy donors or XLP1 patients by Ficoll-Paque PLUS (GE Health Care) density gradient centrifugation, washed, and resuspended at 2 x 10^6 cell/mL in RPMI-GlutaMAX (GIBCO, Life technologies) containing 10% heat inactivated FCS (LONZA) and antibiotics/antimycotics (Sigma-Aldrich). T cells were activated with 1 μg/mL anti-CD3 (clone OKT3) and anti-CD28 (clone CD28.2) antibodies for 3 days. After 3 days, activated T cells were washed and cultured in complete RPMI-GlutaMAX supplemented with 100 IU/mL rhIL-2 (Peprotech) at 1.2 x 10^6 cells/mL for ≥7 days before all the assays were conducted (media was replaced every 2-3 days).

Jurkat A3 cells were from ATCC. Cells were cultured in RPMI-GlutaMAX (GIBCO, Life Technologies) with 10% FCS and antibiotics/antimycotics (Sigma-Aldrich) in humidified atmosphere 5% CO_2 at 37°C.

The DGKα inhibitor R59949 (Sigma-Aldrich) was dissolved in DMSO; equal amounts of DMSO were used in the control samples. All reagents are from Sigma-Aldrich apart: human recombinant IL-2 (Peprotech), FR180204 (ERK inhibitor II # 328007, Calbiochem), 1,2-dioctanoyl-sn-glycerol (DG 08:0, # 800800O, Avanti), SL0101-1 (Tocris Bioscience, Cat n. 2250).

Antibody	Vendor	Type	Catalog number	clone
anti-actin	Santa Cruz	monoclonal	sc-8432	C-2
anti-tubulin	Sigma-Aldrich	monoclonal	T0926	
anti-DGKα	Shaap et al., 1993	monoclonal mix		
anti-DGKα	Abcam	polyclonal	AB 64845	
anti-human CD3ε	in house	monoclonal		OKT3
anti-human CD3	eBiosciences	monoclonal	16-0038-85	UCHT1

anti-human CD28	eBiosciences	monoclonal	16-0289-85	CD28.2
anti-SAP	Cell Signaling	polyclonal	5272S	
anti p44/p42 MAPK	Cell Signaling	polyclonal	9102	
anti-phospho T_{202}/Y_{204} p44/p42 MAPK	Cell Signaling	polyclonal	9101S	
anti-S6	Cell Signaling	polyclonal	2217	
anti-phospho S6	Cell Signaling	polyclonal	4856	
anti-RasGRP1	Santa Cruz	polyclonal	sc-28581	
anti-PKCθ	Santa Cruz	polyclonal	sc-212	
anti-phospho S351 Nur77	Cell Signaling	polyclonal	5095	
Anti-Nur77	Cell Signaling	polyclonal	3960	
Anti-rabbit Alexaflour 488	Life Technologies	polyclonal	A-21206	
anti-mouse HRP	Perkin Elmer	polyclonal	NEF822001EA	
anti-rabbit HRP	Perkin Elmer	polyclonal	NEF812001EA	

siRNA for transient silencing

Activated human PBLs were prepared as described above and transfected with 200 pmol of siRNA oligonucleotides specific for the target protein (Stealth Select siRNA, Life Technologies) or a non-specific control oligo (Life Technologies). Transient silencing was obtained by transfection using the Amaxa nucleofector kit "Human T cell nucleofector kit" (VPA-1002, Lonza) and the Amaxa Nucleofector II system (program T-20, Lonza) according to manufacturer's instructions. The cells were maintained in culture in presence of IL-2 (100 IU/ml) for 4 day to allow target gene knockdown. siRNA sequences were: SAP forward UGUACUGCCUAUGUGUGCUGUAUCA, reverse UGAUACAGCAGACAUAGGCAGUACA; DGKα forward CGAGGAUGGCGAGAUGGCUAAAUAU, reverse AUAUUUAGCCAUCUCGCCAUCCUCG; DGKζ forward GCCGCUUUCGGAAUAAGAUtt, reverse AUCUUAUUCCGAAAGCGGCtg; PKCθ forward CGUUGGAUGAGGUGGAUAAtt, reverse UUAUCCACCUCAUCCAACGga; RasGRP1 forward CUACGACAAUUACCGGCGAtt, reverse UCGCCGGUAAUUGUCGUAGtt. Nur77 forward GGUCCCUGCACAGCUUGCUUGUCGA, reverse UCGACAAGCAAGCUGUGCAGGGACC. Nor1 forward AGAUCUUGAUUAUUCCAGATT, reverse UCUGGAAUAAUCAAGAUCUCT. The efficiency of all the siRNAs was validated by WB or qPCR

analysis. Stealth RNAi Negative Control Duplexes (# 12935-300, Life Technologies) was used as negative control.

Jurkat cells live imaging, Raji loading and conjugate experiments

For the experiment performed with the DGKα inhibitor R59949, Jurkat shSAP or shCNTR were transfected with DMRIE-C (Invitrogen) according to the manufacturers' instructions, and after 48 hours R59949 10 μM was added 30 min before cells conjugation.

For the experiments performed with siRNA, 0.5 x 10^6 Jurkat shSAP or shCNTR cells were microporated (Neon® Transfection System, Life Technologies) according to the manufactures' instructions (1400V, 30 sec, 1 pulse). Cells were then transferred into 2 ml fresh, pre-warmed complete RPMI and incubated for 96 hours prior to performing the conjugation experiments.

For the Raji B cells loading and the conjugation experiments, Raji B cells were washed once in PBS and resuspended in RMPI 0% FCS + 5 μM of CellTracker Red CMPTX (Invitrogen) for 30 min at 37 °C. Cells were then washed twice with RMPI 10% FCS, and resuspended in RPMI 10% FCS + Staphylococcal enterotoxin E (SEE, Toxin technology #ET404) 1 μg/ml for 1 hour at 37 °C. Then cells were washed twice with RMPI 10% FCS and resuspended in conjugation medium (RPMI/0.2 % BSA (endotoxin low, f.a.f.)/50 mM HEPES pH 7.5).

Jurkat cells (1 x 10^5) were resuspended in conjugation medium and mixed with Raji cells SEE-loaded 1:1, centrifugated at 100 x g for 1 min to force conjugate formation, and then incubated for 10 min at 37°C. Cells conjugates were then resuspended in warm conjugation medium, seeded on polylisine-coated glasses and let adhere for 5 min at 37 °C. Live cells were imaged with an Zeiss LSM 510 (Carl Zeiss) inverted laser scanning microscope (LSM) using a C- Apochromat X63 water immersion objective (Zeiss).

Immunofluorescence experiments with primary human PBLs

Freshly isolated human PBLs were isolated and cultured as described before and transfected with Amaxa Nucleofector™ Kit for Human T Cells (Cat. VVPA-1002) with control, SAP-specific and/or DGKα-specific siRNA. After 72 hours T cells were incubated with Raji B cells loaded with mixed SEE (1 μg/ml) and SEB (0.5 μg/ml) for 15 minutes, fixed and stained for either PKCθ or RasGRP1. For the experiments performed with the DGKα inhibitor R59949, CNTRL or SAP-silenced PBLs were pre-treated with R59949 (10 μM, 30 minutes, 37°C) or DMSO before allowing conjugation.

Quantification and data processing

To quantify the mean fluorescence intensity (MFI) of Lifeact-GFP or PKCθ-CRD at the contact site between T cell and Raji B cell, we have programmed an automatic cell image segmentation algorithm that yields masks for Raji B cell (always labeled in red, blue in the mask) and T cell transfected with GFP-plasmids of interest (green, shown in green in the mask). The algorithm arbitrary takes in account a 2 μm width area in the juxtaposed zone between the two masks (red area). The data processing is a step-by-step procedure performed as follow:

1. Creating a Microsoft Office Excel file, which contains the sorted data. This file tracks the measurements automatically.
2. Loading the image in the LSM format (which contains all the meta-information about the image)
3. Adjusting contrast and brightness, while filtering the image to reduce "salt and pepper" noise
4. Exclusion of other cells rather then the two in exam by drawing a tight ROI around the conjugate
5. Segmentation which allows to automatically recognize the regions of interest (ROIs)
6. Selection of the perimeter: it allows fixing the size of the contact area.

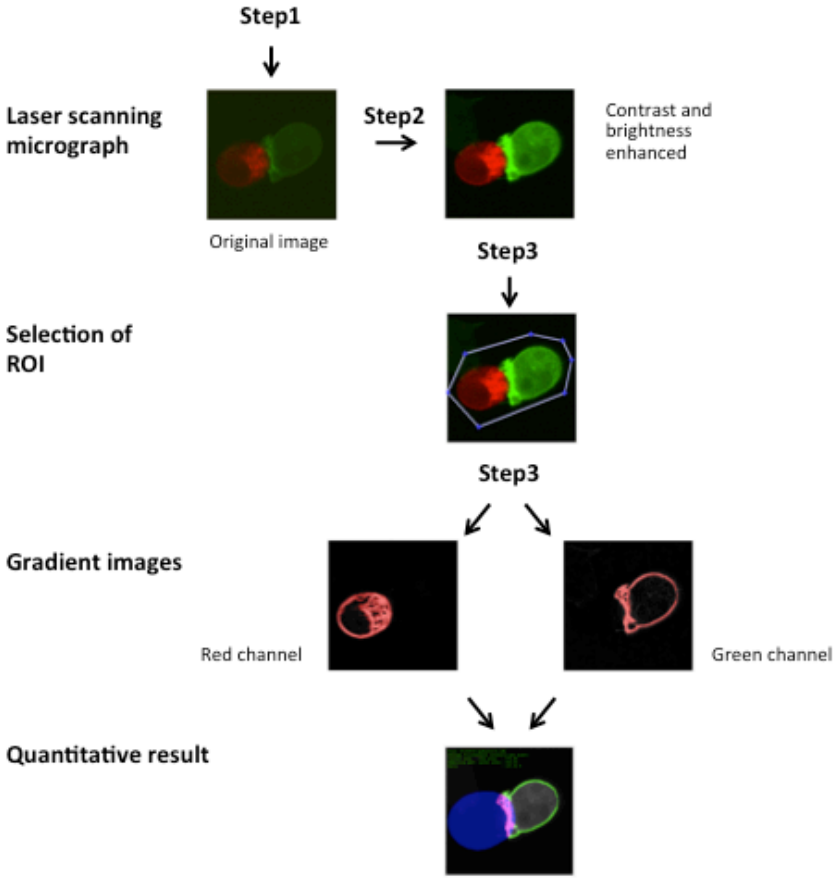

Figure 8. Step-by-step procedure of the automated segmentation process.

The automatic segmentation algorithm was created by using MatLab software. Input: loading the original image in the LSM Zeiss format. Output: MFI of ROI1 (contact area, in red) and ROI2 (remaining part, in

green) and the ratio MFI-ROI1/MFI-ROI2, which was used for the statistic. The steps are described in details in the text above. The algorithm was modified from a previous one originally created to quantify native Ras activation in single living cells from Christoph Biskup [126]

The MTOC repositioning in the conjugate experiments was analyzed by calculating a polarization index equal to the distance from the MTOC to the immunological synapse divided by the distance from the immunological synapse to the distal pole of the T cell [52]. Distances in micrometers were measured by using the LSM software, Zeiss.

PKCθ and RasGRP1 localization at the IS were scored by counting cells which display accumulation on the total cells analyzed (100 cells were scored for each individual experimental point in each experiment).

Cytofluorimetry

To test the restimulation induced cell death (RICD), activated T cells (10^5 cells/well) were plated in triplicate in 96-well round-bottom plate and treated with anti-CD3 mAb OKT3 (1-100 ng/ml) in RPMI-GlutaMAX supplemented with 100 IU/ml rhIL-2 for 24 hours. In some assays R59949 (5-10 μM) or DAG (50 μM) or U0126 (5 μM)/FR180204 (10 μM)/Rottlerin (6 μM) inhibitors were added 30 minutes before the restimulation. 24 hours after treatment, cells were stained with 1 μg/ml propidium iodide and collected for a constant time of 30 seconds per sample on a FACScan flow cytometer (FACS Calibur, BD). Cell death was analyzed with CellQuest software (BD) or Flowing software (Turku Bioimaging) as percentage of cell loss = (1 – [number of viable cells (treated) / number of viable cells (untreated)]) × 100 as described before [90].

Alternatively, for Annexin V^+ assays, cells were plated in triplicate (1.5 x 10^6 cells/well) in 12-well plate and treated with anti-CD3 clone OKT3 (10 ng/ml) in RPMI-GlutaMAX supplemented with 100 IU/ml rhIL-2 for 24 hours. 24 hours after treatment, cells were stained with the Kit Alexa Fluor® 488 Annexin V^+/Dead Cell Apoptosis Kit (Invitrogen) according to manufacturer's instructions and analysed on a FACScan flow cytometer (FACS Calibur, BD).

Western blotting

The activated lymphocytes were stimulated at density of 15 x 10^6 cell/ml in RPMI-GlutaMAX 10% H.I. FCS with 10 μg/ml anti-CD3 clone OKT3 for 5, 30 minutes or 4 hours. In some western blots

R59949 (5 µM) was added 30 minutes before the restimulation. The restimulation was stopped by washing the cells with cold (4°C) PBS and the cells were lysate at 15 X 10^6 cell/ml in lysis buffer (25mM Hepes, pH 8, 150mM NaCl, 0.5/1% Nonidet P-40, 5 mM EDTA, 2 mM EGTA, 1 mM ZnCl2, 50 mM NaF, 10% glycerol supplemented with fresh 1 mM Na3VO4, and protease inhibitors), clarified after centrifugation of 15 minutes at 12000 rpm at 4°C, heat-denatured with Laemmli buffer (100°C for 5 minutes) and separated by SDS-PAGE (Biorad). Proteins were then transferred on PVDF membrane (Hybond P, Amersham) by using semi-dry system (Biorad). Membranes were then blocked with 5% BSA in TBS and incubated at 4°C overnight with primary antibodies diluted in TBS-tween (150 mM NaCl, 20 mM Tris, pH 7.5, 0.1 % Tween), BSA 2%, 0.01% azide. After 4 washes with TBS-Tween 0.1%, membranes were incubated with secondary antibodies and washed again. Western blots were visualized using Western Lightening Chemiluminescence Reagent Plus (Perkin Elmer) and the images were acquired by using Versadoc Model 4000 Imaging System (Biorad) whose software was used for densitometry.

Quantitative RT-PCR

The activated lymphocytes were stimulated at density of 15 x 10^6 cell/ml in complete RPMI-GlutaMAX with 10 µg/ml anti-CD3 clone OKT3 for 4 hours. Where indicated, R59949 (5 µM) was added 30 minutes before the restimulation. Cells were washed with cold PBS and the mRNA was extracted by ChargeSwitch Total RNA Cell Kit (Life Technologies). The RNA was retrotranscribed with High-Capacity cDNA Reverse Transcription Kits (Applied Biosystems) and cDNA quantified by real time PCR (C1000 Thermal Cycler CFX96 realtime system, Biorad) using GUSB as normalizer.
TaqMan gene expression assays were from Life Technologies: Hs00939627_m1 (GUSB), Hs00176278_m1 (DGKα), Hs00174114_m1 (IL-2), Hs00158978_m1 (SH2D1A), Hs01076940_m1 (BCL2L11), Hs00181225_m1 (FASLG), Hs 00374226_m1 (NR4A1) and Hs 00545007_m1(NR4A3).

Mice and in vivo experiments

Sap KO mice were as described [127]. C57BL/6 (B6) were purchased from Jackson Laboratories (Bar Harbor, ME). Experimental procedures were approved by the Institutional Animal Care and Use Committee at The Children's Hospital of Philadelphia. To establish LCMV infection, mice received 2x10^5 plaque-forming units (PFU) of LCMV-Armstrong ($LCMV_{arm}$) by intraperitoneal (i.p) injection on day 0 and experiments were carried out until day +8 post-infection. Beginning at day

4, mice were given twice daily i.p injections of R59022 (Sigma-Aldrich, St. Louis, MO) dissolved in DMSO (2mg/kg body weight). Mice in all groups were sex and age matched.

Mouse splenocytes in vitro stimulations, flow cytometry and ELISA

Splenocytes were cultured at a concentration of 10 x 10^6 cells/mL with or without gp33 peptide (0.4 ng/μL, AnaSpec, Fremont, CA) in the presence of monensin and fluorochrome conjugate anti-CD107α (BD Biosciences, San Jose, CA) for 5 hours. Cells were washed, fixed and permeabilized with cytofix/cytoperm (BD Biosciences, San Diego, CA) and stained for intracellular cytokines. Fluorochrome conjugated anti-mouse CD4, CD8, TCRβ, and IFNγ monoclonal antibodies were from BD Biosciences (San Jose, CA, USA). Anti-mouse CD44 and TNFα antibodies were purchased from eBioscience (San Diego, CA, USA). APC-conjugated MHC-I restricted LCMV gp33 tetramer was provided by John Wherry (The University of Pennsylvania). Data were collected on an LSRII flow cytometer (BD Biosciences) and analyzed using FlowJo software (Tree Star; Ashland, OR). Serum IFNγ levels were determined by enzyme linked immunosorbent assay (ELISA; R&D Systems, Minneaoplis, MN).

Histology

Livers were fixed overnight in 10% formalin (w/v) (Fischer Scientific, Fair Lawn, New Jersey), embedded in paraffin, cut in 5 μm sections, and stained with hematoxylin and eosin. Images were captured using a Nikon Eclipse 90i equipped with a Nikon DS-Fi1 camera and NIS-Elements BR 3.0 software (Nikon, Japan). For each sample, five random fields were captured at 20x magnification (Nikon Plan Apo 10x; NA 0.45) and subjected to computer-based quantification of inflammatory infiltrates using the BZ-II Analyzer Hybrid Cell Count software (Keyence, Japan). The average number of inflammatory foci (defined as clusters containing > 8 lymphocytes) was determined for each treatment group, along with the area of the inflammatory infiltrate.

Statistics

Data are shown as the mean ± SEM. For statistical analysis, Student's t-test was used. Experiments shown are representative of at least 3 independent experiments. Statistical analyses of *in vivo* experiments and of data presented in Figs 1, 2 and 4 were calculated with GraphPad software (GraphPad PRISM software; San Diego, CA), using One-way ANOVA Kruskal-Wallis test followed by a Dunn's multiple comparison test. Group comparisons of cell percentages and absolute numbers,

serum cytokine levels and organ/body weight ratios were performed using Student's t-test. Data are representative of 2 independent experiments with 6-10 mice analyzed in each cohort and all error bars indicate SD. A *p*-value less than or equal to 0.05 was deemed to be significant in all experiments.

Results

In SAP-silenced cells, DGKα activity impairs IS formation.

We previously showed that SAP-deficient T cells fail to inhibit DGKα upon TCR triggering, resulting in decreased DAG-mediated signaling [116]. As DAG signaling at the IS is relevant for IS organization [124], we hypothesized that the aberrant DGKα activity in SAP deficient cells may perturb IS organization and signaling. Indeed, prior studies provided evidences that SAP is required to form stable interactions between the T cells and the APCs [86, 128].

We reasoned that if the DGKα aberrant activity in SAP-deficient cells was responsible for the IS defects, then the silencing or inhibition of DGKα would rescue the T : B cells conjugation in SAP-deficient cells. To address this hypothesis, we tracked actin dynamics using Lifeact-GFP in control or SAP-deficient Jurkat T cells (shCNTRL and shSAP, respectively) during conjugation with superantigen (SEE)-loaded Raji B cells. As previously reported in murine CTLs [128], shSAP Jurkat cells failed to assemble F-actin at the IS with SEE-loaded Raji B cells (**Fig. 1a-d**). DGKα silencing or inhibition with R59949 rescued IS formation in those cells, suggesting that excessive DGKα activity is responsible for the defective IS assembling of SAP-deficient cells (**Fig. 1a-d**). Notably, DGKα silencing or inhibition had no effect on F-actin polarization of control cells (**Fig. 1a-d**).

In response to TCR stimulation, SAP recruitment is specifically responsible for DGKα inhibition, while the activity of DGKζ is not affected [116]. Nevertheless, both DGKζ and DGKα were found to be recruited at the IS upon TCR engagement [52, 125]. Therefore, we did the experiments by co-transfecting DGKζ-specific siRNA and Lifeact-GFP in shCNTRL or shSAP Jurkat cells. In SAP-deficient cells, silencing of DGKζ showed a trend in restoring actin polarization at the IS, although without reaching statistical significance (**Fig. 1e,f**).

These data confirm that excessive activity of the α isoform of DGK in SAP-deficient lymphocytes interferes with the actin remodeling at the IS, likely by metabolizing DAG.

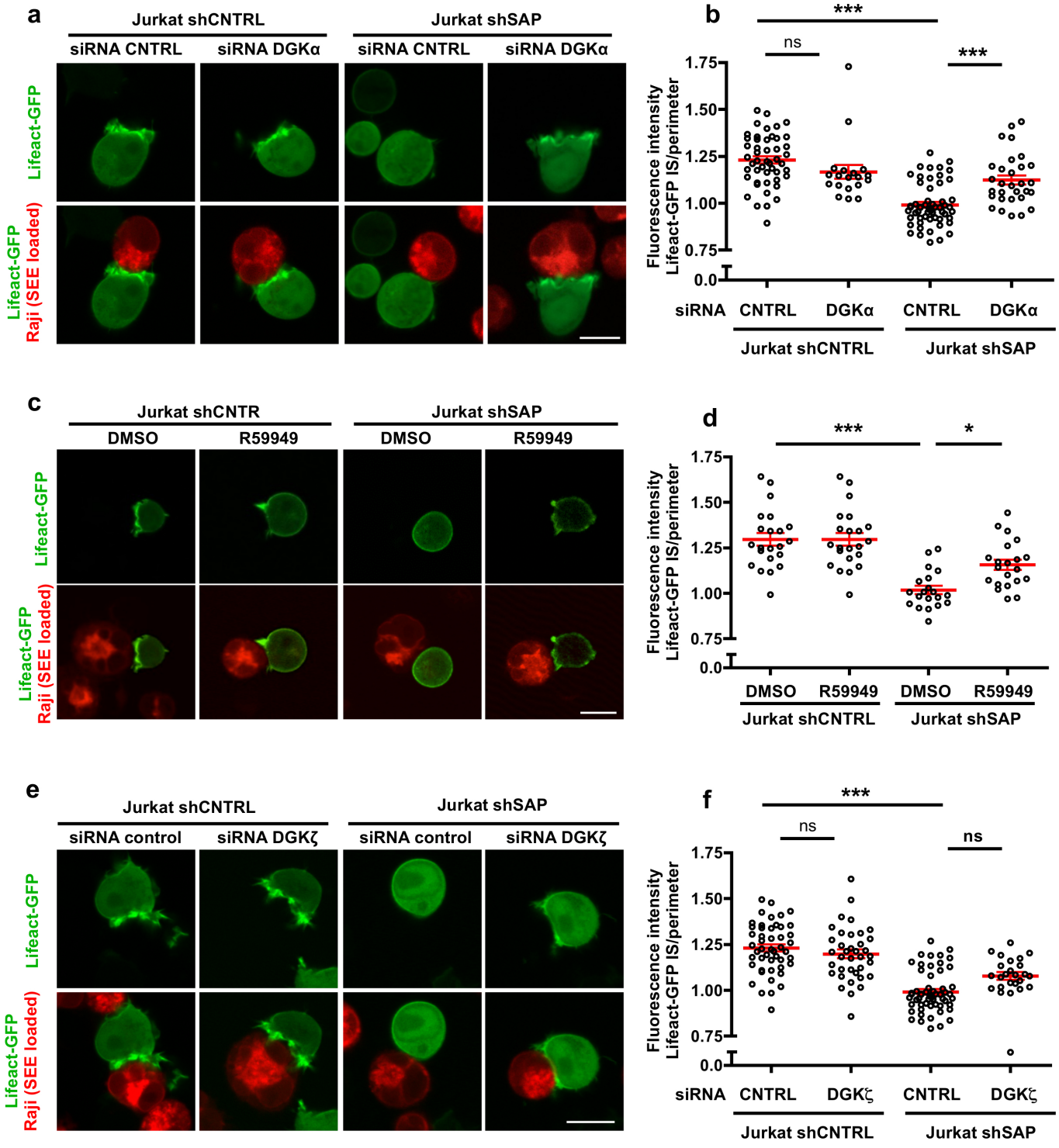

Figure 1. In SAP-silenced cells, DGKα activity impairs IS formation. Live-cells imaging analysis of shCNTRL or shSAP Jurkat cells transfected with Lifeact-GFP to follow F-actin movements during the conjugation with SEE-loaded Raji B cells (**a**) Jurkat shCNTRL or shSAP were transiently cotransfected with DGKα-specific siRNA or non specific siRNA as control together with Lifeact-GFP (green). 4 days later, cells were mixed 1:1 with SEE-loaded Raji B cells (Red) to allow conjugate formation. Representative pictures are shown, scale bar 10 μm (**b**) Synaptic localization of Lifeact-GFP was quantified ratiometrically comparing the mean fluorescence intensity (MFI) of GFP at the contact zone between the Jurkat cell and the Raji B cell and the MFI at the perimeter of the Jurkat cell (see material and methods for details). Data are derived from n > 20 conjugates per condition. Red lines and error bars in the scatter plots denote means and SEM, respectively. ***P < 0.001, ns P > 0.05. Data are representative of at least three independent experiments. (**c**) Jurkat shCNTRL or shSAP were pretreated with DMSO or R59949 10 μM for 30 min before allowing conjugation with

SEE-loaded Raji B cells. R59949 was maintained in the medium for all the time of the experiment. Representative pictures are shown, scale bar 10 μm (**d**) Graph shows the quantification of the MFI at the IS measured as in (b), n > 20, ***P < 0.001, ns P > 0.05. Data are representative of at least three independent experiments. (**e**) Jurkat shCNTRL or shSAP were transiently cotransfected with DGKζ-specific siRNA or non specific siRNA as control together with Lifeact-GFP (green). 3 days later, cells were mixed 1:1 with SEE-loaded Raji B cells (Red) to allow conjugate formation. Representative pictures are shown, scale bar 10 μm. (**f**) Quantification performed as in (b), n > 20, ***P < 0.001, ns P > 0.05. Data are representative of at least three independent experiments.

In SAP-silenced cells, DGKα activity impairs DAG accumulation at the IS.

We next sought to investigate whether in SAP-deficient cells the increased DGKα activity was responsible for an impaired DAG accumulation at the IS. With this purpose, we transfected control or SAP-deficient Jurkat cells with a DAG biosensor containing the tandem C1 domains of PKCθ fused to GFP (PKCθ-CRD) [48], together with control or DGKα-specific siRNA. In control cells, PKCθ-CRD was recruited to the contact zone between T and APC cell, while in absence of SAP this recruitment was impaired. Notably, silencing or inhibition of DGKα were able to restore DAG polarization toward the IS in SAP-deficient cells (**Fig. 2a-d**). As DGKζ plays a major role in DAG metabolism at the IS [103, 125], we did similar experiments by silencing DGKζ. In SAP-deficient cells, DGKζ-specific silencing did not significantly rescue PKCθ-CRD accumulation at the IS, although we noticed a positive trend (**Fig. 2e,f**). Interestingly, in control cells DGKα, but not DGKζ, silencing perturbed the localization of the biosensor, which accumulated also at the periphery of the cells (**Fig. 2a,b**), thus indicating a role of DGKα in localizing DAG at the IS. Indeed, DGKα plays a specific role in limiting the area in which DAG accumulates at the IS [52].

Those data confirm that an increased DGKα activity metabolizes DAG in SAP-deficient cells and consequently impairs IS organization. According with a key role of polarized DAG signaling in the synapse organization, we observed that administration of exogenous PMA, a DAG analog which potently activates ERK1/2 (**Fig. 3c**), during the conjugation experiments strongly inhibited F-actin polarization in both in control and SAP-deficient cells (**Fig. 3a,b** and [124]).

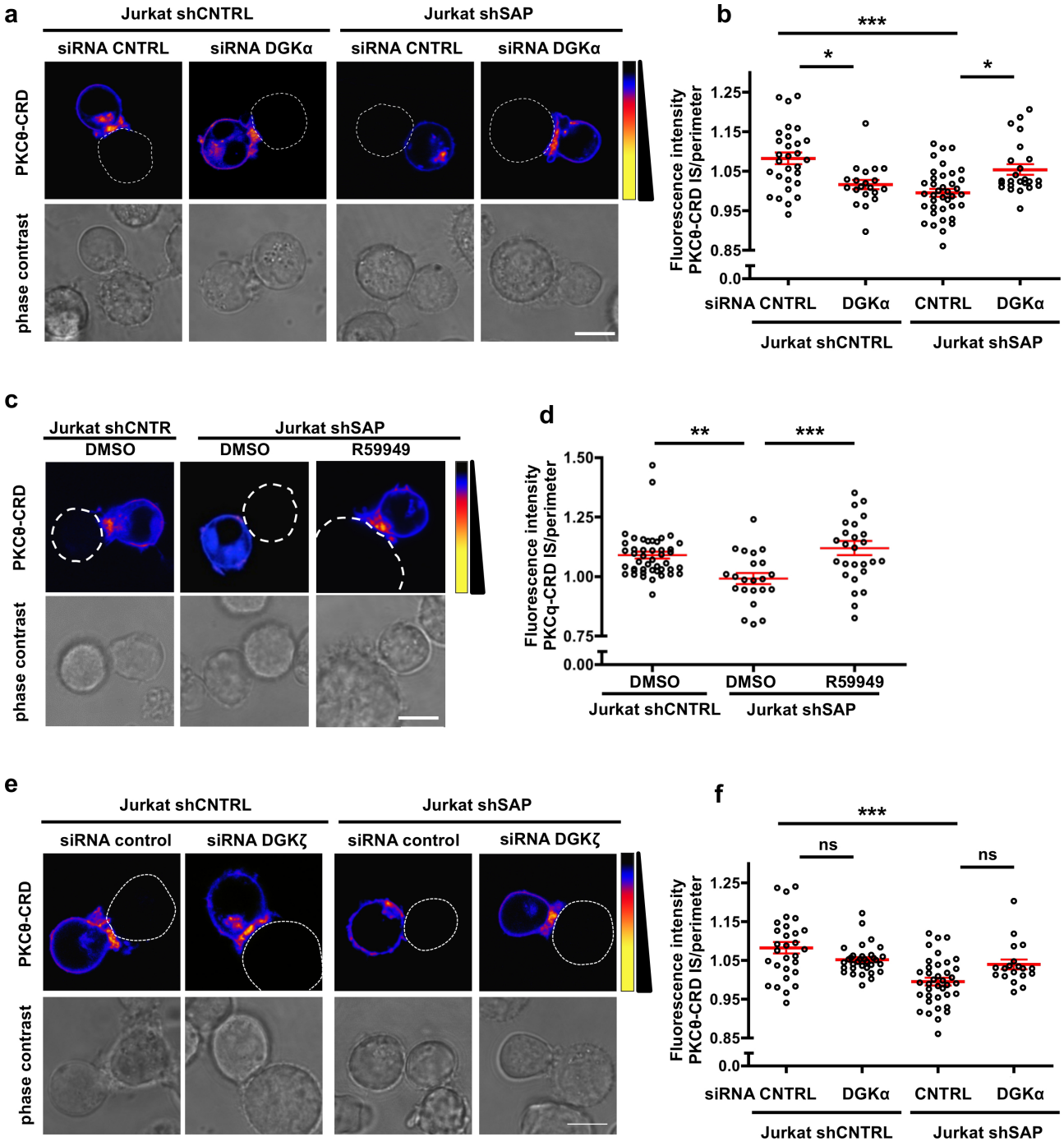

Figure 2. In SAP-silenced cells, DGKα activity impairs DAG accumulation at the IS.

Live-cells imaging analysis of shCNTRL or shSAP Jurkat cells transfected with EGFP-PKCθ-CRD to follow DAG accumulation during the conjugation with SEE-loaded Raji B cells.

shCNTRL and shSAP Jurkat T cells were transiently co-transfected with EGFP-tagged PKCθ-CRD and DGKα-specific (**a**), DGKζ-specific (**e**), or non specific siRNA. After 4 days were stimulated with SEE-loaded Raji B cells, and confocal live cell images were taken during T cell-APC conjugation. The fluorescence intensity of EGFP-tagged PKCθ-CRD is shown by pseudocolor as indicated in the calibration bar, with the position of the APC indicated in white dotted line (top row). The bottom row shows the corresponding phase contrast images. Scale bar 10 µm. (**b, d** and **f**) Quantification of the EGFP-tagged PKCθ-CRD accumulation at the IS (see Materials and Methods for details), which was calculated as the ratio of the mean fluorescence intensity (MFI) of GFP at the contact zone between the Jurkat cell and the Raji B cell and the MFI at the perimeter of the Jurkat cell. Data are derived from n > 20 conjugates per condition. Red lines and error bars in the scatter plots denote means and SEM, respectively. ***P < 0.001, ** P < 0.01, *P < 0.05, ns P > 0.05. All data are representative of at least three independent experiments. (**c**) shCNTRL or shSAP Jurkat T cells were

transiently transfected with EGFP-tagged PKCθ-CRD. After 48 h, cells were pretreated for 30 minutes with R59949 10 µM or DMSO and stimulated with SEE-loaded Raji B cells. Confocal live cell images were taken during T cell-APC conjugation. Representative images are shown in pseudo-colors as indicated in the calibration bar, with the position of the APC indicated in white dotted line. Scale bar 10 µm.

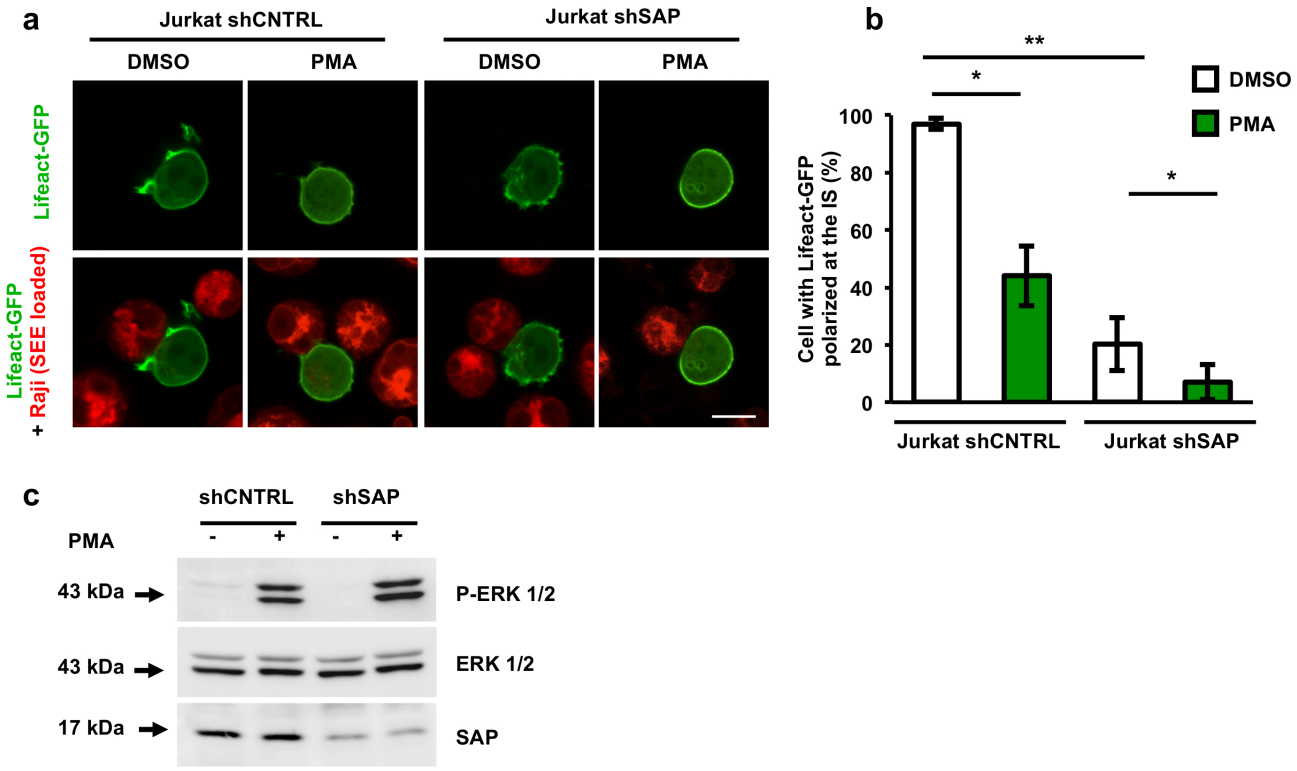

Figure 3. PMA disrupts the IS formation.
(**a**) Jurkat shCNTRL or shSAP were transiently transfected with Lifeact-GFP (green). 48 hours later, cells were treated for 15 min with PMA (200 ng/ml) mixed 1:1 with SEE-loaded Raji B cells (Red) to allow conjugate formation. Representative pictures are shown. Scale bar 10 µm. (**b**) Quantification of Lifeact-GFP polarized to the IS. The histogram shows the means and SEM of the % of polarized cells on the total of the cells counted, n > 20 conjugates for each condition, for at least three independent experiments. Statistic was calculated by using the unpaired two-tailed *t* test, where **P < 0.01, *P < 0.05. (**c**) shCNTRL and shSAP Jurkat cells were treated with PMA (200 ng/ml, 15 min), lysed and analyzed by WB for P-ERK 1/2, ERK and tubulin content.

In SAP-silenced cells, DGKα activity impairs MTOC reorientation.

DAG gradients and actin polymerization at the IS are required to orient the MTOC toward the IS [50, 124]. Indeed, CTLs from SAP KO mice exhibit both F-actin polarization defects and impaired MTOC reorientation towards B cell targets [128]. To determine whether DGKα inhibition may also restore MTOC docking at the IS, we performed conjugation experiments in control and SAP-deficient cells expressing GFP-Tubulin in the presence of the DGK inhibitor R59949. We found that, compared to shCNTRL Jurkat cells, shSAP Jurkat cells exhibit a defect in MTOC polarization, measured as distance between MTOC and the IS. Here, DGKα inhibition was able to drive the MTOC relocation behind the IS, while did not have any significant effect on MTOC positioning in control cells (**Fig. 4a,b**).

These data collectively indicates that DGKα plays a pivotal role in regulating the DAG gradient that is required for both actin dynamics and MTOC repositioning toward the IS.

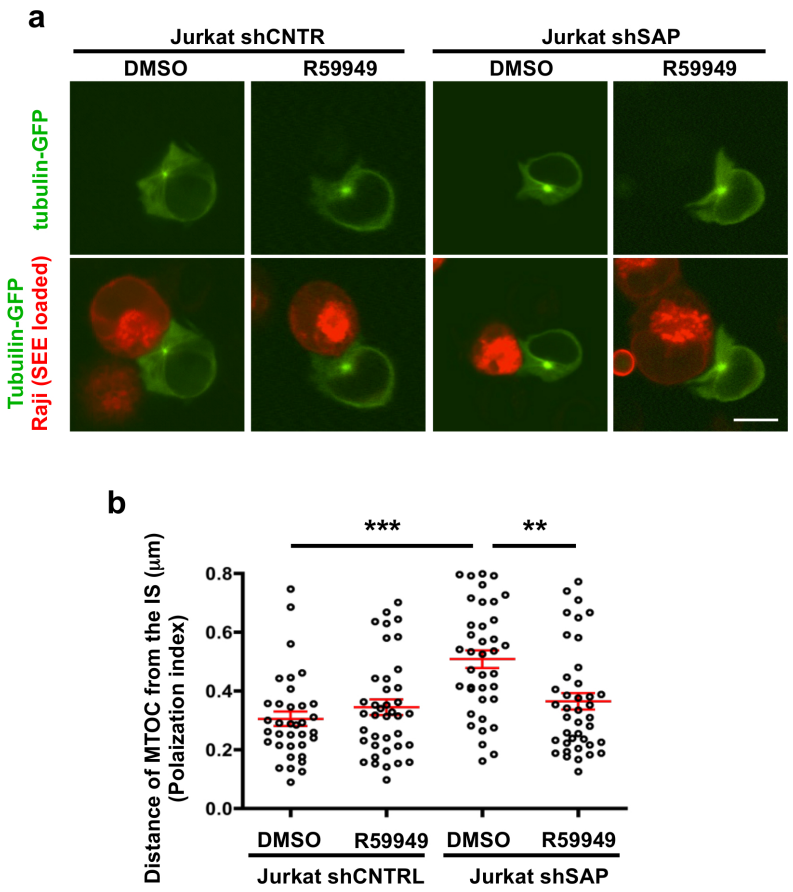

Figure 4. In SAP-silenced cells, DGKα activity impairs MTOC reorientation.
(**a**) shCNTRL and shSAP Jurkat cells were transfected with GFP-Tubulin (green). Two days later, cells were pretreated for 30 minutes with R59949 10 µM or DMSO and mixed 1:1 with SEE-loaded Raji B cells (red) to allow conjugate formation, seeded on polylysine-coated glasses and acquired. Representative images are shown, scale bar 10 µm. (**b**) The polarization index was measured by calculating the distance from the MTOC to the immunological synapse divided by the distance from the immunological synapse to the distal pole of the T cell. Red lines and error bars in the scatter plots denote means and SEM, respectively. ***P < 0.001, **P < 0.01. n > 20 conjugates for each experimental condition, all data are representative of at least two independent experiments.

In SAP-silenced cells, DGKα activity impairs DAG-dependent signaling.

We next sought to investigate whether inhibition or silencing of DGKα restores the defective DAG signaling of SAP-deficient cells.

At first, we used primary T lymphocytes to track the recruitment to the IS of two DAG-dependent signal transducers: PKCθ [129] and RasGRP1 [130]. Consistent with our previous findings, recruitment of PKCθ and RasGRP1 to the IS was strongly reduced in SAP-silenced T cells (**Fig. 5a-h**). Silencing or inhibition of DGKα did not influence the recruitment of PKCθ and RasGRP1 in control T cells, but fully restored localization at the IS in SAP-silenced cells (**Fig. 5a-h**). These data are consistent with previous observation in Jurkat T cells [116] and suggest that in the absence of SAP, excessive DAG metabolism limits TCR signaling and cytoskeletal remodeling at the IS.

Since is known that inhibition of DGKα activity potentiates DAG-dependent signaling [131-134], and we found that was sufficient to rescue RasGRP1 recruitment at the IS in SAP-deficient primary T cells, we asked whether DGKα inhibition could also restore the defective ERK activation observed in SAP-deficient primary T cells [66, 68]. Indeed, we observed that silencing or pharmacologic inhibition of DGKα did not affect basal ERK activity in resting control T cells, but potentiated ERK1/2 phosphorylation following TCR stimulation (**Fig. 6a,b)**. Compared to control cells, SAP-silenced cells exhibited decreased ERK activation upon TCR stimulation; however, DGKα knockdown or inhibition restored TCR-driven ERK activation bringing it back to nearly normal levels (**Fig. 6a,b**).

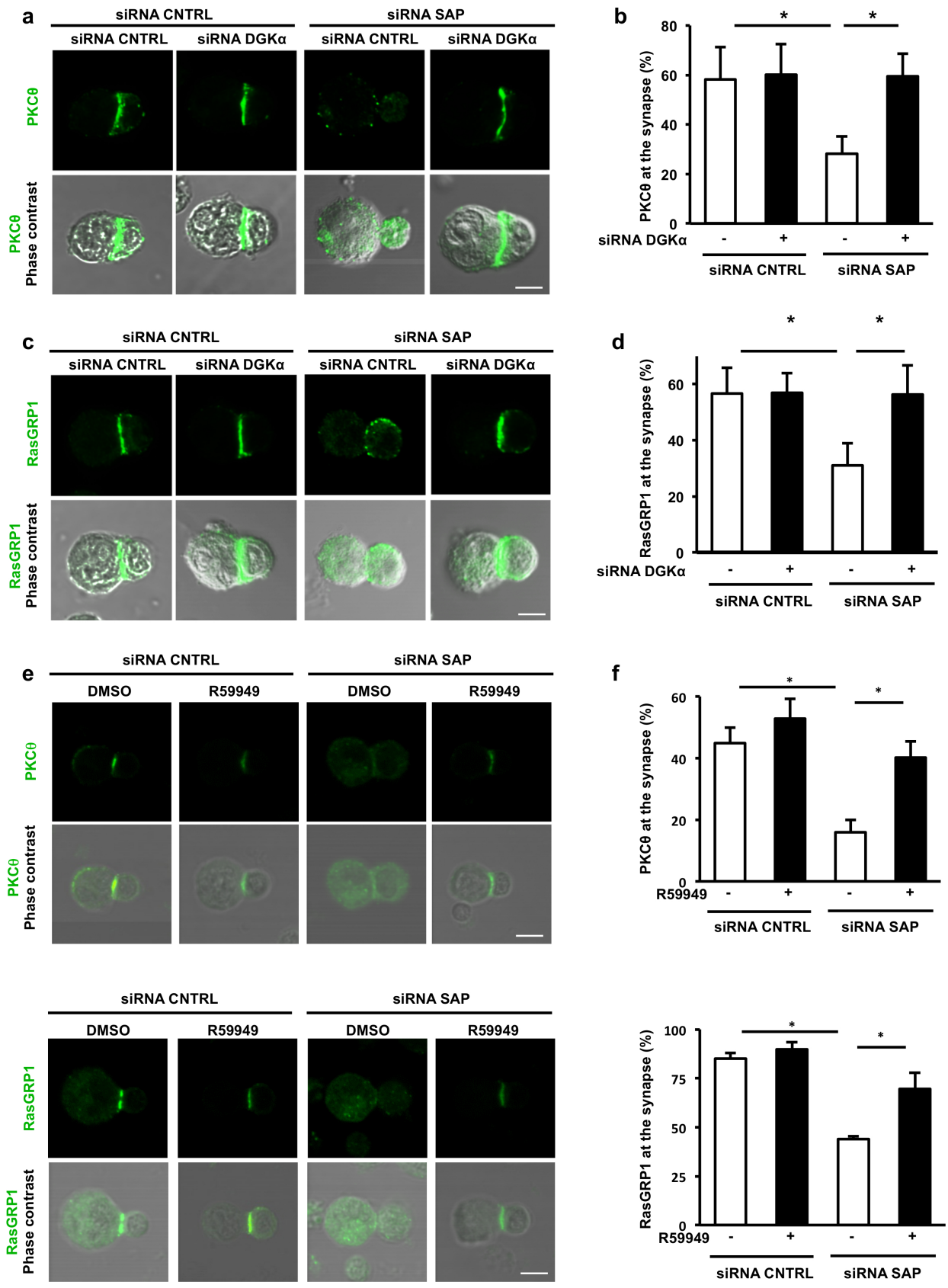

Figure 5. In SAP-silenced cells, DGKα activity impairs PKCθ and RasGRP1 recruitment to the IS.

Primary human PBLs were transfected with the indicated siRNA and after 72 hours incubated 1:1 with Raji B cells loaded with mixed SEE and SEB superantigens for 15 minutes, fixed and stained for PKCθ (**a**) or RasGRP1 (**c**), both in

green. Scale bar 10 µm. Histograms show the percentage of cells displaying PKCθ (**b**) and RasGRP1 (**d**) at the IS. n = 100 conjugates were counted in six replicates from two independent experiments as mean ± SEM (unpaired two-tailed *t* test, *P < 0.01).

Human PBLs were transfected with control or SAP-specific siRNA. After 72 hours were pretreated with R59949 (10 µM, 30 minutes) and incubated with Raji B cells loaded with mixed SEE and SEB superantigens for 15 minutes, fixed and stained for PKCθ (**e**) or RasGRP1 (**g**). Representative pictures are shown. Scale bar 5 µm. Histogram shows the percentage of cells displaying PKCθ (**f**) and RasGRP1 (**h**) at the IS. Data are derived from three independent experiments as mean ± SEM (unpaired two-tailed *t* test, *P < 0.05).

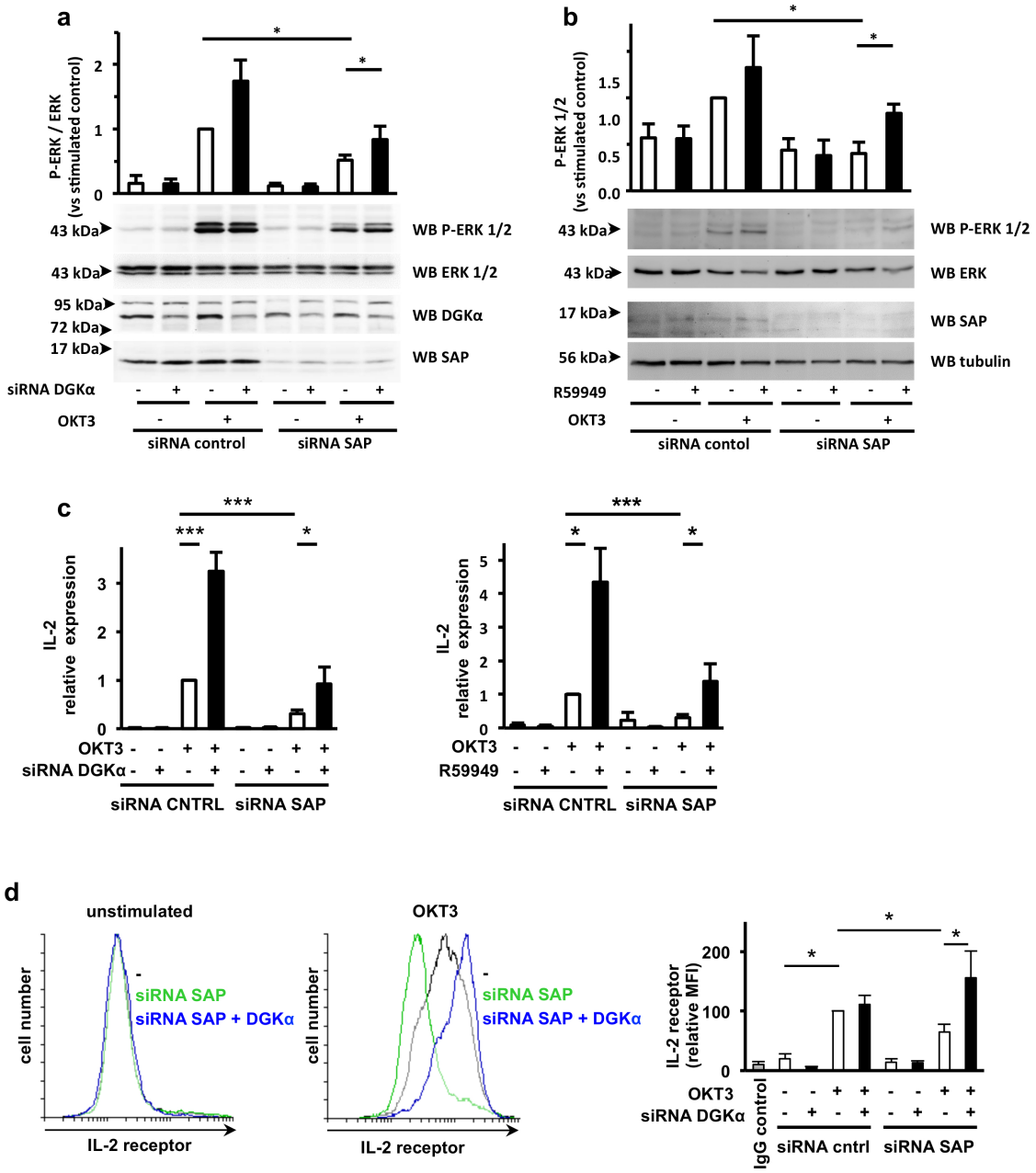

Figure 6. DGKα silencing or inhibition enhances ERK1/2 phosphorylation, IL-2 expression and CD25 membrane exposure in WT and SAP-deficient primary T cells.

(**a**) Primary human PBLs were transfected with the indicated siRNA. After 4 days, cells were stimulated with OKT3 (10 µg/ml) for 30 min, lysed and analysed by WB for P-ERK 1/2, ERK, DGKα and SAP content. (**b**) Primary human PBLs were transfected with a SAP-specific siRNA. After 4 days, cells were pretreated with R59949 (5 µM, 30 min) and then stimulated with OKT3 (10 µg/ml) for 5 min, lysed and analysed by WB for P-ERK 1/2, ERK, tubulin and SAP content. Histograms in (a) and (b) shows the mean ± SEM of the corresponding densitometries. 5 independent experiments were performed for (a) and 6 for (b), unpaired two-tailed *t* test, *P < 0.05. (**c**) Primary human PBLs were transfected with the indicated siRNA. 4 days later, they were restimulated with 10 µg/ml OKT3 for 4 hours (left), or pretreated with R59949 (5 µM, 30 minutes) and then restimulated (right). IL-2 was quantified by quantitative RT-PCR using GUSB as reference gene. Graphs show the mean ± SEM of six independent experiments. Unpaired *t* test ***P < 0.001, *P < 0.05. (**d**) Primary human PBLs were transfected with control, SAP, or SAP + DGKα-specific siRNAs. After 4 days, cells were treated with OKT3, fixed and stained for CD25. The histograms show the FACS analysis of the CD25 MFI in untreated (left) and OKT3-treated (right) cells. On the right, the graph shows the mean ± SEM of the MFI relative to the stimulated control (unpaired two-tailed *t* test, *P < 0.05).

DGKα knockdown or inhibition reinforces the strength of the signal upon TCR ligation in SAP-deficient T lymphocytes.

We next sought to examine to what extent DGKα silencing or inhibition restore TCR signaling in SAP-silenced T cells. To this purpose, we selected a panel of TCR responsive genes, with a specific attention to genes involved in apoptosis previously reported to be less expressed in T lymphocytes from XLP1 patients [90].

First, as T cells derived from XLP1 patients show defective induction of IL-2 and IL-2 receptor α chain (CD25) [135], we evaluated the TCR-stimulated induction of IL-2 mRNA in SAP silenced PBLs upon DGKα silencing or inhibition. As previously described [8, 116], we found that DGKα silencing or inhibition strongly potentiated TCR-induced IL-2 mRNA expression (**Fig. 6c**) without altering induction of CD25 (**Fig. 6d**). In SAP-deficient cells, we observed a lower induction of IL-2 mRNA compared to SAP-sufficient cells, which was completely rescued by DGKα silencing or inhibition (**Fig. 6c**). Similarly, SAP-silenced cells displayed a reduced induction of CD25, which was completely rescued by DGKα silencing (**Fig. 6d**).

Altogether, these data suggest that DGKα silencing or inhibition in both control and SAP knockdown cells enhances IL-2 production and CD25 exposure, thus potentiating the TCR-induced IL-2 autocrine loop.

Among other genes whose activation is strongly induced downstream the TCR-triggering, we selected BIM (*BCL2L11*), FASL (*FASLG*), Nur77 (*NR4A1*) and Nor1 (*NR4A3*), which were shown to have also pro-apoptotic functions [34, 35, 88, 89, 136, 137]. Particularly, XLP1-derived T lymphocytes features a defective induction of BIM and FASL [90]. Accordingly, we observed a reduced TCR-induced transcription of BIM (*BCL2L11)* and FASL (F*ASLG*) in SAP-silenced PBLs (**Fig. 7a-d**). However, the expression of these two genes was not rescued by DGKα silencing or inhibition (**Fig. 7a-d**). Similarly, the DGKα inhibitor R59949 did not restore FASL and BIM expression at the protein level in XLP1 derived T lymphocytes (**Fig. 7e**). When we measured FASL in the supernatants (sFASL) of TCR-stimulated T cells, we detected a substantial reduction of sFASL released from T cells from XLP1 patients, which was not rescued by R59949 or by the other DGKs inhibitor R59022 (**Fig. 7f**).

On the other hand, Nur77 expression has been used as a report of the TCR receptor signal strength [138] and, together with its closed homolog Nor1, mediates activation-induced cell death [139]. The transcription of both Nur77 (*NR4A1*) and Nor1 (*NR4A3*) was severely impaired in SAP-

silenced cells and both DGKα silencing and inhibition were able to fully rescue their expression in SAP-silenced cells, without affecting their induction in control cells (**Fig. 7g-j**). A similar trend was observed at the protein level in Jurkat cells, were Nur77 was induced between 2 and 4 hours of TCR stimulation in a SAP-dependent manner (**Fig. 7k**). The defective induction in Jurkat shSAP was fully rescued by the DGKα inhibitor R59949 (**Fig. 7k**). Finally, the DGKα inhibitors R59949 and R59022 were also capable of partially restoring Nur77 and Nor1 induction in XLP1 patients-derived T cells (**Fig. 7l).**

Those data indicates that DGKα silencing or inhibition selectively rescues the expression of some TCR-dependent target genes in SAP deficient cells, and also suggest that in SAP-deficient cells the defective induction of IL-2, CD25, Nur77 and Nor1 is due to a reduced TCR signaling strength caused by excessive DGKα activity.

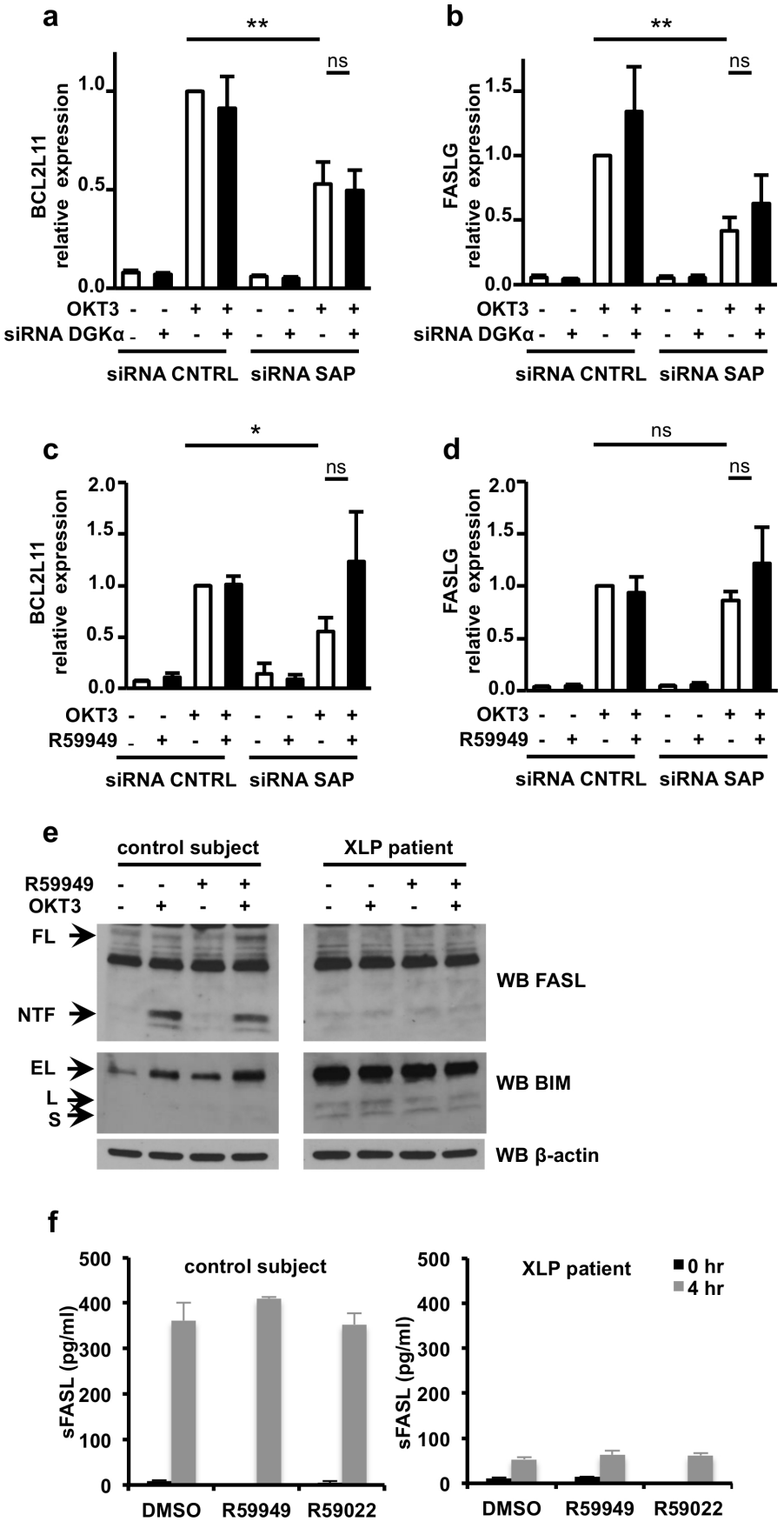
a
**
ns
BCL2L11 relative expression
1.0
0.5
0.0
OKT3 - - + + - - + +
siRNA DGKα - + - + - + - +
siRNA CNTRL
siRNA SAP
b
**
ns
FASLG relative expression
1.5
1.0
0.5
0.0
OKT3 - - + + - - + +
siRNA DGKα - + - + - + - +
siRNA CNTRL
siRNA SAP
c
*
ns
BCL2L11 relative expression
2.0
1.5
1.0
0.5
0.0
OKT3 - - + + - - + +
R59949 - + - + - + - +
siRNA CNTRL
siRNA SAP
d
ns
ns
FASLG relative expression
2.0
1.5
1.0
0.5
0.0
OKT3 - - + + - - + +
R59949 - + - + - + - +
siRNA CNTRL
siRNA SAP
e
control subject
XLP patient
R59949 - - + + - - + +
OKT3 - + - + - + - +
FL
NTF
EL
L
S
WB FASL
WB BIM
WB β-actin
f
control subject
XLP patient
0 hr
4 hr
sFASL (pg/ml)
500
400
300
200
100
0
DMSO
R59949
R59022

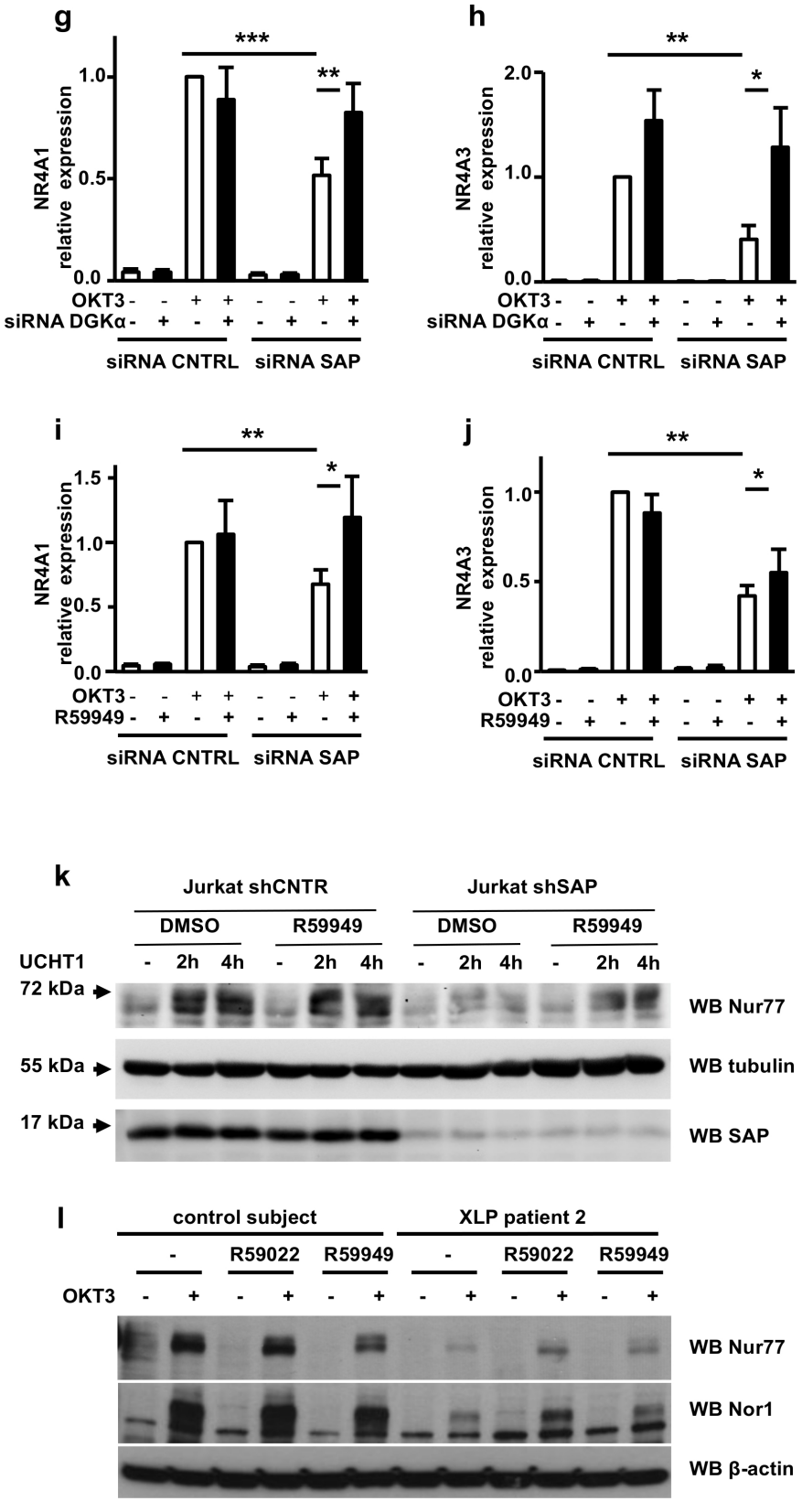

Figure 7. DGKα silencing or inhibition enhances Nur77 and Nor1 expression in WT and SAP-deficient primary T cells. Primary human PBLs were transfected with the indicated siRNA. 4 days later, they were stimulated with 10 µg/ml OKT3 for 4 hours (**a,b**), or pretreated with R59949 (5 µM, 30 minutes) and then restimulated (**c,d**). BIM (**a,c**) and FASL (**b,d**) were quantified by quantitative RT-PCR using GUSB as reference gene. Graphs show the mean ± SEM of six independent experiments. Unpaired *t* test **P < 0.01, *P < 0.05, ns P > 0.05.

(**e**) Primary human PBLs from healthy donor or XLP1 patient were pretreated with DMSO or R59949 (5 μM, 30 minutes) and then restimulated for 4 hours. BIM and FASL expression was verified by WB analysis. (**f**) Primary human PBLs from healthy donor or XLP1 patient were pretreated or not with R59022 or R59949 (5 μM, 30 minutes) and then unstimulated or restimulated for 4 hours. sFASL release was quantified by ELISA. (**g-j**) The same cDNA of the experiments performed in (a-d) was used to measure by quantitative RT-PCR NR4A1 (Nur77) and NR4A3 (Nor1), using GUSB as reference gene. Graph shows the mean ± SEM of six independent experiments. Unpaired *t* test ***P < 0.001, **P < 0.01, *P < 0.05. (**k**) shCNTR or shSAP Jurkat T cells were pretreated with R59949 (5 μM, 30 min), stimulated with anti-CD3 (UCHT1 clone) for 0, 2 and 4 hours, lysed and analysed by WB for Nur77, tubulin and SAP content. (**l**) PBLs from healthy donor or XLP1 patient were pretreated with R59022 or R59949 (5 μM, 30 min) and stimulated or not with anti-CD3 (OKT3 clone). 4 hours later, cells were lysed and analysed by WB for Nur77, Nor1 and β-actin content.

DGKα silencing or inhibition rescues RICD in SAP-deficient T cells from healthy donors or T lymphocytes from XLP1 patients.

XLP1 patients exhibit resistance to restimulation-induced cell death (RICD) due to a reduced signaling strength and impaired induction of pro-apoptotic proteins [90]. Therefore, we asked if the RICD defect observed in cells from XLP1 patients could depend on the aberrant DGKα activity, which - by consuming DAG - lowers the TCR signal strength, and whether the inhibition of DGKα could reestablish RICD in SAP-deficient T lymphocytes.

We performed RICD experiments in T cells from healthy donors transfected with SAP-specific siRNA, in presence or not of the two commercial inhibitors of DGKs, R59949 and R59022. While both inhibitors did not show significant effects on cell death of control cells, at any of the concentration used, R59949 and R59022 treatment rescued the cell death of SAP-silenced cells to nearly normal levels (**Fig. 8a,b**). We then repeated the experiments on T cells from XLP patients. Again, the two DGKs inhibitors did not affect RICD in cells from healthy donors, while partially rescued the cell death in 4 different XLP1 patients-derived T lymphocytes (**Fig. 8c-f**). We next performed the same experiments transfecting cells with a siRNA specific for DGKα. In both our experimental systems (i.e. T cells from healthy donors silenced for SAP or T cells from XLP1 patients), silencing of DGKα is sufficient to completely rescue the RICD defect (**Fig. 8g,h**). Those data indicate a specific involvement of DGKα activity in the RICD resistance of these cells and suggest a key role for DAG signaling in the induction of cell death in a context of restimulation. To further support this hypothesis, we performed the RICD experiments in SAP-deficient T cells treated with a soluble, short form of DAG (C8-DAG). As showed in **Fig. 8i**, 50 μM DAG did not affect RICD in control cells, while completely rescued the defective cell death of SAP-deficient T cells.

As DGKζ is the main responsible for DAG metabolism in T cells [103, 125], we verified the effect of DGKζ silencing on RICD. We found that DGKζ-specific silencing did not affect RICD in control cells but partially restored it in SAP silenced cells (**Fig. 8j**), suggesting that the strength of TCR-induced DAG signaling controls RICD.

As RICD is an apoptotic process, we analyzed phosphatidylserine exposure and propidium iodide uptake during the assay to exclude a toxic/necrotic side effects of our treatments. DGKα silencing or inhibition in control cells did not affect apoptosis, while in SAP-deficient T cells or T cells from XLP patients both silencing or inhibition of DGKα restored the size of the AnnV+ cell population. The small necrotic/late apoptotic fraction is not perturbed (**Fig. 9a,b)**

Collectively, our data show that the RICD defect observed in T lymphocytes from XLP1 patients is due to the aberrant activity of DGKα. Therefore, DGKα inhibition could potentially overcome the cell death defects of T cells from XLP1 patients. Moreover, also other approaches to increase DAG levels within the cells - i.e. silencing of DGKζ, or administration of exogenous DAG at the beginning of the death assay – were able to rescue the RICD. This suggests that DGKα, by consuming DAG, terminates the signal responsible for the apoptosis in T cells from XLP1 patients, thus explaining their resistance to RICD.

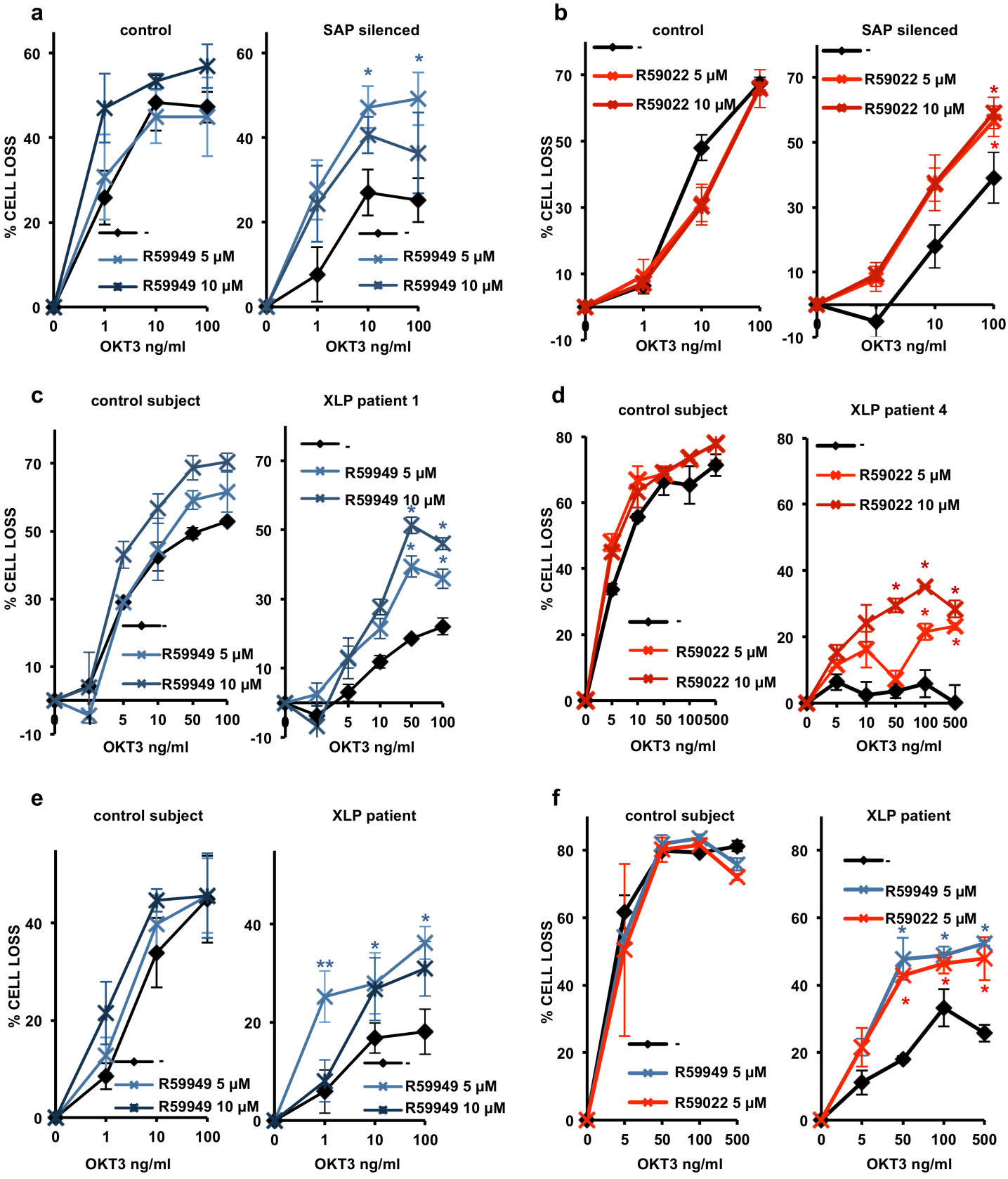
a
control
SAP silenced
% CELL LOSS
OKT3 ng/ml
-
R59949 5 µM
R59949 10 µM
b
control
SAP silenced
R59022 5 µM
R59022 10 µM
c
control subject
XLP patient 1
d
control subject
XLP patient 4
e
control subject
XLP patient
f
control subject
XLP patient

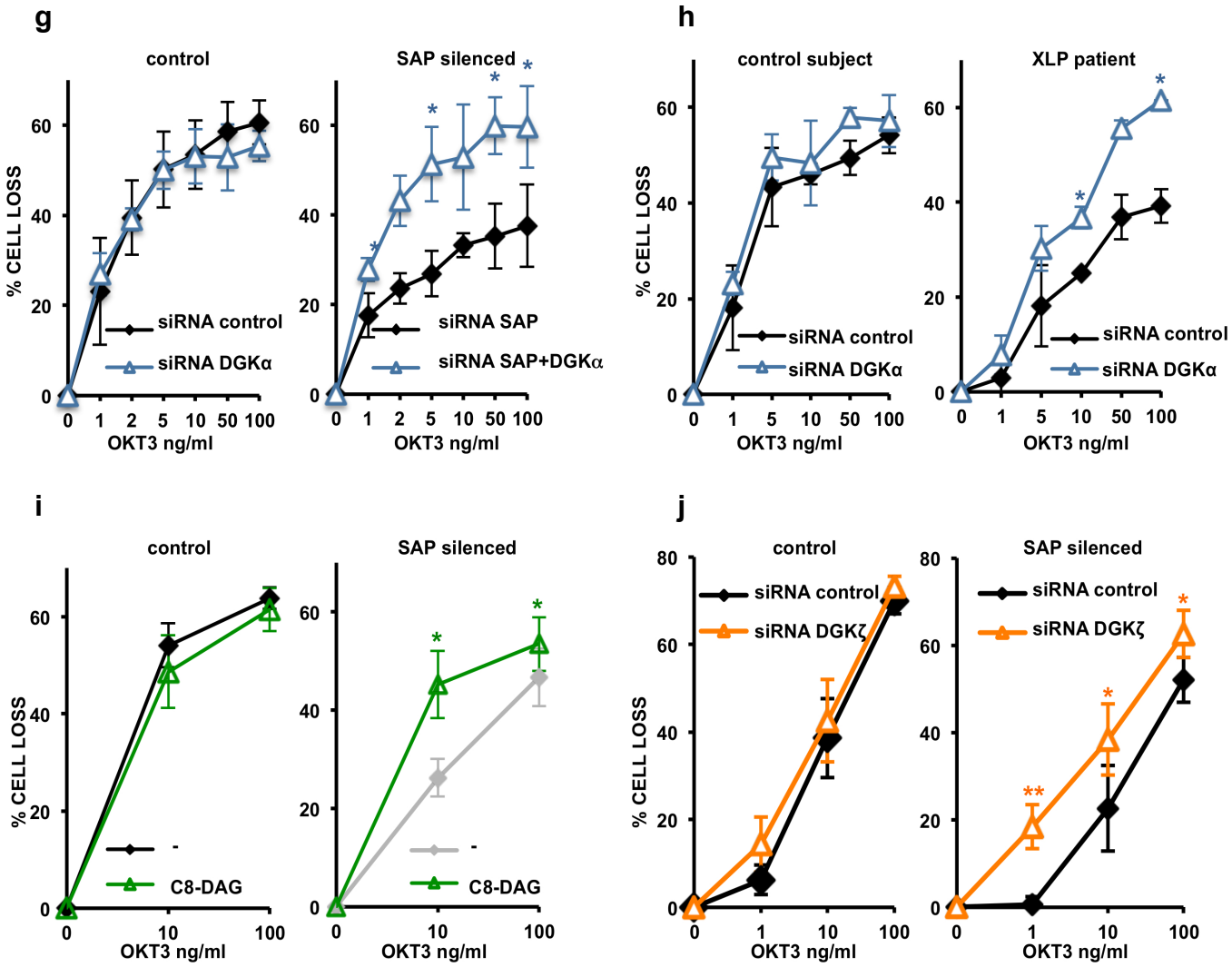

Figure 8. DGKα silencing or inhibition rescues RICD in SAP-deficient T cells from healthy donors or T lymphocytes from XLP1 patients. Lymphocytes from control subjects were transfected with a SAP-specific siRNA and after 4 days pretreated with the indicated doses of R59949 for 30 min (**a**) or R59022 (**b**) and then restimulated with increasing doses of CD3 agonist OKT3. After 24 hours the % of cell loss was evaluated by PI staining. Data are the mean ± SEM of three independent experiments performed in triplicate. Lymphocytes from control subject or XLP patient were pretreated with the indicated doses of R59949 for 30 min (**c,e,f**) or R59022 (**d,f**) and then restimulated with increasing doses of CD3 agonist OKT3. After 24 hours the % of cell loss was evaluated by PI staining. Data are the mean ± STDEV of one experiment performed in triplicate.

(**g**) Lymphocytes from control subjects were transfected with the indicated siRNA and after 4 days restimulated with increasing doses of CD3 agonist OKT3. After 24 hours the % of cell loss was evaluated by PI staining. Data are the mean ± SEM of three independent experiments performed in triplicate. (**h**) Lymphocytes from control subject or XLP patient were transfected with a DGKα-specific siRNA and after 4 days restimulated with increasing doses of CD3 agonist OKT3. After 24 hours the % of cell loss was evaluated by PI staining. Data are the mean ± STDEV of one experiment performed in triplicate. (**i**) Lymphocytes from control subjects were transfected with a SAP-specific siRNA and after 4 days pretreated with 50 µM of C8-DAG and then restimulated with increasing doses of CD3 agonist OKT3. After 24 hours cells were washed and the % of cell loss was evaluated by PI staining. Data are the mean ± SEM of three independent experiments performed in triplicate. (**j**) Lymphocytes from control subjects were transfected with the indicated siRNA and after 4 days restimulated with increasing doses of CD3 agonist OKT3. After 24 hours the % of cell loss was evaluated by PI staining. Data are the mean ± SEM of three independent experiments performed in triplicate.

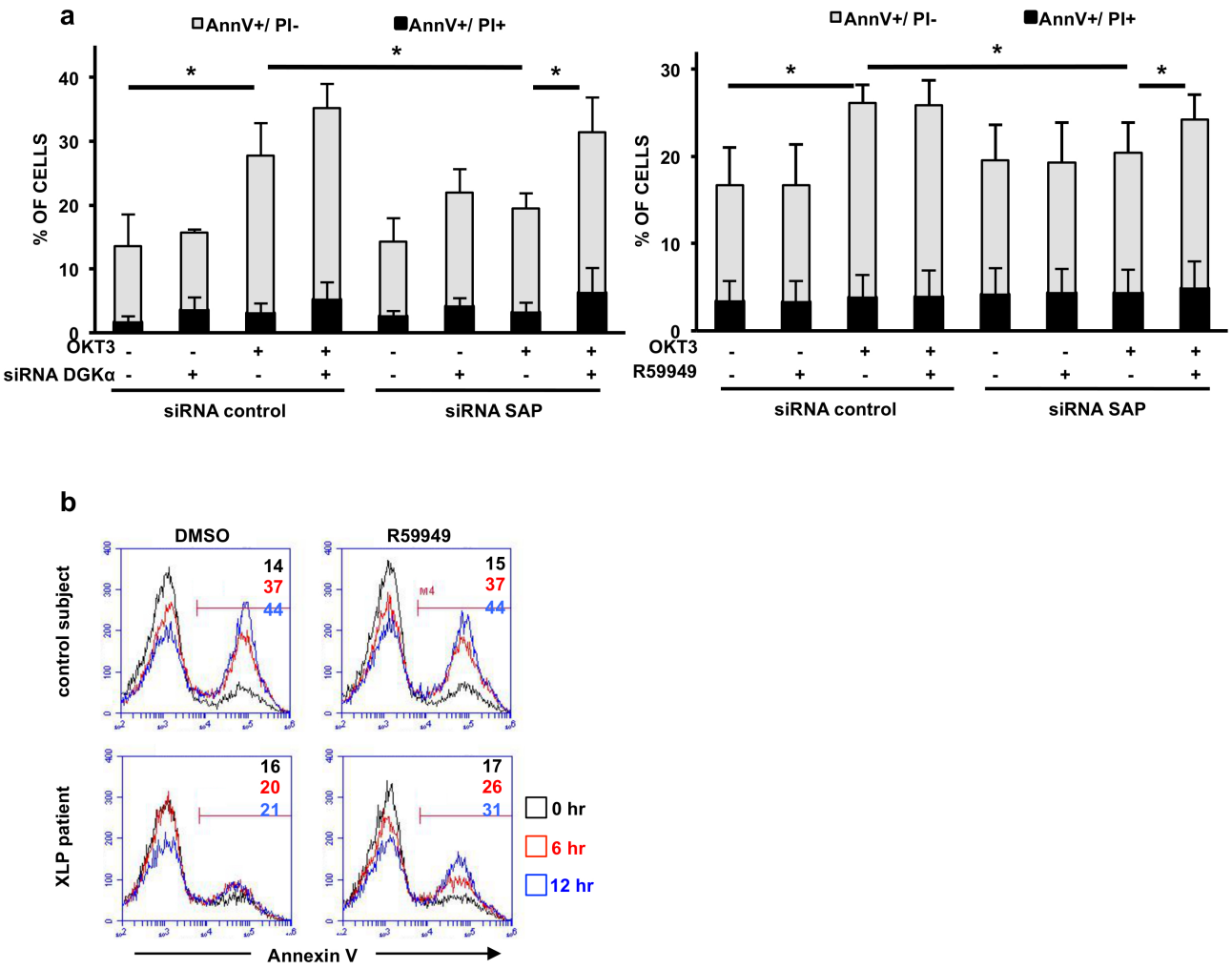

Figure 9. DGKα silencing or inhibition increased the apoptotic fraction of SAP-deficient cells or cells from XLP1 patients.

(**a**) AnnexinV/PI analysis of the experiments showed in Fig. 8a,b (right) and Fig. 8g (left). Data are the mean ± SEM of three independent experiments performed in triplicate. Paired *t* test, * P < 0.05 (**b**) AnnexinV staining of the experiments showed in Fig.8c,e. A representative experiment is showed.

DGKα knockdown restores RICD by activating DAG signaling through PKCθ and the MAPK cascade.

We already showed that DGKα inhibition in SAP-deficient cells is able to restore DAG-dependent PKCθ and RasGRP1 recruitment at the IS, and to activate ERK1/2. Interestingly, these pathways are relevant for the induction of RICD [140, 141], prompting us to verify whether they mediates the restoration of apoptosis upon DGKα knockdown in SAP-deficient T cells. Indeed, by silencing PKCθ and RasGRP1, we observed that both were required for RICD in both control cells and SAP+DGKα silenced cells, while their silencing did not affect the residual apoptosis of SAP-deficient cells (**Fig. 10a,b)**.

Similarly, Rottlerin, an inhibitor of nPKCs (including PKCθ isoform) [142], at 6 μM concentration had minimal effects on RICD of control cells. However, it completely abolished the rescue of RICD mediated by DGKα silencing in SAP-deficient cells (**Fig. 10c**). Equally, the MEK and ERK inhibitors (U0126 [143] and FR180204 [144], respectively) at doses that showed a slight effect on RICD of control cells, were able to completely abolish the induction of cell death mediated by DGKα silencing in SAP-deficient cells (**Fig. 10d**). Those results indicate that silencing of DGKα reestablish RICD by activating PKCθ activity and the RasGRP1/MEK/ERK signaling cascade, prompting us to focus on the RSK2 S6 kinase, which is activated downstream of ERK, and phosphorylates Nur77. This phosphorylation is in turn responsible for Nur77 mitochondrial translocation and, ultimately, for cell apoptosis [33, 34].

The RSK inhibitor SL0101-1 (100 μM) drastically induced resistance to RICD in control cells, confirming that RSK activity is required for RICD, likely by promoting Nur77 phosphorylation (**Fig. 10e**). Notably, SL0101-1 also abolished the rescue of RICD induced by DGKα silencing in SAP-deficient cells, indicating that DGKα knockdown restores RICD via RSK activation (**Fig. 10e**). We observed similar effects on T cells derived from XLP1 patients. Here, the rescue of RICD upon R59949 treatment was totally blunted by the RSK inhibitor SL0101-1 (**Fig. 10f**).

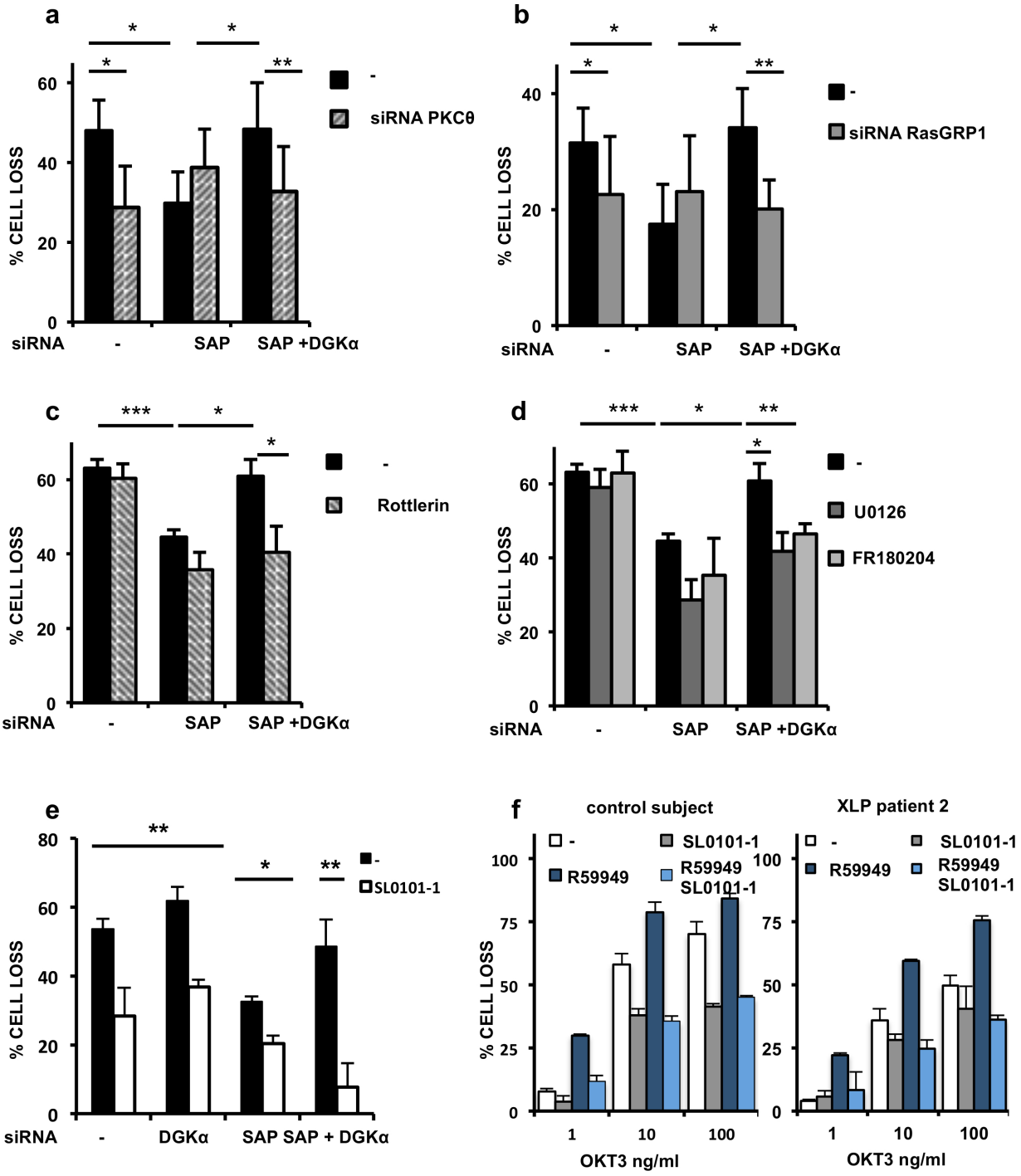

Figure 10. DGKα knockdown restores RICD by activating DAG signaling through PKCθ and the MAPK cascade. Lymphocytes were transfected with SAP siRNA and PKCθ-specific (**a**) or RasGRP1-specific siRNA (**b**) and after 4 days were restimulated with CD3 agonist OKT3 (10 ng/ml). After 24 hours the % of cell loss was evaluated by PI staining. Data are the mean ± SEM of four independent experiments performed in triplicate. Paired T test **P < 0.01, *P < 0.05. (**c**) Lymphocytes were transfected with the indicated siRNA and after 4 days were pretreated with the PKCs inhibitor Rottlerin (6 μM). After 30 minutes cells were restimulated with CD3 agonist OKT3 (100 ng/ml). After 24 hours the % of cell loss was evaluated by PI staining. Data are the mean ± SEM of four independent experiments performed in triplicate. Paired T test ***P < 0.001, **P < 0.01, * P < 0.05. (**d**) Experiments performed as in (c), except that cells were pretreated with MEK (U0126, 5 μM) and ERK (FR180204, 10 μM) inhibitors. (**e**) Experiments performed as in c, except that cells were pretreated with the RSK2 inhibitor (SL0101-1, 100 μM). (**f**) Lymphocytes from control subject (left) or XLP1 patient 2 (right) were pretreated for 30 minutes with R59949, 5 μM and restimulated for 24 hours with increasing doses of OKT3. A representative experiment is shown.

RSK-dependent Nur77 phosphorylation is required for the RICD.

Altogether, our data suggest that, upon DGKα silencing, Nur77 induction and phosphorylation by RSK2 may be the key events required for restoring the RICD in SAP-silenced cells.

Thus, we evaluated the amount and phosphorylation of the Nur77 protein in primary T cells upon SAP or SAP+DGKα silencing treated or not with SL0101-1. In these experiments, P-S6 was used as a read out for RSK activity. In line with the experiments shown in Fig. 7, we saw a defect in TCR-induced Nur77 expression in SAP-silenced cells which is rescued by DGKα silencing (**Fig. 11a**). In parallel, we observed that SAP-deficient cells displayed a severely decreased phosphorylation of Nur77 on the RSK-dependent phosphorylation site S351, which is fully rescued by DGKα silencing in a RSK dependent manner (**Fig. 11a**).

Moreover, in XLP1-derived T cells, the simultaneous silencing of Nur77 and Nor1 reduced the effect on RICD induced by DGKα inhibition, indicating a synergistic role for those two factors in boosting the RICD (**Fig. 11b**). Indeed, Nur77 knockdown alone had no effect on RICD (data not shown). Interestingly, Nur77 and Nor1 silencing did not affect apoptosis of control cells from healthy donors, indicating that in those cells other apoptotic pathways concur in achieving the RICD (**Fig. 11b**).

Altogether, those results indicate that the reestablishment of DAG signaling at the IS observed upon DGKα knockdown restores apoptosis in SAP-deficient cells by activating PKCθ and the MAPK cascade, leading to RSK-mediated phosphorylation of Nur77 and Nor1, whose induction is specifically required for the rescue of the RICD mediated by DGKα silencing or inhibition.

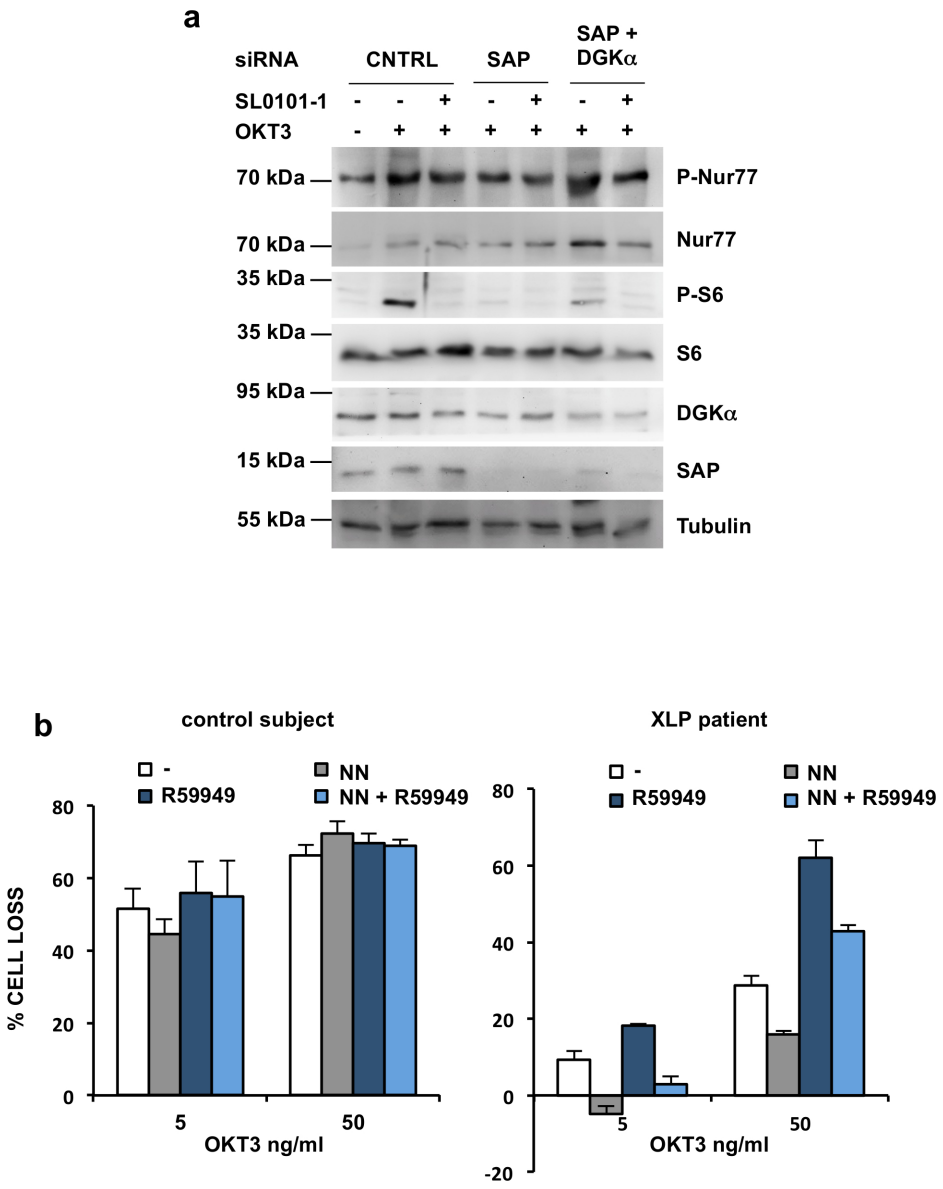

Figure 11. RSK-driven phosphorylation of Nur77 and Nor1 is required for the RICD.

(**a**) Human primary T lymphocytes were transfected with control, SAP and SAP+DGKα siRNAs. After 4 days, cells were pretreated with SL0101-1 (100 µM, 30 minutes) and stimulated with OKT3 (10 µM, 4 hours), lysed and analyzed by WB for P-Nur77 (S531), Nur77, P-S6, S6, DGKα, SAP and tubulin content. P-S6 was used as read out for SL0101-1 activity. A representative experiment is shown, n = 3 (**b**) Primary T lymphocytes from control subject or XLP1 patient were co-transfected with Nur77 and Nor1 specific antibodies (NN). After 4 days, cells were pretreated with DMSO or R59949 (5 µM, 30 minutes) and stimulated with 5 or 50 ng/ml of anti-CD3 OKT3. A representative experiment is shown, n = 3.

Discussion

SAP deficiency in XLP1 causes multiple defects in the immune response. In particular, XLP1 patients display uncontrolled lymphoproliferation and extensive tissue damage upon EBV infection, which leads to fulminant infection mononucleosis (FIM). The lymphocyte expansion involves primarily the CD8+ compartment and mediates the tissue damage and illness [145]. A critical contribution to this process is due to resistance to restimulation-induced cell death (RICD), which depends on the NTB-A/SAP signaling pathway [90, 96].

We based this work on the finding that TCR-triggering inhibits DGKα in a SAP-dependent manner, thus allowing an efficient downstream DAG signaling [116, 146]. Inhere we demonstrate that the resistance to RICD observed in SAP-deficient lymphocytes from XLP1 patients is due, at least partially, to the uncontrolled DGKα activity. Moreover, we identified a strong correlation between DAG levels and the induction of the expression of the pro-apoptotic orphan nuclear receptors Nur77/Nor1. In an *in vivo* model of XLP1, we also provide evidence that DGKα inhibition attenuates the expansion of CD8+ lymphocytes and tissue damage. This suggests potential therapeutic applications for DGKα inhibitors, such as the stabilization of patients before the hematopoietic stem cell transplant.

The demonstration of a crucial role of uncontrolled DGKα activity in promoting resistance to RICD comes from the striking finding that DGKα silencing or inhibition is sufficient to fully restore cell death in SAP-silenced T cells but also in T lymphocytes from XLP1 patients (**Fig. 8**).

Interestingly, DGKα knockdown had no effect on RICD in SAP-sufficient cells (**Fig. 8**). This result confirms that, in normal T lymphocytes, DGKα activity is limited by SAP and couples with previous findings indicating that, despite high expression levels, DGKα plays a minor role in DAG metabolism in TCR-activate lymphocytes [125, 134].

Interestingly, the observation that also the specific silencing of DGKζ restored RICD in SAP-deficient cells (**Fig. 8j**) suggests that the crucial regulator of RICD is DAG signaling. Indeed, exogenous administration of a short chain C8-DAG was sufficient to restore RICD as well (**Fig. 8i**). Conversely, stimulation with phorbol ester (PMA), a DAG analog which bypass early TCR signaling events, strongly potentiated the signal, thus enhancing cell death while perturbing the IS formation (**Fig. 3a-c** and data not shown). These data strongly suggest that a localized DAG signaling is required for RICD.

The DAG accumulation induced by the TCR-triggering is highly localized at the immune synapse and controls both the organization of the actin cytoskeleton and the downstream events, leading to MTOC orientation towards the IS and activation of downstream effectors [37, 47]. DGKα and DGKζ are both recruited at the immune synapse, but they have distinct and non-redundant functions: while the ζ isoform prevalently phosphorylates the bulk of DAG, the α isoform plays a specific role in the controlling the synapse organization and T cell polarization [52, 125]. Interestingly, lymphocytes from SAP KO mice display several defects in the IS signaling, which couple with variable alterations in the IS assembly and MTOC polarization, depending on the cell type. Specifically, CTLs exhibit impaired actin reorganization and MTOC reorientation towards B cell targets, iNKT shows normal actin polymerization but are defective in MTOC orientation, while CD4+ T cells display normal IS but decreased DAG-dependent PKCθ recruitment [67, 128, 147]. To verify the correlation between these defects and DGK activity, we developed specific algorithms to quantify the accumulation of the PKCθ-CRD DAG biosensor, Lifeact-GFP and Tubulin-GFP in conjugates between SEE-loaded Raji B cells and Jurkat T cells, to follow DAG, actin and MTOC movements, respectively. Our results indicates that the defects of the IS morphology and function in SAP deficient cells are due to the increased DAG metabolism by DGKα. Indeed, DGKα-specific silencing restores not only the DAG accumulation at the IS but also the IS morphology and the MTOC orientation in SAP-deficient cells (**Fig. 1,2,4**). We can also confirm that in control SAP-sufficient cells, DGKα limits DAG polarization at the IS, without affecting conjugate formation [52, 124]. In contrast, DGKζ silencing was not sufficient to significantly rescue actin accumulation to the IS in SAP-deficient cells (**Fig. 1**), or to disrupt the polarity in control cells (**Fig. 1,2)**, accordingly to the prominent role of the α isoform in regulating the polarity of the T cells [52].

Notably, the MTOC repositioning controls the secretion of cytotoxins, which travel along microtubules to the centrosome, and are then released towards the target cell [50]. It is likely that DGKα inhibition in SAP-deficient cells, by controlling MTOC reorientation, might restore the cytotoxic activity of CTLs (and possibly of NK cells). It would be interesting to test this hypothesis, since XLP patients not only display impaired T cell restimulation-induced cell death, but also have impaired clearance of EBV+ B cells leading to HLH and lymphomas.

Altogether, our data demonstrates that DGKα controls the IS formation, the strength of the signaling, and the RICD in SAP-deficient cells, thus suggesting that DAG at the IS might regulates the RICD process. Indeed, SAP-deficient cells show decreased recruitment of the DAG-dependent signal transducer PKCθ and impaired activation of the DAG-dependent MAPK pathway [64, 67,

116]. Therefore, we immuno-localized PKCθ and RasGRP1 to follow DAG signaling at the IS of primary T lymphocytes, confirming a decreased recruitment in SAP-deficient cells which is fully rescued by DGKα silencing or inhibition (**Fig. 5a-h**). Accordingly, the TCR-induced activation of ERK1/2 kinases is reduced in SAP absence but fully rescued by DGKα silencing or inhibition (**Fig. 6a,b**).

Both PKCθ and RasGRP1 were previously implicated in apoptosis induced by the activation of the TCR [140, 141]. Therefore, we tested whether DGKα silencing might induce rescue of RICD in SAP deficient cells by reestablish PKCθ and RasGRP1 pathways. Indeed, we found that both PKCθ and RasGRP1-specific siRNA decreased the RICD in control cells without affecting the residual RICD of SAP-deficient cells, while blunted the rescue of RICD promoted by DGKα silencing (**Fig. 10a,b**). Similar results were obtained when we used inhibitors of the DAG-dependent effectors PKCs and MEK/ERK, confirming the relevance of those pathways downstream to DGKα silencing (**Fig. 10c,d**). Those results indicate that the residual RICD in SAP-deficient cells is not mediated by DAG signaling, while the rescue of cell death mediated by DGKα silencing in those cells is completely dependent on DAG signaling at the IS (**Fig.10**).

To investigate to what extent the potentiation of DAG signaling restores the TCR signaling levels required to initiating the RICD, we evaluated a set of TCR-responsive genes involved in the control of the cell death.

We found that DGKα silencing or inhibition in control cells do not altered TCR-induced exposure of IL-2 receptor (CD25), nor the expression of pro-apoptotic genes such as FASL, BIM, Nur77 or Nor1, while potently enhanced IL-2 expression (**Fig.6** and **Fig.7**), in line with published data [8, 123]. Conversely, SAP-deficient cells present a reduced TCR signaling strength with decreased expression of IL-2, CD25 and pro apoptotic proteins (**Fig. 6** and **7**), as previously demonstrated in [68, 90, 116, 135].

Surprisingly, among them, DGKα knockdown selectively rescued IL-2 expression, CD25 membrane exposure, Nur77 and Nor1 expression in SAP-deficient cells (**Fig.6, Fig.7g-j**), while the expression of FASL and BIM, as well as sFASL secretion, remain low and not responsive to TCR triggering (**Fig.7a-f**). This selectivity may reflect the inability of DGKα inhibition to compensate for the reduced LCK recruitment and activation to the NTB-A receptor in SAP absence [96], which is responsible for the decreased FASL and BIM expression in SAP-deficient cells [96].

Our results also suggest that DGKα silencing rescues cell death in SAP deficient cells by promoting FASL and BIM independent pathways. Therefore, we turned our attention on Nur77 and Nor1, as

those two orphan nuclear receptors are known mediators of apoptosis in T cells [34-36, 139, 148]. Moreover, their pro-apoptotic activity is promoted by RSK-mediated phosphorylation downstream to the MAPK pathway [33, 34]. Upon phosphorylation, Nur77 binds Bcl-2, which acquires pro-apoptotic functions [35]. This signaling pathway is taking place upon DGKα silencing in SAP-deficient cells as in those cells we noted a strong increase of Nur77 protein and phosphorylation as compared to both control and SAP-deficient cells (**Fig. 7k,l** and **Fig. 11a**). Strikingly, the RSK-specific inhibitor SL0101-1 completely abolishes apoptosis in double SAP/DGKα-deficient cells, thus demonstrating the key role of the kinase in mediating the DGKα KD effects on the RICD process (**Fig. 10e,f**). Furthermore, Nur77/Nor1 double knockdown had a minimal effect on RICD of control cells, while reduces the R59949-mediated boost of cell death in XLP1 patient derived cells (**Fig. 11b**). These results demonstrate that by inhibiting DGKα we potentiate the MAPK pathway leading to Nur77/Nor1 induction and phosphorylation, which contributes to the RICD onset. However, other DAG-dependent signaling pathways possibly contribute to cell death in those cells, as the effects obtained by silencing Nur77/Nor1 are relatively small when compared to RSK inhibition (**Fig. 10e,f** and **Fig. 11b**).

By collaborating with K. E. Nichols, we tested the efficacy of the R59022 DGK inhibitor in a mouse model of XLP1. In this model, SAP KO mice are infected by Lymphocytic Choriomeningitis virus Armstrong (LCMV), which induces hepatosplenomegaly and potent CD8+ T cell activation [127, 145, 149]. Following LCMV infection, SAP KO mice developed significant hepatosplenomegaly when compared to uninfected mice (**Fig. 12a,b**). This organomegaly was associated with a marked expansion in the absolute number of total ($CD8^+$), activated ($CD8^+CD44^+$) and LCMV-specific ($CD8^+CD44^+gp33^+$) T lymphocytes in both spleen and liver (**Fig. 12e,g**). We then tested the efficacy of DGKα inhibition in the reduction of the CD8+ expansion by adopting a "curative" protocol, in which SAP KO mice were infected with LCMV and after 4 days treated with twice-daily intraperitoneal injections of R59022 (2mg/kg body weight). We selected this inhibitor and the current dosage as it has been previously reported to inhibit DGKα activity *in vivo* without inducing significant toxicity [150]. Compared to LCMV-infected untreated SAP KO mice, R59022-treated mice had smaller spleens (**Fig. 12a**). Moreover, both spleens and livers contained significantly fewer lymphocytes (**Fig. 12a,b**). The decrease was due to a reduction of the number of activated and LCMV-specific CD8+ lymphocytes (**Fig. 12e,g**).

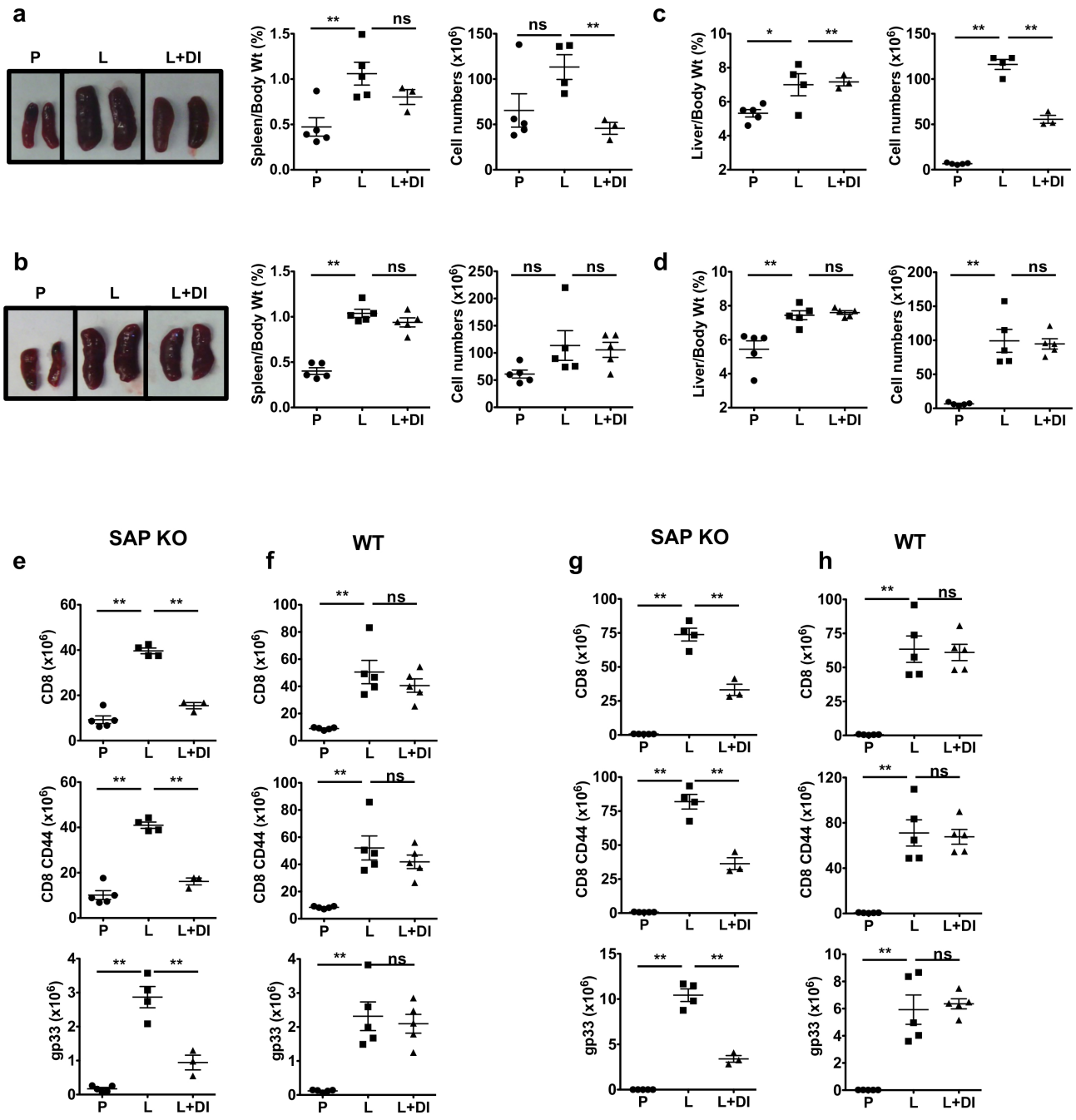

Figure 12. The DGK inhibitor R59022 reduces the numbers of activated LCMV-specific CD8+T cells in LCMV-infected SAP KO mice. Representative images, ratio over body weight, and total splenocytes count of spleen from SAP KO (**a**) and WT (**b**) mice injected with PBS (P) or LCMV, without (L) or with R59022 treatment (L+DI). Ratio over body weight and total intra-hepatic lymphocyte count of liver from SAP KO (**c**) and WT (**d**) mice injected with PBS (P) or LCMV, without (L) or with R59022 treatment (L+DI). (**e-f**) Absolute number of CD8+, CD8+CD44+ and CD8+CD44+gp33+ cells in the spleens of PBS (P), LCMV (L) and LCMV+ R59022 (L+DI) treated SAP KO (**e**) or WT mice (**f**). (**g-h**) Absolute number of CD8+, CD8+CD44+ and CD8+CD44+gp33+ cells in the liver of PBS (P), LCMV (L) and LCMV+ R59022 (L+DI) treated SAP KO (**g**) or WT mice (**h**).

Data are from 1 of 2 experiments in which a total of 6-10 mice in each cohort was examined. Error bars represent SD. Statistical significance was determined by unpaired two-tail t-test. * $P < 0.05$, ** $P < 0.001$, ns: not significant.

To assess whether DGKα inhibition influenced CD8+ cytokine production and effector functions, we performed *in vitro* stimulation experiments using splenic T cells isolated from control, LCMV-infected, and LCMV infected but R59022 treated SAP KO mice. In these assays, splenocytes were cultured directly *ex vivo* with the MHC class I restricted LCMV peptide gp33. Five hours later, cells were harvested and analyzed for intracellular TNFα and IFNγ and for expression of CD107, a marker of degranulation commonly used as a surrogate for cytolytic potential. Interestingly, we observed a significant reduction in the absolute number of TNFα+, IFNγ+ and CD107+ CD8+ T cells (**Fig. 13a**). In agreement with the reduction of the absolute number of IFNγ-producing cells, we found significant lower serum IFNγ levels in the R59022 treated mice (**Fig. 13b**) and a reduced number and size of lymphocytic infiltrates within the livers (**Fig. 13e,f**). Taken together, these data indicate that the pharmacologic inhibition of DGKα *in vivo* reduces virus-induced $CD8^+$ T cell expansion, spleen enlargement, liver infiltration and the cytokine storm that characterize this pathology. The first phase of LCMV-induced illness is similar in WT mice, but R59022 treatment had minimal to no effect on CD8+ expansion (**Fig. 12b,d,f,h**), cytokine production (**Fig. 13c,d**) or liver infiltration (**Fig. 13g,h**) indicating that R59022 is not impairing immune response to LCMV. These results are consistent with a recent work of Shin and colleagues that elegantly demonstrated that CD8+ T cells from DGKα KO mice infected with LCMV do not show enhanced expansion compared to T cells from WT mice. [151]. We consider that those data are in line with our observation that DGKα inhibition or silencing did not affect apoptosis of SAP-sufficient cells (**Fig. 8**), and reflect the physiological inhibition exerted by SAP on DGKα.

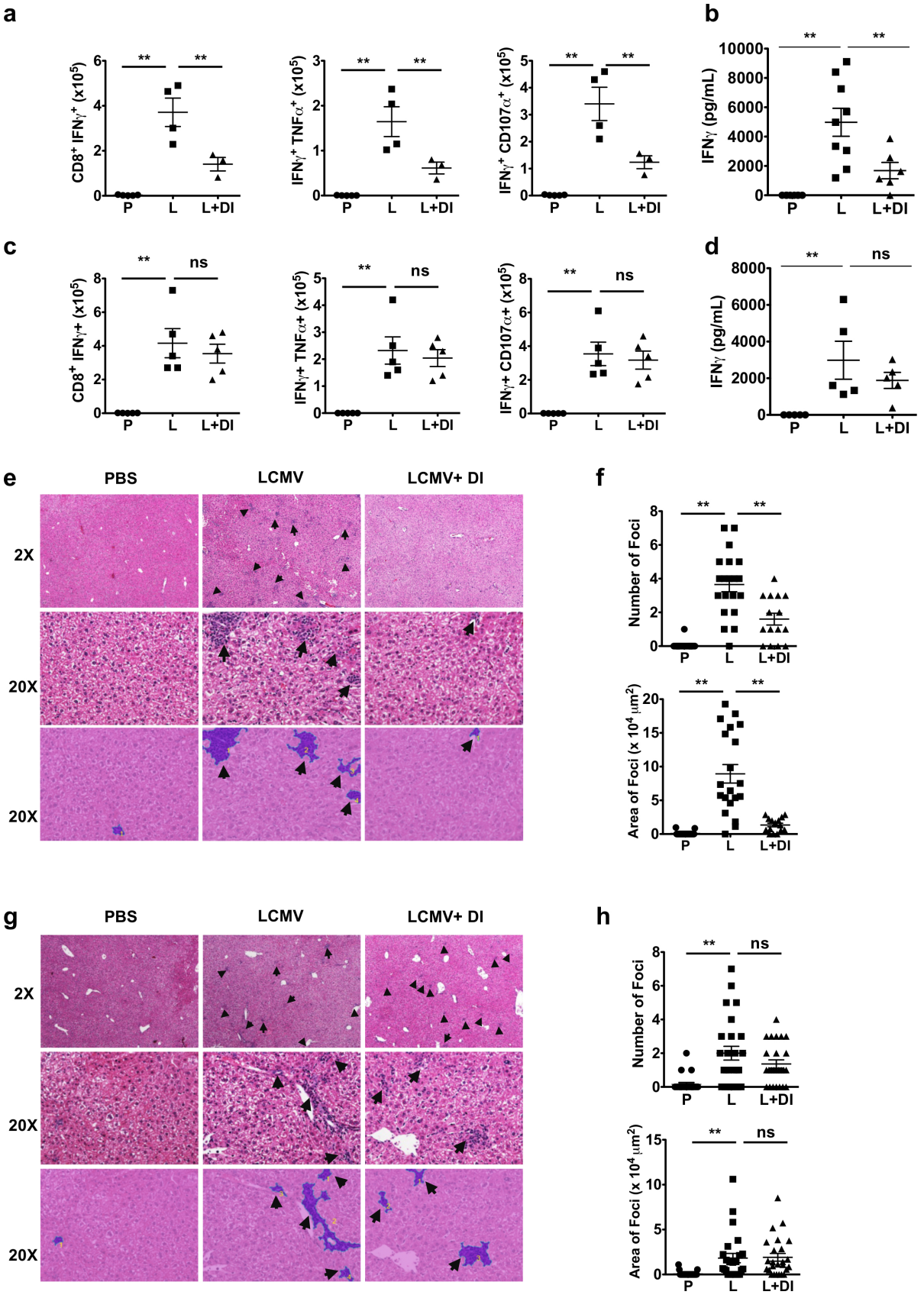

Figure 13. The DGK inhibitor R59022 reduces the number of virus-specific activated CD8+ cytokine producing cells in the spleens of LCMV-infected SAP KO mice.

2×10^6 splenocytes were left unstimulated or stimulated with 0.4 ng/mL gp33 peptide, in the presence of 1000 µg/mL monensin for 5 hours and analyzed for intracellular cytokines production and degranulation. Absolute number of

CD8+IFNγ+, IFNγ+TNFα+ and IFNγ+CD107α+ cells from SAP KO (**a**) and WT mice (**b**). Error bars represent SD. Statistical significance was determined by unpaired two-tail t-test. * P < 0.05, ** P < 0.001, ns: not significant. (**c-d**) Serum IFNγ levels from SAP KO (**c**) and WT (**d**) mice were assayed on day 8 post-infection by ELISA. Data are compiled from 2 experiments, n= 6-10. Error bars represent SEM. Statistical significance was determined by unpaired two-tail t-test. ** P < 0.001, ns: not significant. (**e-f**) Histology of livers from representative SAP KO (**e**) and WT (**f**) mice under low (top row, 2X) and high (middle row, 20X) power magnification. Arrows point to inflammatory foci (top) and a representative inflammatory focus (middle row). (**g-h**) Histological sections were analyzed for the number and area of the inflammatory foci in each group of SAP KO (**g**) or WT (**h**) mice. Micrographs in the bottom row are the respective analyzed images shown in the middle row. Statistical significance was determined by unpaired two-tail t-test. * P < 0.05, ** P < 0.001, ns: not significant.

Altogether, these findings suggest that the reduction of CD8+ expansion in R59022-treated SAP KO mice might be due to the reestablishment of the T cell apoptosis, since also splenocytes from SAP KO mice display a RICD defect which is rescued in vitro by DGKα inhibition (data not shown).

This work is the result of an international collaboration aimed to verify the relevance of SAP-mediated DGKα inhibition in the regulation of TCR signaling strength. In this study we provide evidence that in SAP-deficient T cells the IS morphology is altered and the TCR signaling strength is reduced by excessive DGKα activity, leading to a defective restimulation-induced cell death.

Collectively, with our *in vitro* results we characterized a crucial signaling pathway that leads to RICD, providing new insights in understanding this complex process, which is initiated with DAG accumulation and, through PKCθ and RasGRP1, terminates with the RSK activation and Nur77 phosphorylation.

Notably, with the *in vivo* data we identified the inhibition of DGKα as a promising approach to reduce the life-threatening hyperproliferation of the T lymphocytes that occurs during the acute phase of EBV infection in XLP1 patients. Also, the same strategy might be used for the treatment of other diseases, which, as XLP1, exhibit an increased signal strength threshold required for undergo apoptosis, such as ITK deficiency [152, 153].

Appendix

During my PhD fellowship, I have been involved in other two projects, which have been published in two international journals.

Particularly, the first project (Rainero *et al.*, 2014) was meant to elucidate the mechanism of the SDF-1α-induced matrix invasion of the invasive carcinoma breast line MDA-MB-231. We based this work on previous publication in which we demonstrated that, in epithelial cells, DGKα activity promotes cytoskeletal remodeling and matrix invasion by recruiting atypical PKCs at ruffling sites [154] and by promoting RCP-mediated recycling of α5β1 integrin to the tip of pseudopods [155].

Here, we found that DGKα is activated and translocates to the cell protrusion in response to SDF-1α stimulation, thus promoting Rac and PKCs-mediated elongation of protrusion, MMP-9 metalloproteinase secretion, matrix invasion and cell elongation. Phosphatidic acid generated by DGKα at the cell protrusion was able to recruit atypical PKCs, which in turn was responsible for the recruitment of β1 integrin and MMP-9 to the cell tip. Finally, we demonstrated that the DGKα/atypical PKCs/β1 integrin axis is required for MDA-MB-231 cells matrix invasion.

I enthusiastically contributed to this work by generating the inducible MDA-MB-231 shDGKα cell line and the MDA-MB-231 OST-tagged DGKα cell line. Also, I've designed and carried out the experiments performed with both the inducible cell lines, which were used for the localization of DGKα, for the invasion, migration and wound healing experiments, and for the evaluation of DGKα, atypical PKCs, Rac and β1 integrin contribution to the protrusion elongation of the cells.

The second project came from collaboration with the Immunology group led by Prof. Umberto Dianzani (Dianzani *et al.*, 2014). The work was based on the observations that a soluble form of ICOS (ICOS-Fc) inhibits the adhesion of different tumor cells lines to HUVECs expressing B7h, the ICOS ligand, suggesting that may act as an anti-tumoral agent by preventing metastatic dissemination. Here, we performed migration assays to evaluate the efficacy of ICOS-Fc in inhibiting cell migration on a number of different cell lines. ICOS-Fc specifically inhibited the migration of HUVECs, human dermal lymphatic ECs, and the HT29, HCT116, PC-3, HepG2, JR8, and M14 tumor cell lines expressing high levels of B7h, whereas it was ineffective in the RPMI7932, PCF-2, LM, and BHT-101 cell lines expressing low levels of B7h. Moreover, ICOS-Fc was able to prevent the epithelial-mesenchimal transition induced by HGF treatment of Hep-G2 cells, but not

in low B7h BHT-101 cells. Those effects of ICOS-Fc on both HUVECs and tumor cell lines were shown to be dependent on the dowmodulation of FAK phosphorylation and β-PIX expression.

Finally, treatment with ICOS-Fc inhibited the development of lung metastases upon injection of NOD-SCID-IL2Rγnull mice with CF-PAC1 cells, as well as C57BL/6 mice with B16-F10 cells. Therefore, the B7h-ICOS interaction may modulate the spread of cancer metastases, which suggests the novel use of ICOS-Fc as an immunomodulatory drug. However, in the B16-F10–metastasized lungs, ICOS-Fc also increased IL-17A/RORc and decreased IL-10/Foxp3 expression, which indicates that it also exerts positive effects on the antitumor immune response.

My contribution to this project was to perform the morphological and scatter experiments in response to hepatocytes growth factor stimulation on different cancer cells types, with the aim to evaluate the antitumoral effects of ICOS-Fc.

OPEN ACCESS Freely available online

PLOS ONE

The Diacylglycerol Kinase α/Atypical PKC/β1 Integrin Pathway in SDF-1α Mammary Carcinoma Invasiveness

Elena Rainero[1], Cristina Cianflone[2], Paolo Ettore Porporato[2¤b], Federica Chianale[2¤a], Valeria Malacarne[2], Valentina Bettio[2], Elisa Ruffo[2], Michele Ferrara[2], Fabio Benecchia[2], Daniela Capello[2], Wolfgang Paster[3], Irene Locatelli[2¤c], Alessandra Bertoni[2], Nicoletta Filigheddu[2], Fabiola Sinigaglia[2], Jim C. Norman[1], Gianluca Baldanzi[1]*, Andrea Graziani[1]

1 Integrin Biology Laboratory, Beatson Institute for Cancer Research, Glasgow, Scotland, United Kingdom, **2** Department of Translational Medicine, Università del Piemonte Orientale, Novara, Italy, **3** Sir William Dunn School of Pathology, University of Oxford, Oxford, United Kingdom

Abstract

Diacylglycerol kinase α (DGKα), by phosphorylating diacylglycerol into phosphatidic acid, provides a key signal driving cell migration and matrix invasion. We previously demonstrated that in epithelial cells activation of DGKα activity promotes cytoskeletal remodeling and matrix invasion by recruiting atypical PKC at ruffling sites and by promoting RCP-mediated recycling of α5β1 integrin to the tip of pseudopods. In here we investigate the signaling pathway by which DGKα mediates SDF-1α-induced matrix invasion of MDA-MB-231 invasive breast carcinoma cells. Indeed we showed that, following SDF-1α stimulation, DGKα is activated and localized at cell protrusion, thus promoting their elongation and mediating SDF-1α induced MMP-9 metalloproteinase secretion and matrix invasion. Phosphatidic acid generated by DGKα promotes localization at cell protrusions of atypical PKCs which play an essential role downstream of DGKα by promoting Rac-mediated protrusion elongation and localized recruitment of β1 integrin and MMP-9. We finally demonstrate that activation of DGKα, atypical PKCs signaling and β1 integrin are all essential for MDA-MB-231 invasiveness. These data indicates the existence of a SDF-1α induced DGKα - atypical PKC - β1 integrin signaling pathway, which is essential for matrix invasion of carcinoma cells.

Citation: Rainero E, Cianflone C, Porporato PE, Chianale F, Malacarne V, et al. (2014) The Diacylglycerol Kinase α/Atypical PKC/β1 Integrin Pathway in SDF-1α Mammary Carcinoma Invasiveness. PLoS ONE 9(6): e97144. doi:10.1371/journal.pone.0097144

Editor: Donald Gullberg, University of Bergen, Norway

Received November 27, 2013; **Accepted** April 15, 2014; **Published** June 2, 2014

Funding: This work was supported by: AIRC, Italian Association for Cancer Research, (IG 13524 and IG 5392 grants) www.airc.it, and CARIPLO Foundation (2010-0737 grant) www.fondazionecariplo.it. CC was supported by a mobility grant of CIB, Consorzio Interuniversitario Biotecnologie www.cibiotech.it. GB was supported by EMBO (short term fellowships) www.embo.org and University Piemonte Orientale (Young Investigators) www.unipmn.it. VM was supported by Compagnia di San Paolo www.compagnia.torino.it/. DC was supported by Fondo Di Solidarieta' Edo Tempia Valenta Per Lotta Contro I Tumori www.fondoedotempia.it. The funders had no role in study design, data collection and analysis, decision to publish, or preparation of the manuscript.

Competing Interests: The authors have declared that no competing interests exist.

* E-mail: gianluca.baldanzi@med.unipmn.it

¤a Current address: Physical Biology of the Cancer Cell, IRCC Institute for Cancer Research and Treatment, Candiolo, Turin, Italy
¤b Current address: Unit of Pharmacology & Therapeutics, Angiogenesis and Cancer Research Group, University of Louvain Medical School, Brussels, Belgium
¤c Current address: Department of Health Sciences, Università del Piemonte Orientale, Novara, Italy

Introduction

Most cancer-associated mortality is caused by metastatic dissemination of primary tumors and the outgrowth of secondary tumors at distant sites. Among the microenvironment signals sustaining the invasive phenotype of cancer cells, stromal cell-derived factor-1α (SDF-1α, also named CXCL12), plays a major role in promoting cancer metastasis in several cancers, including breast cancer [1]. SDF-1α is a chemokine secreted by tumor-associated fibroblasts and bone marrow stromal cells, which through activation of its CXCR4 receptor, promotes migration and invasion of malignant cells and their homing to target organs [2,3]. Indeed CXCR4 is a poor prognosis predictor in several cancer types [4].

In breast cancer, the chemotactic and invasive activity of SDF-1α/CXCR4 is mediated by both $G\alpha_{13}$-mediated activation of RhoA and Gαi-mediated activation of Rac1 via DOCK180/ELMO, which regulate cytoskeletal remodeling [5,6]. In myeloid cells, Rac1 mediates SDF-1α-induced increase of integrin affinity, while RhoA mediates formation of membrane protrusions and CXCR4 trafficking to the cell surface in Rab11+ endosomes [7,8]. Moreover, in gastric cancer cells SDF-1α invasive and proliferative activity is also stimulated by Gαi- and PI3Kβ-mediated activation of mTOR complex 1, which contributes to Rac1 activation as well [9]. Finally, atypical protein kinases C (PKCζ and ι, hereafter aPKCs), which do not bind diacylglycerol (DG), play a key role in mediating chemotaxis of bone marrow and muscle stem cells, and of lymphocytes [10,11]. However neither the mechanisms by which SDF-1α stimulates aPKCs nor their role in SDF-1α invasive signaling in breast cancer cells have been elucidated.

DGKs are a multigenic family of ten enzymes phosphorylating DG to generate phosphatidic acid (PA), thus reciprocally regulating in a highly compartmentalized manner the concentration of both lipid second messengers and their signaling activities [12]. Indeed, activation of DGKs results in the termination of DG-mediated signals, while triggering PA-mediated ones. Increasing evidence points to DGKα as a critical node in oncogenic signaling

and as a putative novel therapeutic target in cancer: inhibition or silencing of DGKα has been shown to reduce tumor growth and mortality in glioblastoma and hepatic carcinoma xenograft models [13,14]. Moreover, we recently showed that DGKα activity sustains the pro-invasive activity of metastatic p53 mutations, by promoting the recycling of α5β1 integrin to the tip of invasive protrusions in tridimensional matrix [15]. DGKα is activated and recruited to the membrane by growth factors, estrogen and tyrosine kinase oncogenes through Src-mediated phosphorylation. Upon growth factor stimulation, activation of DGKα mediates cell migration, invasion and anchorage-independent growth [16–21]. Indeed, activation of DGKα is a central element of a novel lipid signaling pathway involving PA-mediated recruitment at the plasma membrane and activation of aPKCs in a complex with RhoGDI and Rac1, thus providing a positional signal regulating Rac1 activation and association to the membrane [22,23].

Altogether these data suggest that DGKα and aPKCs may act as signaling nodes in the molecular crosstalk between soluble chemotactic factors and the extracellular matrix, thus prompting us to investigate the involvement of DGKα in cell migration and invasion induced by SDF-1α in breast cancer cells. In here we show that upon SDF-1α stimulation of breast cancer cells, DGKα activity mediates aPKCs localization at protrusion sites and the subsequent recruitment of β1 integrin and MMP-9 secretion. Conversely over-expression of DGKα is sufficient to induce aPKCs-dependent cell elongation. Finally, we observed that the DGKα – aPKCs – β1 integrin pathway is an essential mediator of chemokine-promoted cell migration and matrix invasion.

Materials and Methods

Cells Culture and Reagents

MDA-MB-231 cells were from ATCC, 293FT were from Life Technologies. Cells were cultured in DMEM (Life Technologies) with 10% FCS (LONZA) and antibiotics/antimycotics (Sigma-Aldrich) in humidified atmosphere 5% CO_2 at 37°C.

R59949 (Sigma-Aldrich) was dissolved in DMSO; equal amounts of DMSO were used in the control samples. All reagents are from Sigma-Aldrich apart: matrigel growth factor reduced (BD Bioscences), human recombinant SDF-1α and HGF (Peprotech), Myr-PKCζ/ι peptide inhibitor (BIOMOL) and NSC23766 (Tokris bioscience).

Antibodies: myc (clone 9E10 Santa Cruz), MMP-9 (2C3 Santa Cruz for western blotting and immunofluorescence or IC9111F RDsystems); PKCζ/ι (P0713 Sigma); β1 integrin (cat. 610467 BD Transduction Laboratories for western blotting and immunofluorescence or BV7 Abcam for cytofluorimetry); StrepMab-tag II (2-1507-001 IBA); actin (C-2 Santa Cruz); tubulin (DM1A Sigma-Aldrich); DGKα (Shaap et al., 1993), human RCP (rabbit in-house Ab raised against RCP residues 379–649); Cdc42 (2462 Cell signaling). Secondary antibodies HRP-mouse and HRP-rabbit were from Perkin Elmer. Secondary antibodies anti-rabbit Ig Alexa Flour-488 and anti-mouse Ig Alexa Flour-488 were from Life Technologies as well as Alexa Flour 546-phalloidin, TO-PRO-3 is from Life Technologies.

Invasion Assay

Invasion assay were performed in BD BioCoat Matrigel Chambers. 50,000 cells/well were plated in the upper chamber whereas SDF-1α (100 ng/ml) or 10% FCS were added to the lower chamber in serum free medium. After 22 hours of incubation in a humidified atmosphere 5% CO_2 at 37°C, non invading cells were removed from the upper surface of the membrane and invading cells were fixed and stained with Diff-Quik (Medion Diagnostic) before counting.

Wound Healing Assay

Cells were grown to confluence in 12 wells plates and the monolayer wounded with a pipet tip. Cell debris were removed and monolayer maintained in serum free medium for 24 hours with or without HGF (50 ng/ml). The cells were stained with Diff-Quik (Medion Diagnostic) and for each experimental point 8 fields photographed (Axiovert inverted microscope with a 4x objective and a digital camera). Cells migrating inside 2.3 mm of wound were counted.

DGKα Activation Assay

Cells homogenates were prepared by collecting the cells with a rubber scraper in buffer B (25 mM Hepes (pH 8), 10% glycerol, 150 mM NaCl, 5 mM EDTA, 2 mM EGTA, 1 mM ZnCl2, 50 mM ammonium molibdate, 10 mM NaF, 1 mM sodium orthovanadate and Protease Inhibitor Cocktail), homogenizing them with a 23 G syringe and by spinning at 500 g for 15 min. Protein concentration was determined by the bicinchoninic acid method (Pierce) and equalized for each point with buffer.

DGKα activity in cell homogenates (25 μl) was assayed by measuring initial velocities (5 min at 30°C) in presence of saturating substrates concentration (1 mg/ml diolein, 5 mM ATP, 3 μCi/ml γ^{32}P-ATP (Perkin Elmer), 10 mM MgCl2, 1 mM ZnCl2, 1 mM EGTA in 25 mM Hepes pH 8, final reaction volume 50 ml). Reaction was terminated with 0.1 M HCl and lipids were extracted with cloroform methanol (1:1). PA was separated by TLC in chloroform:methanol:water:25% ammonium hydroxide (60:47:11:4). ^{32}P-PA was identified by co-migration with PA standards stained by incubation in iodine chamber. Radioactive signals were detected and quantified by Molecular Imager (Bio-Rad).

Immunofluorescence

Cells (30,000/well) were plated on matrigel coated coverlips in 24 wells cell culture plate and serum deprived for 16–24 hours before stimulation. After stimulation cells were washed with PBS, fixed in PBS containing 3% paraformaldehyde and 4% sucrose and permeabilized in cold Hepes-Triton buffer (20 mM Hepes, 300 mM sucrose, 50 mM NaCl, 3 mM MgCl2, 0.5% Triton X-100, pH 7.4). PBS containing 2% BSA was used as blocking reagent for 15 minutes and as diluting agent for primary and secondary antibodies (incubated for at least 1 hour). Intermediate washing was performed with PBS containing 0.2% BSA.

Antibodies were added directly onto each glass coverslip in a humidified chamber. Finally, each glass coverslip was washed briefly in water and mounted onto a glass microscope slide using Mowiol (20% Mowiol 4–88, 2.5% 1, 4-diazabicyclo [2.2.2] octane in PBS, pH 7.4).

Confocal images were acquired with Leica confocal microscope TCS SP2 using a 63x objective, NA = 1.32, equipped with LCS Leica confocal software. Basal planes are shown. Each experimental point was performed in duplicate. Depending on preparation quality in each replicate roughly 30 images were taken, containing between 70 and 100 cells.

Morphometry

For cell length analysis cells were plated in 24 wells plates and phase contrast images of live cell were acquired with an Axiovert inverted microscope equipped with a 40x objective and a digital camera (Carl-Zeiss) and total cell length was measured with

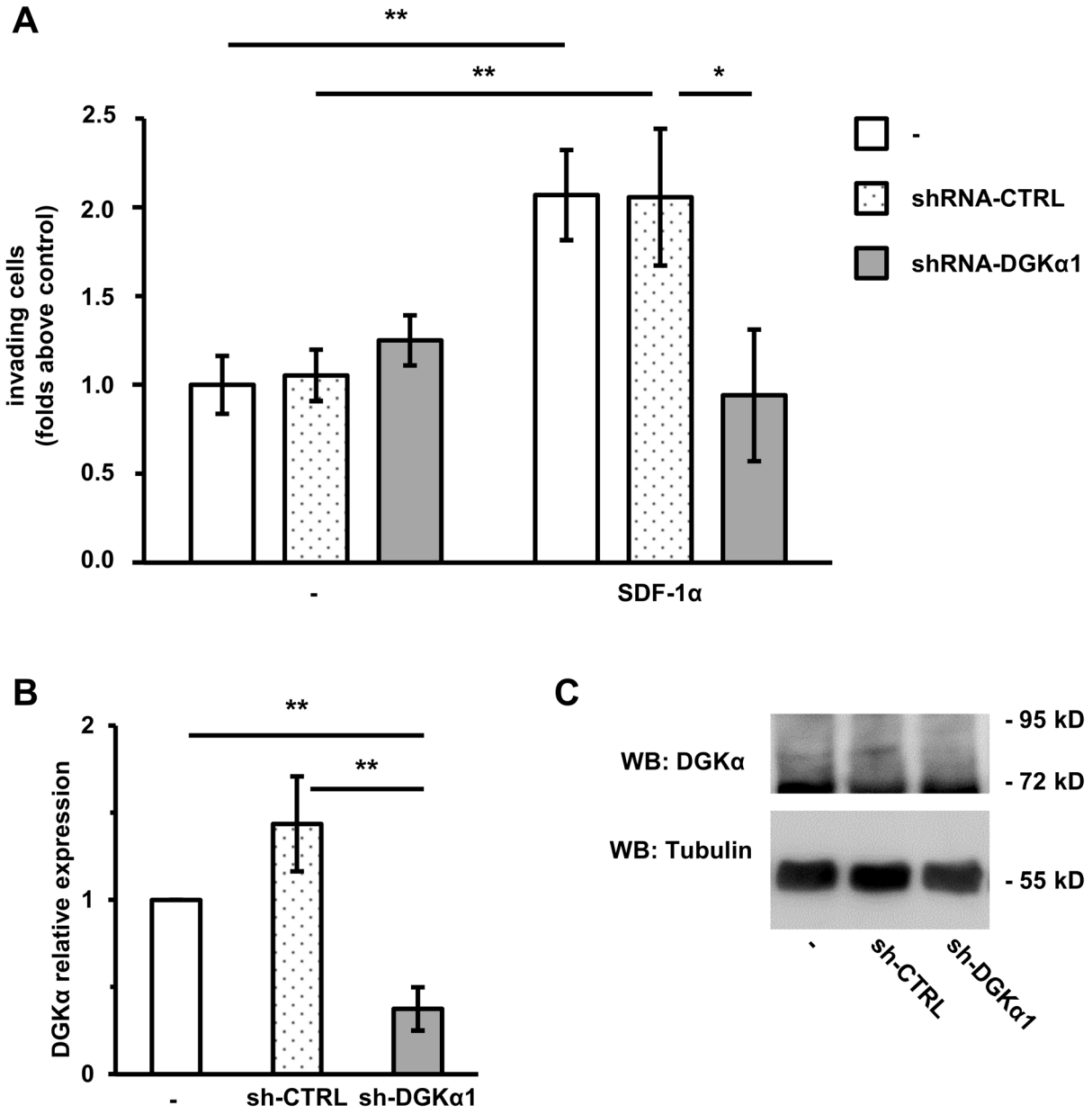

Figure 1. DGKα is necessary for SDF-1α-induced cell invasion. MDA-MB-231 cells were infected with lentiviral vectors expressing an inducible shRNA against DGKα (shRNA-DGKα1) or an inducible control shRNA (shRNA-CTRL). Parental and infected cells were treated with 1 μg/ml doxycycline for 72 hours to promote shRNA transcription. A) 50,000 cells were plated on matrigel invasion chamber and incubated for 24 hours in presence or in absence of SDF-1α (100 ng/ml). Histogram reports mean ± SE of fold over control values from 3 independent experiments with *t-test $p<0.05$, **t-test $p<0.01$. B) The efficiency of DGKα down–regulation by shRNA was verified by quantitative RT-PCR. **t-test $p<0.01$. A) Cells were lysed and the efficiency of DGKα down–regulation by shRNA was verified by western blot, tubulin was used as a loading control.
doi:10.1371/journal.pone.0097144.g001

Image-Pro Plus software (MediaCybernetics). Alternatively in Fig. 6D and Fig. S5B we used a 10x Plan Fluor objective, NA 0.3, and an inverted microscope (TE200; Nikon) with a digital camera (CoolSNAP HQ; Photometrics) and Metamorph software (Molecular Devices). For each experimental condition 5 random fields were photographed containing more than 100 cells.

Cytofluorimetry

Cells were detached with ice could PBS 4 mM EDTA, fixed with PBS containing 3% paraformaldehyde and stained as indicated for 30 min. After washing with PBS containing 0.2% BSA cells were analyzed with a FACScalibur instrument an CellQuest software (BD) or Flowing software (Turku Bioimaging).

siRNA for Transient Silencing

Transient silencing was obtained by transfection of siRNA (Sigma Genosys or Life Technologies). Briefly were plated on matrigel coated coverlips to 30–50% confluence the day before transfection and transfected using lipofectamine 2000 (Life Technologies) according to manufacturer's instructions. The day after transfection cells were serum deprived for further 18 hours before immunofluorescences or western blotting.

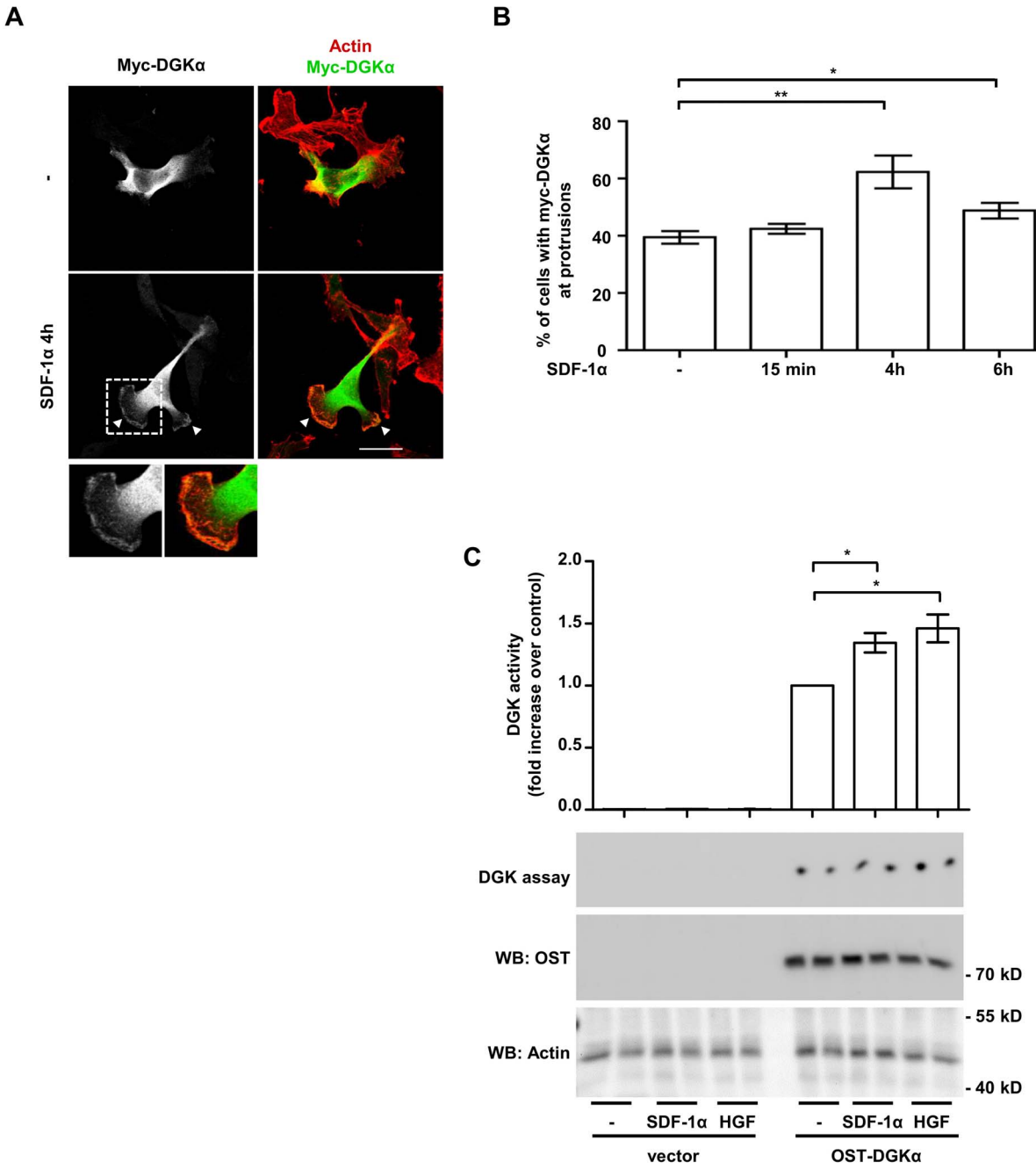

Figure 2. SDF-1α stimulates DGKα activity and localization at protrusions site. A) MDA-MB-231 cells, stably expressing myc-DGKα, were plated on matrigel-coated coverslips for 20 hours in FCS containing medium and cultured for further 20 hours in serum free medium. Cells were then stimulated with 50 ng/ml of SDF-1α for the indicated times, fixed and stained for actin (red) and myc-DGKα (green). Representative images at 4 hours after stimulation. Arrowheads indicate DGKα at protrusions. Histogram (B) reports the percentage of cells displaying myc-DGKα at protrusion as mean ± SE of 5 independent experiments, *t-test $p<0.05$, **t-test $p<0.005$. Scale bar 24 μm. C) MDA-MB-231 cells were infected with a lentiviral vector expressing inducible OST-tagged DGKα or an empty vector. To induce DGKα expression, cells were treated overnight with doxycycline (1 μg/ml) in serum free medium. Cell were homogenized with buffer B in absence of detergent and analysed for DGK activity (upper panel). Values are mean ± SE of 4 independent experiments with *t-test $p<0.05$. OST-DGKα and actin protein expression was verified by anti-OST and anti-actin western blot (lower panel).
doi:10.1371/journal.pone.0097144.g002

Validated siRNA DGKα [17] sense 5′ GGAUGGCGAGAUGGCUAAAtt 3′ antisense 5′UUUAGCCAUCUCGCCAUCCgg 3′.

siRNA PKCζ sense 5′CGUUCGACAUCAUCACCGAtt3′antisense 5′UCGGUGAUGAUGUCGAACGgg3′.

siRNA PKCι sense 5′CGUUCGACAUCAUCACCGAtt3′ antisense 5′UCGGUGAUGAUGUCGAACGgg3′.

siRNA β1 integrin sense 5′GGAGGAAUGUUACACGGCU3′ antisense 5′ AGCCGUGUAACAUUCCUCCag 3′.

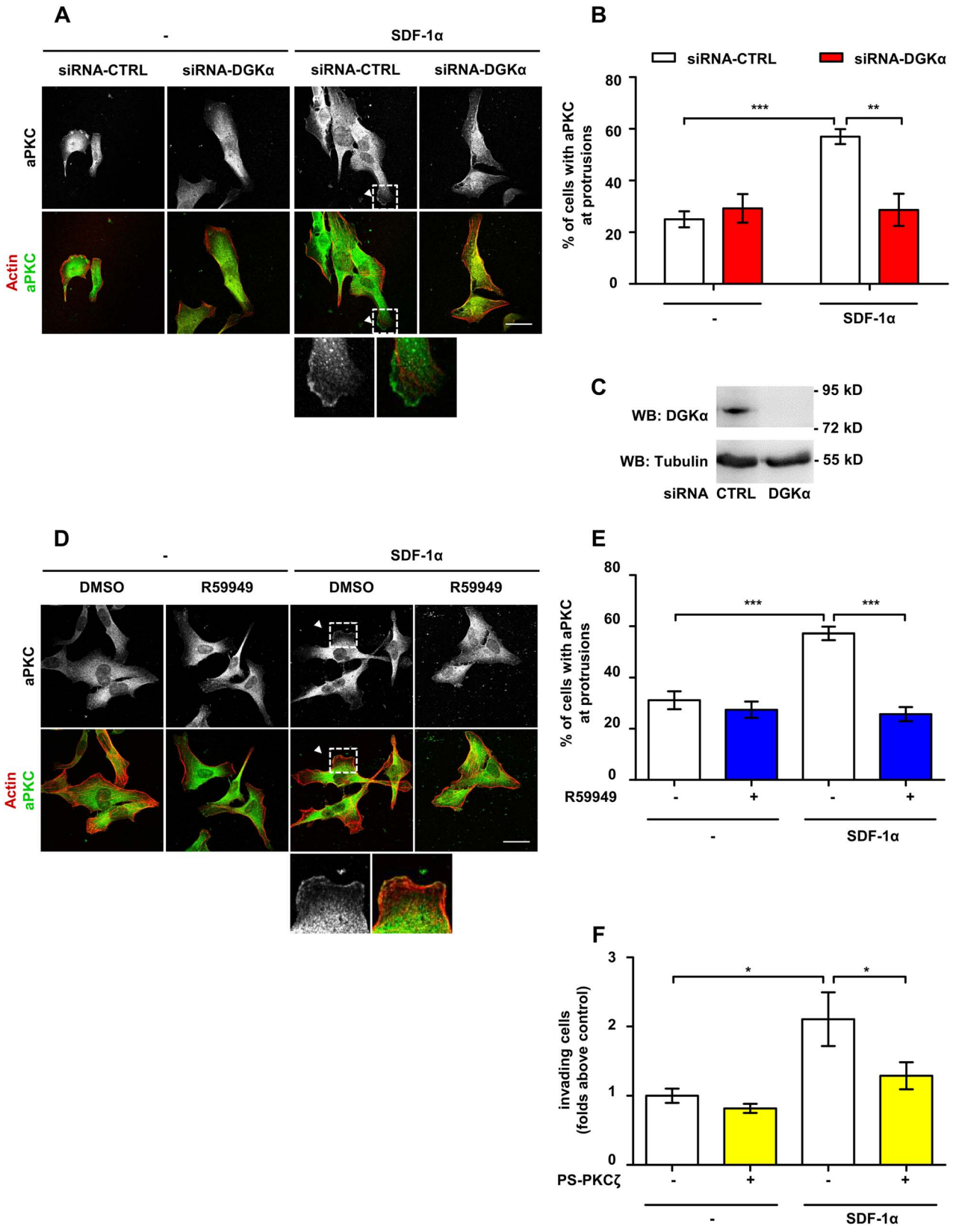

Figure 3. DGKα mediates SDF-1α-induced cell invasion by regulating aPKCs recruitment to cell pseudopods. A) MDA-MB-231 cells were plated on matrigel-coated coverslips for 20 hours in FCS containing medium, transfected with CTRL or DGKα –specific siRNA and cultured for further 20 hours in serum free medium. Cells were then stimulated for 6 hours with 50 ng/ml SDF-1α, fixed, and stained for actin (red) and aPKCs (green). Arrowhead indicates aPKCs at protrusions. Scale bar 24 μm. B) Histogram reports the percentage of cells displaying aPKCs at protrusions as mean ± SE of 3 independent experiments with **t-test $p<0.005$, ***t-test $p<0.0005$. C) MDA-MB-231 cells were transfected with CTRL or DGKα –

specific siRNA and lysed. The efficiency of DGKα down–regulation by siRNA was verified at 48 hours after transfection by western blot, tubulin was used as loading control. D) MDA-MB-231 cells were plated on matrigel-coated coverslips for 20 hours in FCS containing medium and cultured for further 20 hours in serum free medium. Cells were then stimulated for 6 hours with 50 ng/ml SDF-1α, in presence or in absence of 1 μM R59949, fixed and stained for actin (red) and aPKCs (green). Arrowheads indicate aPKCs at protrusions. Scale bar 24 μm. E) Histogram reports the percentage of cells displaying aPKCs at protrusions as mean ± SE of 3 independent experiments with ***t-test $p<0.0005$. F) MDA-MB-231 cells (10^6/well) were plated on matrigel invasion chamber and stimulates for 24 hours with SDF-1α (50 ng/ml) in presence or absence of PKCζ pseudosubstrate (PS-PKCζ, 10 μM). Histogram reports mean ± SE of folds over control values from 3 independent experiments with *t-test $p<0.05$.
doi:10.1371/journal.pone.0097144.g003

siRNA RCP: ON-TARGETplus RAB11FIP1 siRNA L-015968-00-0005 (Dharmacon). Silencer negative control siRNA AM4611 (Life Technologies) was used as negative control.

Generation of Tet-inducible Strep-tagged DGKα Construct and Cell Infection

Human DGKα was amplified from pMT2- DGKα [24] by PCR using the primers DGKα_ScII_fw (5′-CCGCGGGCAGCATGGCCAAGGAGAGGGGC-3′) and DGKα_H3_rv (5′-AAGCTTTTAGCTCAAGAAGCCAAA-3′) and cloned into pEXPR-IBA-105 (IBA GmbH) via SacII and HindIII to generate pEXPR-Strep-DGKα. In a further step Strep-DGKα was amplified by PCR using primers IBA_fw_N1 (5′-GCGGCCGCAGACCCACCATGGCTAGC-3′) and 105DGKa_MluI_rv (5′-ACGCGTTTAGCTCAAGAAGCCAAA-3′) and cloned via NotI and MluI to pLVX-Tight-Puro (Clontech). All constructs were verified by DNA sequencing.

The resulting pLVX-Tight-PURO-OST-DGKα presents OST-DGKα after a tetracycline controlled promoter and was used with the Lenti-X Tet-On Advanced Inducible Expression System (Clontec) according to manufacturer's instruction. Lentiviral particles were obtained in 293FT packaging cells co-transfected with helper vectors. After double infection and selection we obtained a polyclonal population of MDA-MB-231 cells expressing OST-DGKα in a tetracycline inducible manner. A control cell line was also generated with an empty vector.

Generation of MDA-MB-231 Stably Expressing Myc-DGKa

Myc-DGKα was amplified from PMT2-myc-DGKα [16] by PCR using the primers sense.

5′CTCGAGACCAATGGAACAAAAGTTGATTTCAGAAGAAGATTTATTAATGGCCAAGGAGG3′, antisense 5′GCCCCTCTCCTTGGCCATTAATAAATCTTCTTCTGAAACAACTTTTGTTCCATGGCTCGAGTGCA3′ and cloned in the pDONOR211 vector using the Gateway system (Life Technologies) according to manufacturer's instructions. The Gateway Technology (Life Technologies) was also used to subclone myc-DGKα into pLenti4/V5-DEST lentiviral vector. Lentiviral particles were obtained in 293FT packaging cells co-transfected with helper vectors. After infection and selection we obtained a polyclonal population of MDA-MB-231 cells constitutively expressing myc-DGKα.

Inducible Silencing of DGKα in MDA-MB-231

We used the commercial pTRIPZ Inducible Lentiviral Human DGKA shRNA Clone ID: V3THS_340705 (shRNA-DGKα1) or pTRIPZ Inducible Lentiviral Non-silencing shRNA Control RHS4743 (shRNA-CTRL). Those vectors express shRNA and turboRFP under a doxycycline regulated promoter (Thermo Scientific Open Biosystems). Lentiviral particles were obtained in 293FT packaging cells co-transfected with helper vectors. After infection and selection we obtained a polyclonal population of MDA-MB-231 cells which upon induction with doxycycline (1 μg/ml, 72 hours) are 100% RFP positive.

Stable Silencing DGKα in MDA-MB-231

The shRNA for DGKα (forward: 5′ GATCCCCGGTCAGTGATGTCCTAAAGTTCAAGAGACTTTAGGACATCACTGACCTTTTTGGAAA reverse: 5′ AGCTTTTCCAAAAAGGTCAGTGATGTCCTAAAGTCTCTTGAACTTTAGGACATCACTGACCGGG) was cloned with H1-Promoter within the lentiviral vector pCCL.sin.PPT.hPGK.GFPWpre [25]. The resulting vector co-express shRNA-DGKα and GFP (shRNA-DGKα2). Empty vector was used as a control. Lentiviral particles were obtained in 293FT packaging cells co-transfected with helper vectors (Life Technologies). At 1 week after infection nearly 100% of cells were GFP^+.

Generation of ShRNA- β1 Integrin MDA-MB-231

ShRNA-β1integrin in pLKO were a kind gift of P. Defilippi [26]. Lentiviral particles were generated with Sigma Mission Lentivaral packaging mix according to manufacturer's instruction in 293FT cells and selected with puromycin. Empty pLKO was used as a control.

Western Blotting

To verified protein down-regulation cells were lysed 48 hours after transfection. Cell were washed with ice cold PBS, scraped on ice in lysis buffer (25 mM Hepes, pH 8, 150 mMNaCl, 0.5/1% Nonidet P-40, 5 mM EDTA, 2 mM EGTA, 1 mM ZnCl2, 50 mM NaF, 10% glycerol supplemented with fresh 1 mM Na_3VO_4, and protease inhibitors) and clarified after centrifugation of 15 minutes at 12000 rpm at 4°C. Samples were then resuspended in Laemmli buffer, heat denatured, and separated by SDS/PAGE. Proteins were then transferred on PVDF membrane by using semi-dry system. Membrane was then blocked with 5% BSA in PBS and incubated at 4°C overnight with primary antibodies diluted in TBS tween 0.1%, BSA 2%, 0.01% azide. After 4 washes with TBS-Tween 0.1%, membranes were incubated with secondary antibodies and washed again. Western blot were visualized using Western Lightning Chemiluminescence Reagent Plus (Perkin Elmer).

Quantitative RT-PCR

RNA was extracted by TRI-Reagent Solution (Life Technologies) retrotrascribed with High-Capacity cDNA Reverse Transcription Kits (Life Technologies) and cDNA quantified by real time PCR using GUSB as normalizer. TaqMan gene expression assays we from Life Technologies: β1 integrin (Hs 00559595), GUSB (Hs 00939627), DGKα (Hs 00176278) and MMP-9 (Hs 00234579).

MMP-9 Secretion

MDA-MB-231 cells (250,000 cells/well) were plated in 6-well cell culture plate and transfected with the indicated siRNA. After 24 hours in serum free media cells were treated with SDF-1α (100 ng/ml in 500 μl serum-free medium). After 24 hours the MMP-9 concentration in the supernatants was determined by ELISA assay (Life Technologies).

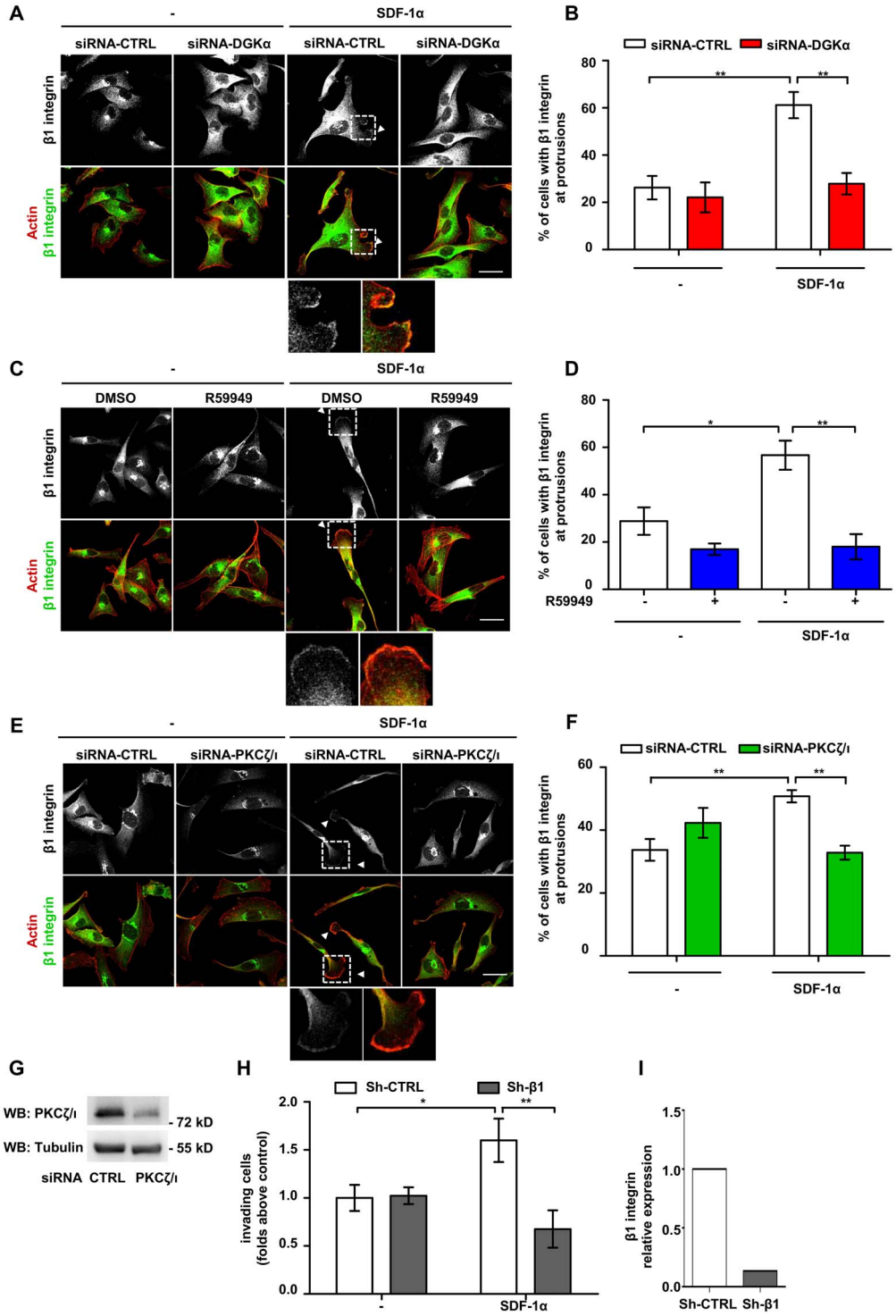

Figure 4. DGKα and aPKCs mediate SDF-1α-induced recruitment of β1 integrin to pseudopods. A) MDA-MB-231 cells were plated on matrigel-coated coverslips for 20 hours in FCS containing medium, transfected with CTRL or DGKα–specific siRNA and cultured for further 20 hours in serum free medium. Cells were then stimulated for 6 hours with 50 ng/ml SDF-1α, fixed and stained for actin (red) and β1 integrin (green). Arrows indicate β1 integrin at protrusions. Scale bar 24 μm. B) Histogram reports the percentage of cells displaying β1 integrin at protrusions as mean ± SE values of 3 independent experiments with **t-test $p<0.005$. C) MDA-MB-231 cells were plated on matrigel-coated coverslips for 20 hours in FCS containing medium and cultured for further 20 hours in serum free medium. Cells were then stimulated for 6 hours with 50 ng/ml SDF-1α, in presence or in absence of 1 μM R59949, fixed and stained for actin (red) and β1 integrin (green). Arrow indicates β1 integrin at protrusions. Scale bar 24 μm. D) Histogram reports the percentage of cells displaying β1 integrin at protrusions as mean ± SE of 3 independent experiments with *t-test $p<0.05$, **t-test $p<0.005$. E) MDA-MB-231 cells were plated on matrigel-coated coverslips for 20 hours in FCS containing medium, transfected with CTRL or PKCζ/ι –specific siRNA and cultured for further 20 hours in serum free medium. Cells were then stimulated for 6 hours with 50 ng/ml SDF-1α, fixed and stained for actin (red) and β1 integrin (green). Arrowheads indicate β1 integrin at protrusions. Scale bar 24 μm. F) Histogram reports the percentage of cells displaying β1 integrin at protrusions as mean ± SE of 3 independent experiments with **t-test $p<0.005$. G) MDA-MB-231 cells

were transfected with CTRL and PKCζ/ι –specific siRNA and lysed. The efficiency of PKCζ/ι down–regulation by siRNA was verified by western bloting, tubulin was used as a loading control. H) MDA-MB-231 cells were infected with lentiviral vectors expressing a shRNA against β1-integrin (shRNA-β1) or a control sequence (shRNA-CTRL). 50,000 cells were plated on matrigel invasion chamber and incubated for 24 hours in presence or in absence of SDF-1α (100 ng/ml). Histogram reports mean ± SE of fold over control values from 3 independent experiments with *t-test $p<0.05$, **t-test $p<0.01$. I) The efficiency of β1-integrin down–regulation by shRNA was verified by quantitative RT-PCR.
doi:10.1371/journal.pone.0097144.g004

Statistical Analysis

Data are shown as the mean ± SEM. For statistical analysis, Student's t-test or *ANOVA* were used. Experiments shown are representative at least 3 independent experiments.

Results

DGKα Is Necessary for SDF-1α-induced Cell Invasion

We previously showed that DGKα is necessary for matrix invasion promoted by Epidermal Growth Factor (EGF) [15] or Hepatocyte Growth Factor (HGF) in MDA-MB-231 breast carcinoma cells [27]. In order to investigate the role of DGKα in chemokine invasive signaling in breast cancer, we knocked down DGKα in MDA-MB-231 using a lentiviral construct expressing a DGKα-specific shRNA under an inducible promoter (shRNA-DGKα1). This construct strongly downregulated DGKα expression when compared with parental cells or a non-targeting control sequence (shRNA-CTRL, Fig. 1 B and C). The invasive ability of parental, DGKα-knocked down and control cells were evaluated in a Matrigel invasion assay. SDF-1α (100 ng/ml) doubles the number of parental as well as shRNA-CTRL MDA-MB-231 invading across the matrigel insert (Fig. 1 A). Conversely, shRNA-DGKα1 cells were unresponsive to SDF-1α stimulation. We confirmed this finding with an independent shRNA (shRNA-DGKα2) giving a comparable inhibition of SDF-1α stimulated matrix invasion (Fig. S1), making off-target effects unlikely.

Those findings indicates that DGKα mediates the pro-invasive signaling promoted not only by tyrosine kinase receptors [22] but also by chemokine receptors involved in tumor cells metastatization, such as those of SDF-1α.

SDF-1α Stimulates DGKα Activity and Localization at Protrusions Sites

The previous findings that HGF, EGF and VEGF activate DGKα and promote its recruitment to the plasma membrane in epithelial and endothelial cells [15,17,22] suggest that SDF-1α may promote localized DGKα activation at ruffling sites. Despite its biological significance, the low level of DGKα expression in MDA-MB-231 cells hampers activation and localization studies of the endogenous protein with currently available antibodies.

Thus, for localization studies, MDA-MB-231 cells were stably infected with a lentiviral vector expressing myc-DGKα and plated on matrigel-coated coverslip to mimic the epithelial microenvironment. In unstimulated serum-deprived cells, myc–DGKα was mainly cytoplasmic, with some cells displaying very little accumulation at cell protrusions (Fig. 2A). Prolonged SDF-1α stimulation (50 ng/ml; 4 to 6 hours) resulted in the localization of DGKα at the tip of large protrusions (Fig. 2A and B). No detectable changes were observed at earlier time points (15 minutes, Fig. 2B).

For enzymatic activation assays, we infected MDA-MB-231 with a lentiviral vector expressing OneStrep-Tagged DGKα (OST-DGKα) under the control of a doxycycline-inducible promoter. Upon 48 hours doxycycline treatment (1 μg/ml), OST-DGKα was strongly overexpressed as compared to endogenous protein (Fig. S2A). Under these conditions the enzymatic activity of OST-DGKα was responsible for almost the entire DGK activity measured in cell homogenates. Both SDF-1α and HGF (a well known DGKα activator) induced a further moderate increase of OST-DGKα activity within 15 minutes of stimulation (Fig. 2C).

Altogether these data indicate that SDF-1α regulates DGKα activity and localization and suggest that DGKα plays a role in the formation and/or extension of cell protrusions induced by SDF-1α.

DGKα Mediates SDF-1α-induced Cell Invasion by Regulating aPKCs Recruitment to Cell Protrusions

DGKα, by producing PA, mediates aPKCs activation and recruitment to the cell surface induced by growth factors [23,28]. Thus, we set to investigate whether DGKα mediates SDF-1α-induced cell invasion by regulating aPKCs. To investigate the role of DGKα in regulating aPKCs localization, MDA-MB-231 cells were transiently transfected with control (siRNA-CTRL) or DGKα-specific siRNA (siRNA-DGKα). Upon 48 hours from transfection with siRNA-DGKα, the expression of DGKα was nearly undetectable as compared to its expression in cells transfected with control siRNA (Fig. 3C). Then, MDA-MB-231 cells were plated on matrigel-coated coverslips, serum starved and stimulated with 50 ng/ml SDF-1α for 6 hours. In control siRNA transfected cells, SDF-1α treatment significantly increased the percentage of cells displaying aPKCs at protrusions, while DGKα silencing strongly impaired aPKCs recruitment to the membrane (Fig. 3A and B). In order to verify the requirement for DGKα enzymatic activity, we carried out aPKCs localization assays in presence or in absence of 1 μM R59949, a rather specific DGKα inhibitor [16,29]. R59949 treatment completely abrogated aPKCs localization at protrusions induced by SDF-1α, while it did not affect aPKCs localization in unstimulated cells (Fig. 3D and E).

In order to investigate the role of aPKCs in SDF-1α-induced invasion through extracellular matrix, MDA-MB-231 cells were treated with 10 μM cell permeable PKCζ pseudosubstrate (PS-PKCζ). In a matrigel invasion assay aPKCs inhibition significantly reduced SDF-1α-induced invasion, while basal invasion was unaffected in unstimulated cells (Fig. 3F).

Altogether, these data demonstrate that in SDF-1α-stimulated breast carcinoma cells, localized activity of DGKα at pseudopodial tips provides a crucial localization lipid signal for aPKCs recruitment, thus mediating SDF-1α-induced invasive signaling.

DGKα and aPKCs Mediate SDF-1α-induced Recruitment of β1 Integrin to Protrusions Sites

Recycling and clustering of β1 integrin at the tip of invasive pseudopods is a key event sustaining the invasive properties of malignant cells [30]. Conversely, growth factors stimulate invasion both by inducing integrin clustering at actin-rich adhesive sites and lamellipodia and by stimulating integrin recycling [26,31]. Thus, we set to investigate whether the DGKα and aPKCs at protrusions promote local accumulation of β1 integrin. In serum starved MDA-MB-231 cells plated on matrigel-coated coverslips β1 integrin is mostly localized in intracellular vesicles in the perinuclear/Golgi area. Upon SDF-1α stimulation, β1 integrin also localized in clusters at the tip of cell protrusions (Fig. 4A, C and E). However, either siRNA-mediated silencing of DGKα or R59949-mediated inhibition of its enzymatic activity impaired SDF-1α-induced localization of β1 integrin at cell extensions

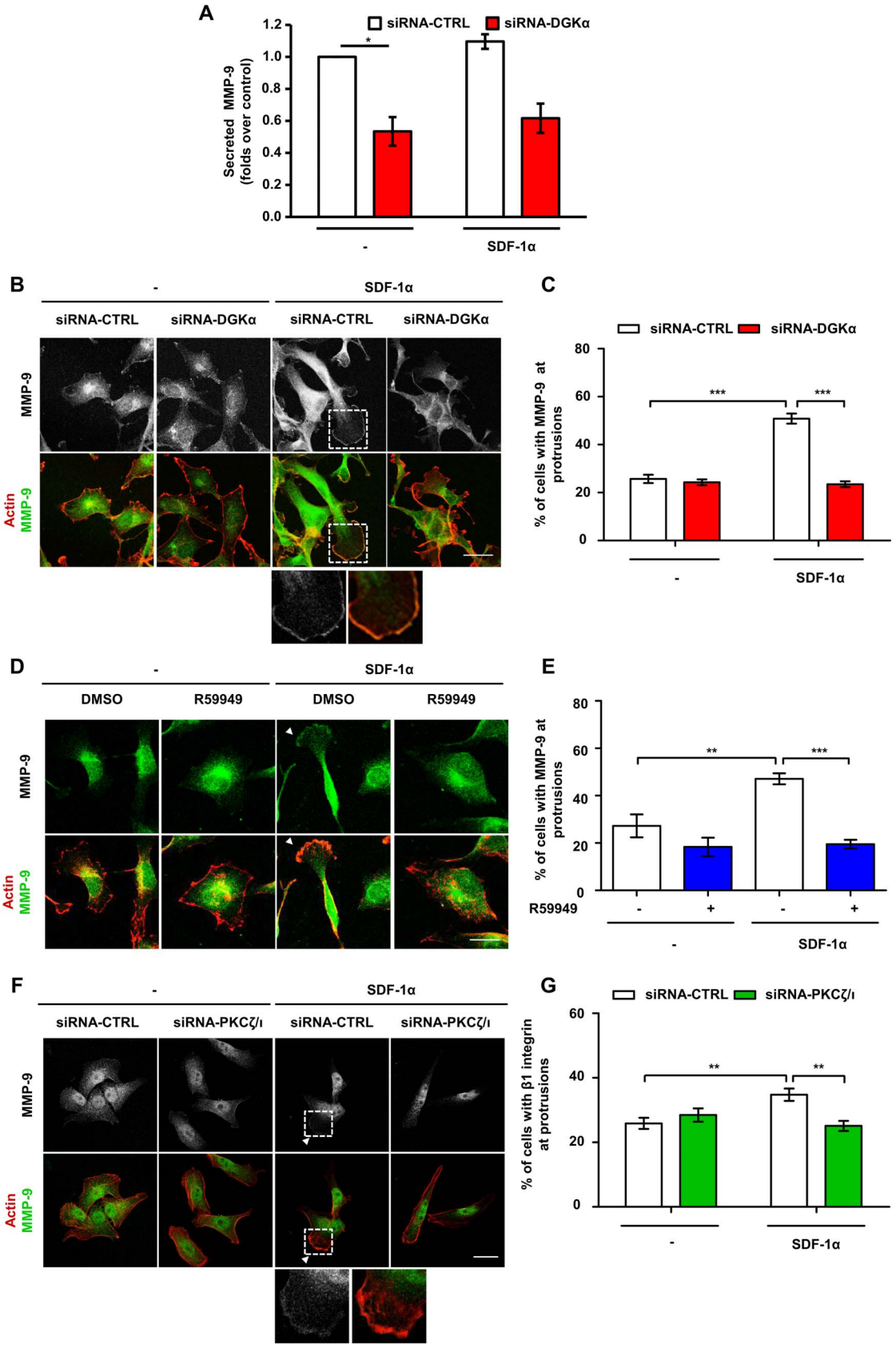

Figure 5. DGKα and aPKCs mediates MMP-9 secretion and localization at protrusions. A) MDA-MB-231 cells were transfected with CTRL or DGKα –specific siRNA and shifted to serum free media. After 24 hours cells were treated with 100 ng/ml SDF-1α in serum free medium for further 20 hours. MMP9 content in the supernatants was measured by ELISA assay, histogram reports secreted MMP-9 as mean ± SE of 3 independent

experiments normalized for control, with *t-test $p<0.05$. B) MDA-MB-231 cells were plated on matrigel-coated coverslips for 20 hours in FCS containing medium, transfected with CTRL or DGKα –specific siRNA and cultured for further 20 hours in serum free medium. Cells were stimulated for 6 hours with 50 ng/ml SDF-1α, fixed and stained for actin (red) and MMP-9 (green). Arrowhead indicates MMP-9 at protrusions. Scale bar 24 μm. C) Histogram reports the percentage of cells displaying MMP-9 at protrusions as mean ± SE of 3 independent experiments with ***t-test $p<0.0005$. D) MDA-MB-231 cells were plated on matrigel-coated coverslips for 20 hours in FCS containing medium and cultured for further 20 hours serum free medium. Cells were stimulated for 6 hours with 50 ng/ml SDF-1α, in presence or in absence of 1 μM R59949, fixed and stained for actin (red) and MMP-9 (green). Arrowhead indicates MMP-9 at protrusions. Scale bar 24 μm. E) Histogram reports the percentage of cells displaying MMP-9 at protrusions as mean ± SE of 3 independent experiments with **t-test $p<0.005$, ***t-test $p<0.01$. F) MDA-MB-231 cells were plated on matrigel-coated coverslips for 20 hours in FCS containing medium, transfected with CTRL or PKCζ/ι –specific siRNA and cultured for further 20 hours in serum free medium. Cells were then stimulated for 6 hours with 50 ng/ml SDF-1α, fixed and stained for actin (red) and MMP-9 (green). Arrowhead indicates MMP-9 at protrusions. Scale bar 24 μm. G) Histogram reports the percentage of cells displaying MMP-9 at protrusions as mean ± SE of 3 independent experiments with *t-test $p<0.05$, **t-test $p<0.005$.
doi:10.1371/journal.pone.0097144.g005

(Fig. 4A, B, C and D). Interestingly SDF-1α stimulation and DGKα inhibition did not affect the expression of β1 integrin at the cell surface, as measured by FACS analysis (Fig. S4A). Since DGKα promotes Rac1 activation and membrane ruffles by regulating aPKCs [15] and as DGKα mediates SDF-1α-induced aPKCs recruitment to the membrane protrusions, we assessed whether aPKCs controls β1 integrin localization. Indeed, siRNA-mediated silencing of aPKCs (Fig. 4G) impaired SDF1-α-induced localization of β1 integrin at cell protrusions (Fig. 4E and F).

Altogether these data suggest that SDF-1α, by activating the DGKα/aPKCs pathway, stimulates the clustering of β1 integrin at cell protrusions, rather than stimulating its bulk translocation at the plasma membrane.

Since the expression of constitutively-membrane bound myr-DGKα stimulates cell invasion by triggering RCP-mediated recycling of integrin α5β1 [15], we set to investigate the role of β1 integrin in SDF-1α-promoted cell invasion. To this purpose we used shRNA mediated knockdown of β1 integrin which resulted in an 80% reduction of its expression in MDA-MB-231 cells (Fig. 4I). We found that, β1 integrin knock down severely impaired the ability of MDA-MB-231 cells to invade through matrigel in response to SDF-1α stimulation (Fig. 4H).

Altogether these data indicate that DGKα, by regulating aPKCs, controls chemokine-induced β1 integrin localization at protrusion sites in breast carcinoma cells, thus confirming the pivotal role of β1 integrin in SDF-1α-promoted matrix invasion.

DGKα and aPKCs Mediate SDF-1α-induced MMP-9 Secretion and Localization at Protrusions

Secretion of matrix metalloproteinases (MMPs) is involved in the extracellular matrix degradation required for invasion of cancer cells [32,33]. SDF-1α stimulates the secretion of MMP-9 in several cancer cells, including MDA-MB-231 cells [34,35]. In migrating cells, MMP-9 is addressed to the cellular extensions involved in cell migration and accumulates at their tips [36]. Thus, we investigated whether SDF1-α regulates intracellular localization and secretion of MMP-9 through the DGKα/aPKCs axis.

MDA-MB-231 cells presented a low, constitutive secretion of MMP-9 (40–80 pg/ml in the supernatant), which was not affected by SDF-1α but was severely reduced by siRNA-mediated silencing of DGKα (Fig. 5A). However, the mRNA levels of MMP-9 were not affected by either SDF-1α stimulation or DGKα inhibition, suggesting that this pathway does not regulate MMP-9 at the transcriptional level in these cells (Fig. S4C). Conversely, SDF-1α stimulated MMP-9 accumulation at protrusions of serum-starved MDA-MB-231 plated on matrigel-coated coverslips (Fig. 5B to E). We cannot rule out that MMP-9 staining may be associated to the plasma membrane, indeed FACS analysis of these cells detected low amounts of membrane-bound MMP-9 with a small increase in MMP-9 surface positive cells following SDF-1α stimulation (Fig. S4B). Silencing of DGKα impaired MMP-9 translocation induced by SDF-1α, while it did not affect its localization in unstimulated cells (Fig. 5B and C). Similarly, DGKα pharmacological inhibition with R59949, completely impaired MMP-9 recruitment induced by SDF-1α (Fig. 5D and E).

Altogether these data suggest that DGKα is essential for MMP-9 accumulation at protrusions and subsequent release in the extracellular space. Given the role of DGKα in regulating aPKCs, we investigated whether aPKCs mediates SDF-1α-induced regulation of MMP-9 localization. Indeed, siRNA-mediated silencing of aPKCs blunted SDF-1α induced MMP-9 localization at pseudopodial tips (Fig. 5F and G).

Altogether these data demonstrate that activation of the DGKα/aPKCs pathway drives both MMP-9 and β1 integrin localization at the pseudopodial tips, thus regulating the extension of invasive protrusions and sustaining the invasive behavior of MDA-MB-231 cells.

DGKα Overexpression Promotes aPKC/Rac Dependent Cell Elongation

We observed that prolonged SDF1α treatment (6 hours, 50 ng/ml) of matrigel plated MDA-MB-231 promotes the transition to an elongated shape with the extension of long protrusions. Interestingly both siRNA downregulation of DGKα and R59949-mediated inhibition impairs this change in shape (Fig. S3A to C) indicating the crucial requirement of DGKα activity.

Since the over-expression of membrane-bound myr-DGKα stimulates cell migration in untransformed cells [18] and pseudopod extension and invasion in A2780 ovarian cancer cells [15], we investigated whether wild type DGKα over-expression was sufficient to further stimulate invasion in MDA-MB-231 cells. The previously described inducible OST-DGKα construct in MDA-MB-231 cells allowed us to verify this issue as doxycycline treatment induced a 30-fold increase in DGKα expression (Fig. 6A and Fig. S2A), with an increase of about 300-fold of the enzymatic activity (Fig. 2C). However, over-expression of OST-DGKα was not sufficient to enhance migration of MDA-MB-231 in wound-healing assay or to increase invasion through matrigel (Fig. S2B and C). Nevertheless, over-expression of OST-DGKα led to elongation of serum-starved MDA-MB-231 cells, while doxycycline did not affect the cell length of empty vector-infected MDA-MB-231 cells (Fig. 6B and D). Both in elongated and in shorter cells, OST-DGKα is localized at the tip of cell protrusions (Fig. 6C) suggesting that despite the absence of cytokines and growth factors the strong up-regulation of DGKα activity is sufficient to recruit the signaling machinery for membrane extension and to establish a feed forward loop recruiting further DGKα.

Consistently, with the reported role of the aPKCs in mediating DGKα-dependent Rac activation and membrane protrusions [23], we observed that siRNA-mediated silencing of aPKCs (Fig. 6G) blunted cell elongation induced by OST-DGKα over-expression (Fig. 6E). Also the Rac inhibitor NSC23766 completely

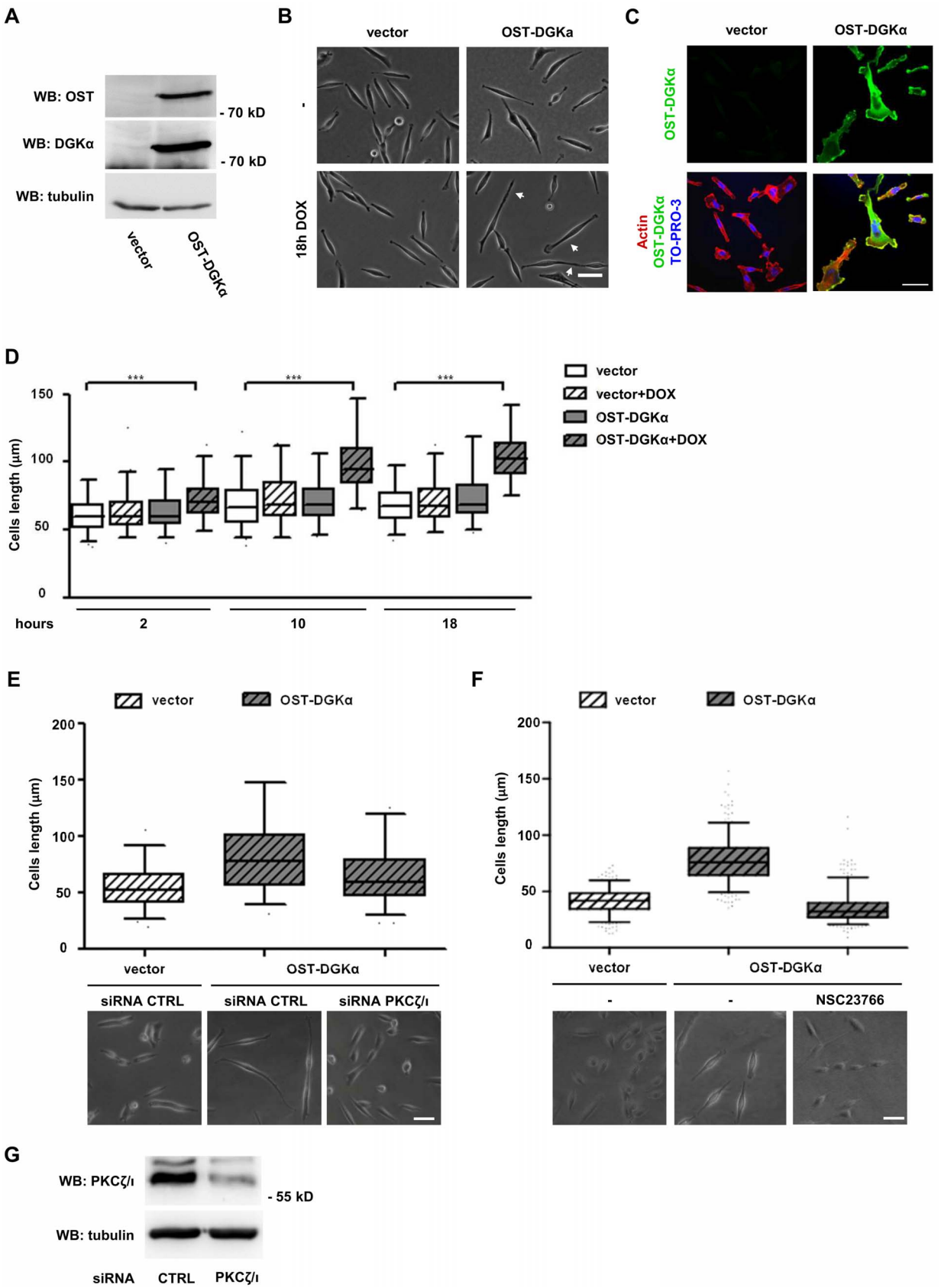

Figure 6. DGKα overexpression promotes a PKC-dependent cell elongation. MDA-MB-231 cells were infected with lentiviral vector expressing inducible OST-tagged DGKα or an empty vector. To induce DGKα expression, cells were treated overnight with doxycycline (1 µg/ml) in serum free medium. A) After cell lysis OST-DGKα induction was verified by western blotting with an antibody recognizing the OST-tag, while the

extent of overexpression was verified with anti DGKα antibodies. Tubulin was used as loading control. B) Phase contrast images of control and OST-DGKα cells cultured in presence or absence of doxycycline. Arrows indicate cells with long protrusions. Scale bar 50 μm. C) Confocal images of doxycycline induced cells showing OST-DGKα localization, cells were stained for actin (red) and OST (green). Scale bar 24 μm. D) Time course of cell elongation at 2, 10 and 18 hours with or without doxycycline treatment. Time lapse videos were recorded and total cell length measured. Box and whiskers plots (black lines show median, whiskers: 5–95 percentile) of data from 3 independent experiments are shown, ***$p<0.0001$, 1 way ANOVA. E) MDA-MB-231 cells expressing OST-DGKα were transiently transfected with control or PKCζ/ι-specific siRNA. After 48 hours DGKα expression was induced by overnight treatment with doxycycline (1 μg/ml) in serum free medium. Images were acquired with a phase contrast microscope, representative images are shown. Scale bar 50 μm. Total cell length was measured for at least 100 cells and reported as box and whiskers plot. F) MDA-MB-231 cells expressing OST-DGKα were induced by overnight treatment with doxycycline (1 μg/ml) in serum free medium with or without NSC23766 (100 μM). Images were acquired with a phase contrast microscope, representative images are shown. Scale bar 50 μm. Total cell length was measured for at least 100 cells and reported as box and whiskers plot. MDA-MB-231 cells were transfected with CTRL and PKCζ/ι –specific siRNA and lysed. The efficiency of PKCζ/ι down–regulation by siRNA was verified by western blotting, tubulin was used as a loading control.
doi:10.1371/journal.pone.0097144.g006

blunted OST-DGKα induced elongation indicating the involvement of Rac family GTPases (Fig. 6F). Those findings confirm the relevance of aPKCs and Rac as DGKα downstream effectors promoting cytoskeletal remodeling and extension of membrane protrusions.

The expression of myr-DGKα drives pseudopodial extension by stimulating RCP-mediated recycling of β1 integrin in A2780 carcinoma cells [15]. However, siRNA-mediated silencing of either β1 integrin or RCP (Fig. S5C and D) did not affect protrusion elongation induced by wild type DGKα in serum starved MDA-MB-231 cells (Fig. S5A and B), suggesting that in this experimental model β1 integrin and its RCP-mediated recycling are not required for protrusion elongation.

These data indicate that up-regulation of DGKα activity by SDF-1α is sufficient to promote the extension of membrane protrusions through the aPKCs – RhoGDI – Rac pathway [22,23], but that additional signaling pathways and/or its localization at specific myrstyoilation-directed membrane compartment are required to trigger cells invasion.

Discussion

We and others established the relevance of DGKα activation and membrane recruitment in growth factors signaling [37]. In normal epithelia, endothelia and lymphocytes DGKα activity is required to convey proliferative [17,38,39] and migratory [16–18,22,23] signaling. Several studies pointed out DGKα involvement in cancer showing that its activity is necessary *in vivo* for glioblastoma and hepatocellular carcinoma progression [13], and *in vitro* for proliferation and survival of endometrial carcinoma [21], anaplastic large cell lymphoma [19], and melanoma [40]. Moreover, DGKα activity mediates matrix invasion sustained by p53 pro-metastatic mutations in cancer cells [15]. However, the molecular pathways by which DGKα controls carcinoma formation and metastatization are poorly known.

Inhere we investigated the role of DGKα in invasive signaling of SDF-1α, one of the key signals driving metastasis [41], whose receptor, CXCR4, is strongly associated to tumor growth and spontaneous metastasis formation [1]. We used MDA-MB-231 cells, a highly invasive human breast cancer cell line, whose invasiveness and tumorigenicity are dependent on the expression of SDF-1α receptor, CXCR4 [42–44]. In these cells we had previously shown that DGKα is required for EGF- [15] and HGF-induced [27] migration in a tridimensional environment.

Interestingly, we show here that DGKα is also regulated by SDF-1α, which stimulates its enzymatic activity and promotes its recruitment at ruffling sites (Fig. 2). Moreover, we show that activation of DGKα provides a key lipid signal required for SDF-1α pro-invasive activity in MDA-MB-231 cells (Fig. 1).

We previously showed that the PA generated by HGF-induced activation of DGKα recruits to the plasma membrane and activates aPKCs in a complex with RhoGDI and Rac1, thus mediating the release of Rac1 from RhoGDI, and its localization and activation at ruffle sites [23]. The aPKCs subfamily comprises the ζ and ι isoforms, which are activated by PA [28] but insensitive to DG.

Several pieces of evidence show that aPKCs and in particular PKCι, play a key role in cancer cell invasion and tumor progression [45]. Interestingly, PKCι is essential for K-Ras-driven invasion in colon cancer by regulating Rac1 [46], while aPKCs mediates EGF-induced cell migration of MDA-MB-231 breast cancer cells [47]. Altogether these data further suggest that the DGKα/aPKCs signaling axis contributes to pro-invasive signaling.

Accordingly, the finding that SDF-1α induces aPKCs localization at protrusion sites through activation of DGKα, indicates that the DGKα/aPKCs signaling axis mediates chemokine-driven mammary carcinoma invasiveness (Fig. 3). DGKα-dependent recruitment of aPKCs at protrusion is an essential signaling event, since the silencing of either DGKα or aPKCs impairs downstream events such as accumulation of β1 integrin and MMP-9 at the plasma membrane (Fig. 4 and 5). The functional relevance of aPKCs as a DGKα effector is further proved by the observation that its silencing impairs DGKα-induced cell elongation (Fig. 6E) and that its inhibition blocks SDF-1α-induced matrix invasion (Fig. 3F).

The findings that aPKCs, RCP and β1 integrin are all required for the invasiveness of MDA-MB-231 (Fig. 3F, 4H and ref. [15]), and that upon SDF-1α stimulation β1 integrin is concentrated at protrusion tips in a DGKα and aPKCs-dependent manner, are consistent with our previous data showing that DGKα-generated PA, through binding to RCP, docks α5β1 recycling vesicles to the tips of invasive pseudopods. Altogether these findings suggest that activation of aPKCs may also contribute to integrin recycling induced by chemokines and growth factors, although there is no experimental evidence for it.

Several pieces of evidence in different cell types indicate that activation of aPKCs regulates MMPs production and secretion [48]. For instance, PKCζ activation mediates MMP-9 secretion induced by SDF-1α in hematopoietic progenitors [11]. MMPs are key players in the tumor microenvironment and play a major role in invasion of extracellular matrix [49]. While some MMPs are transmembrane proteins, most of them are soluble and bind to the extracellular cell surface by interaction with several membrane proteins, including β1 integrin and CD44v [50–54].

Our finding that both DGKα and aPKCs are required for SDF-1α-induced release of MMP9 in the cell medium and for its accumulation at protrusions, provides further strength to our thesis that DGKα/aPKCs axis is a major component of chemokine pro-invasive signaling. Interestingly, in SDF-1α-stimulated cells, MMP-9 localization at cell surface superimposes with that of β1 integrin, suggesting that their function at protrusion tips is coordinately regulated by activation of DGKα/aPKCs signaling.

Finally, the observation that DGKα over expression drives by itself elongation of cell protrusions by regulating aPKCs is consistent with active PKCζ promoting wide cytoskeletal remodeling and protrusions in untrasformed cells [23]. The molecular mechanisms by which aPKCs induces cell elongation downstream to DGKα is still partially known. In line with our previous demonstration that activation of the DGKα/aPKCs signaling module stimulates the RhoGDI driven localization of both Rac1 and Cdc42 at membrane ruffles, we observed that the Rac inhibitor NSC23766 blunts DGKα induced cell elongation (Fig. 6G) and that SDF-1α-induced localization of Cdc42 at protrusions of MDA-MB-231 cells is significantly reduced by DGKα inhibition (Fig. S3D and E). Conversely, protrusion extension occurs even in the absence of β1 integrin and RCP, suggesting that DGKα-dependent activation of aPKCs regulates cytoskeletal remodeling independently from β1 integrin recycling and function, which are required, however, to enable cell migration through a 3D matrix (Fig. 4H). While it is clear that DGKα/aPKCs activity on cell elongation is independent on β1 integrin recycling, these data cannot rule out that accumulation of β1 integrin and MMP-9 at protrusion tips depends on DGKα/aPKCs-induced regulation of Rac1 or Cdc42 and cytoskeletal contractility [31].

Altogether we showed that activation of the DGKα/aPKCs/β1 integrin pathway plays a key role in chemokine-driven matrix invasion in breast cancer cells. Those observations suggest that DGKα inhibition or silencing could be effective not only in reducing primary tumor growth *in vivo* [13,14] but could potentially also reduce the metastatic potential of carcinoma cells.

Supporting Information

Figure S1 DGKα is necessary for SDF-1α-induced cell invasion. MDA-MB-231 cells were infected with lentiviral vectors expressing a shRNA against DGKα (shRNA-DGKα2) or an empty vector. A) Cells were lysed and the efficiency of DGKα down–regulation by shRNA was verified by western blot, tubulin was used as a loading control. B) 50,000 cells were plated on matrigel invasion chamber and incubated for 24 hours in presence or in absence of SDF-1α (100 ng/ml). Histogram reports mean ± SE of fold over control values from 3 independent experiments with *t-test $p<0.05$, ***t-test $p<0.0005$.
(TIF)

Figure S2 DGKα overexpression does not affect migration and invasion of MDA-MB-231 cells. MDA-MB-231 cells were infected with lentiviral vector expressing inducible OST-tagged DGKα or an empty vector. To induce DGKα expression, cells were treated overnight with doxycycline (1 μg/ml) in serum free medium. A) After cell lysis, the extent of DGKα overexpression was verified with anti DGKα antibodies, long and short exposures are shown. Actin was used as loading control. B) Cells were grown to confluence in 12 well plates and subjected to a wound healing assay for 24 hours in serum free medium. HGF (50 ng/ml) was used as a positive control. The cells were stained and those migrating inside 2.3 mm of wound counted. Histogram reports mean ± SE of fold over control values from 3 independent experiments with *t-test $p<0.05$. C) 50,000 cells were plated on matrigel invasion chamber and incubated for 24 hours in serum free medium. Medium with 10% FCS was used as positive control. Histogram reports mean ± SE of fold over control values from 3 independent experiments with *t-test $p<0.05$.
(TIF)

Figure S3 DGKα is required for SDF-1α-induced pseudopod elongation. A) MDA-MB-231 cells were plated on matrigel-coated coverslips for 20 hours in FCS containing medium, transfected with CTRL or DGKα -specific siRNA and cultured for further 20 hours in serum free medium. Cells were then stimulated for 6 hours with 50 ng/ml SDF-1α, fixed and photographed at phase contrast. B) Histogram reports protrusions length in μm as mean ± SE values of 4 independent experiments with *t-test $p<0.005$. C) MDA-MB-231 cells were plated on matrigel-coated coverslips for 20 hours in FCS containing medium and cultured for further 20 hours in serum free medium. Cells were then stimulated for 6 hours with 50 ng/ml SDF-1α, in presence or in absence of 1 μM R59949, fixed and photographed at phase contrast. Histogram reports protrusions length in μm as mean ± SE of 3 independent experiments with *t-test $p<0.005$. D) MDA-MB-231 cells were plated on matrigel-coated coverslips for 20 hours in FCS containing medium and cultured for further 20 hours serum free medium. Cells were stimulated for 6 hours with 50 ng/ml SDF-1α, in presence or in absence of 1 μM R59949, fixed and stained for actin (red) and Cdc42 (green). Arrowhead indicates Cdc42 at protrusions. Scale bar 24 μm. E) Histogram reports the percentage of cells displaying Cdc42 at protrusions as mean ± SE of 3 independent experiments with *t-test $p<0.05$.
(TIF)

Figure S4 SDF-1α is not affecting surface exposition of β1-integrin and MMP-9. A) Surface expression of β1 integrin was analyzed before (turquoise) and after (red) SDF-1α stimulation. Flow cytometry histogram overlay comparing the level of β1 integrin expression before and after SDF-1α expression. Isotype-matched controls mAb staining are given as dashed lines. MFI, median fluorescence intensity. B) Surface expression of MMP-9 was analyzed before (turquoise) and after (red) SDF-1α stimulation. Flow cytometry histogram overlay comparing the level of MMP-9 expression before and after SDF-1α expression. Isotype-matched controls mAb staining are given as dashed lines. MFI, median fluorescence intensity. C) MDA-MB-231 cells were plated on 6 wells dish for 20 hours in FCS containing medium and cultured for further 20 hours serum free medium. Cells were stimulated for 24 hours with 100 ng/ml SDF-1α, in presence or in absence of 1 μM R59949. MMP-9 mRNA was quantified by quantitative RT-PCR. Histogram reports the mean ± SE of 3 independent experiments.
(TIF)

Figure S5 DGKα promoted cell elongation is independent from β1 integrin and RCP. MDA-MB-231 cells were infected with lentiviral vector expressing inducible OST-tagged DGKα or an empty vector. A) Cells were transiently transfected with control or β1 integrin-specific siRNA. After 48 hours DGKα expression was induced by overnight treatment with doxycycline (1 μg/ml) in serum free medium. Images were acquired with a phase contrast microscope, representative images are shown. Scale bar 50 μm. Total cell length was measured for at least 100 cells and reported as box and whiskers plot. B) Cells were transiently transfected with control or RCP-specific siRNA. After 48 hours DGKα expression was induced by overnight treatment with doxycycline (1 μg/ml) in serum free medium. Images were acquired with a phase contrast microscope, representative images are shown. Scale bar 50 μm. Total cell length was measured for at least 100 cells and reported as box and whiskers plot. C) MDA-MB-231 cells were transfected with CTRL and β1 integrin-specific siRNA and lysed. The efficiency of β1 integrin down–regulation by siRNA was verified by western blotting, tubulin was used as a

loading control. D) MDA-MB-231 cells were transfected with CTRL and RCP-specific siRNA and lysed. The efficiency of RCP down–regulation by siRNA and of OST-DGKα induction was verified by western blotting, actin was used as a loading control. (TIF)

Acknowledgments

ShRNA-β1 integrin in pLKO were a kind gift of P. Defilippi [26]. We thank O. Acuto (Oxford, UK) for helpful discussions.

Author Contributions

Conceived and designed the experiments: E. Rainero GB AG JCN. Performed the experiments: E. Rainero CC PEP FC VM VB E. Ruffo MF FB DC WP IL. Analyzed the data: E. Rainero CC FC PEP VM VB E. Ruffo MF DC IL AB NF FS GB AG. Contributed reagents/materials/analysis tools: E. Rainero WP GB AG. Wrote the paper: E. Rainero GB AG.

References

1. Müller A, Homey B, Soto H, Ge N, Catron D, et al. (2001) Involvement of chemokine receptors in breast cancer metastasis. Nature 410: 50–56.
2. Korkaya H, Liu S, Wicha MS (2011) Breast cancer stem cells, cytokine networks, and the tumor microenvironment. J Clin Invest 121: 3804–3809.
3. Teicher BA, Fricker SP (2010) CXCL12 (SDF-1)/CXCR4 pathway in cancer. Clin Cancer Res 16: 2927–2931.
4. Burger JA, Kipps TJ (2006) CXCR4: a key receptor in the crosstalk between tumor cells and their microenvironment. Blood 107: 1761–1767.
5. Li H, Yang L, Fu H, Yan J, Wang Y, et al. (2013) Association between Gαi2 and ELMO1/Dock180 connects chemokine signalling with Rac activation and metastasis. Nat Commun 4: 1706.
6. Yagi H, Tan W, Dillenburg-Pilla P, Armando S, Amornphimoltham P, et al. (2011) A synthetic biology approach reveals a CXCR4-G13-Rho signaling axis driving transendothelial migration of metastatic breast cancer cells. Sci Signal 4: ra60.
7. Azab AK, Azab F, Blotta S, Pitsillides CM, Thompson B, et al. (2009) RhoA and Rac1 GTPases play major and differential roles in stromal cell-derived factor-1-induced cell adhesion and chemotaxis in multiple myeloma. Blood 114: 619–629.
8. Kumar A, Kremer KN, Dominguez D, Tadi M, Hedin KE (2011) Gα13 and Rho mediate endosomal trafficking of CXCR4 into Rab11+ vesicles upon stromal cell-derived factor-1 stimulation. J Immunol 186: 951–958.
9. Chen G, Chen SM, Wang X, Ding XF, Ding J, et al. (2012) Inhibition of chemokine (CXC motif) ligand 12/chemokine (CXC motif) receptor 4 axis (CXCL12/CXCR4)-mediated cell migration by targeting mammalian target of rapamycin (mTOR) pathway in human gastric carcinoma cells. J Biol Chem 287: 12132–12141.
10. Odemis V, Boosmann K, Dieterlen MT, Engele J (2007) The chemokine SDF1 controls multiple steps of myogenesis through atypical PKCzeta. J Cell Sci 120: 4050–4059.
11. Petit I, Goichberg P, Spiegel A, Peled A, Brodie C, et al. (2005) Atypical PKC-zeta regulates SDF-1-mediated migration and development of human CD34n + progenitor cells. J Clin Invest 115: 168–176.
12. Mérida I, Avila-Flores A, Merino E (2008) Diacylglycerol kinases: at the hub of cell signalling. Biochem J 409: 1–18.
13. Takeishi K, Taketomi A, Shirabe K, Toshima T, Motomura T, et al. (2012) Diacylglycerol kinase alpha enhances hepatocellular carcinoma progression by activation of Ras-Raf-MEK-ERK pathway. J Hepatol 57: 77–83.
14. Dominguez CL, Floyd DH, Xiao A, Mullins GR, Kefas BA, et al. (2013) Diacylglycerol kinase α is a critical signaling node and novel therapeutic target in glioblastoma and other cancers. Cancer Discov 3: 782–797.
15. Rainero E, Caswell PT, Muller PA, Grindlay J, McCaffrey MW, et al. (2012) Diacylglycerol kinase α controls RCP-dependent integrin trafficking to promote invasive migration. J Cell Biol 196: 277–295.
16. Cutrupi S, Baldanzi G, Gramaglia D, Maffè A, Schaap D, et al. (2000) Src-mediated activation of alpha-diacylglycerol kinase is required for hepatocyte growth factor-induced cell motility. EMBO J 19: 4614–4622.
17. Baldanzi G, Mitola S, Cutrupi S, Filigheddu N, van Blitterswijk WJ, et al. (2004) Activation of diacylglycerol kinase alpha is required for VEGF-induced angiogenic signaling in vitro. Oncogene 23: 4828–4838.
18. Baldanzi G, Cutrupi S, Chianale F, Gnocchi V, Rainero E, et al. (2008) Diacylglycerol kinase-alpha phosphorylation by Src on Y335 is required for activation, membrane recruitment and Hgf-induced cell motility. Oncogene 27: 942–956.
19. Bacchiocchi R, Baldanzi G, Carbonari D, Capomagi C, Colombo E, et al. (2005) Activation of alpha-diacylglycerol kinase is critical for the mitogenic properties of anaplastic lymphoma kinase. Blood 106: 2175–2182.
20. Baldanzi G, Pietronave S, Locarno D, Merlin S, Porporato P, et al. (2011) Diacylglycerol kinases are essential for HGF-dependent proliferation and motility of Kaposi's Sarcoma cells. Cancer Sci.
21. Filigheddu N, Sampietro S, Chianale F, Porporato PE, Gaggianesi M, et al. (2011) Diacylglycerol kinase α mediates 17-β-estradiol-induced proliferation, motility, and anchorage-independent growth of Hec-1A endometrial cancer cell line through the G protein-coupled estrogen receptor GPR30. Cell Signal 23: 1988–1996.
22. Chianale F, Cutrupi S, Rainero E, Baldanzi G, Porporato PE, et al. (2007) Diacylglycerol kinase-alpha mediates hepatocyte growth factor-induced epithelial cell scatter by regulating Rac activation and membrane ruffling. Mol Biol Cell 18: 4859–4871.
23. Chianale F, Rainero E, Cianflone C, Bettio V, Pighini A, et al. (2010) Diacylglycerol kinase alpha mediates HGF-induced Rac activation and membrane ruffling by regulating atypical PKC and RhoGDI. Proc Natl Acad Sci U S A 107: 4182–4187.
24. Schaap D, de Widt J, van der Wal J, Vandekerckhove J, van Damme J, et al. (1990) Purification, cDNA-cloning and expression of human diacylglycerol kinase. FEBS Lett 275: 151–158.
25. Taulli R, Accornero P, Follenzi A, Mangano T, Morotti A, et al. (2005) RNAi technology and lentiviral delivery as a powerful tool to suppress Tpr-Met-mediated tumorigenesis. Cancer Gene Ther 12: 456–463.
26. Morello V, Cabodi S, Sigismund S, Camacho-Leal MP, Repetto D, et al. (2011) β1 integrin controls EGFR signaling and tumorigenic properties of lung cancer cells. Oncogene 30: 4087–4096.
27. Filigheddu N, Cutrupi S, Porporato PE, Riboni F, Baldanzi G, et al. (2007) Diacylglycerol kinase is required for HGF-induced invasiveness and anchorage-independent growth of MDA-MB-231 breast cancer cells. Anticancer Res 27: 1489–1492.
28. Limatola C, Schaap D, Moolenaar WH, van Blitterswijk WJ (1994) Phosphatidic acid activation of protein kinase C-zeta overexpressed in COS cells: comparison with other protein kinase C isotypes and other acidic lipids. Biochem J 304 (Pt 3): 1001–1008.
29. Sato M, Liu K, Sasaki S, Kunii N, Sakai H, et al. (2013) Evaluations of the selectivities of the diacylglycerol kinase inhibitors r59022 and r59949 among diacylglycerol kinase isozymes using a new non-radioactive assay method. Pharmacology 92: 99–107.
30. Desgrosellier JS, Cheresh DA (2010) Integrins in cancer: biological implications and therapeutic opportunities. Nat Rev Cancer 10: 9–22.
31. Trusolino L, Cavassa S, Angelini P, Andó M, Bertotti A, et al. (2000) HGF/scatter factor selectively promotes cell invasion by increasing integrin avidity. FASEB J 14: 1629–1640.
32. Nabeshima K, Inoue T, Shimao Y, Sameshima T (2002) Matrix metalloproteinases in tumor invasion: role for cell migration. Pathol Int 52: 255–264.
33. Itoh Y, Nagase H (2002) Matrix metalloproteinases in cancer. Essays Biochem 38: 21–36.
34. Yuecheng Y, Xiaoyan X (2007) Stromal-cell derived factor-1 regulates epithelial ovarian cancer cell invasion by activating matrix metalloproteinase-9 and matrix metalloproteinase-2. Eur J Cancer Prev 16: 430–435.
35. Fernandis AZ, Prasad A, Band H, Klösel R, Ganju RK (2004) Regulation of CXCR4-mediated chemotaxis and chemoinvasion of breast cancer cells. Oncogene 23: 157–167.
36. Legrand C, Gilles C, Zahm JM, Polette M, Buisson AC, et al. (1999) Airway epithelial cell migration dynamics. MMP-9 role in cell-extracellular matrix remodeling. J Cell Biol 146: 517–529.
37. Mérida I, Avila-Flores A, García J, Merino E, Almena M, et al. (2009) Diacylglycerol kinase alpha, from negative modulation of T cell activation to control of cancer progression. Adv Enzyme Regul.
38. Flores I, Casaseca T, Martinez-A C, Kanoh H, Merida I (1996) Phosphatidic acid generation through interleukin 2 (IL-2)-induced alpha-diacylglycerol kinase activation is an essential step in IL-2-mediated lymphocyte proliferation. J Biol Chem 271: 10334–10340.
39. Flores I, Jones DR, Ciprés A, Díaz-Flores E, Sanjuan MA, et al. (1999) Diacylglycerol kinase inhibition prevents IL-2-induced G1 to S transition through a phosphatidylinositol-3 kinase-independent mechanism. J Immunol 163: 708–714.
40. Yanagisawa K, Yasuda S, Kai M, Imai S, Yamada K, et al. (2007) Diacylglycerol kinase alpha suppresses tumor necrosis factor-alpha-induced apoptosis of human melanoma cells through NF-kappaB activation. Biochim Biophys Acta 1771: 462–474.
41. Luker KE, Luker GD (2006) Functions of CXCL12 and CXCR4 in breast cancer. Cancer Lett 238: 30–41.
42. Kang H, Mansel RE, Jiang WG (2005) Genetic manipulation of stromal cell-derived factor-1 attests the pivotal role of the autocrine SDF-1-CXCR4 pathway in the aggressiveness of breast cancer cells. Int J Oncol 26: 1429–1434.
43. Kang H, Watkins G, Parr C, Douglas-Jones A, Mansel RE, et al. (2005) Stromal cell derived factor-1: its influence on invasiveness and migration of breast cancer

cells in vitro, and its association with prognosis and survival in human breast cancer. Breast Cancer Res 7: R402–410.
44. Lapteva N, Yang AG, Sanders DE, Strube RW, Chen SY (2005) CXCR4 knockdown by small interfering RNA abrogates breast tumor growth in vivo. Cancer Gene Ther 12: 84–89.
45. Murray NR, Kalari KR, Fields AP (2011) Protein kinase Cι expression and oncogenic signaling mechanisms in cancer. J Cell Physiol 226: 879–887.
46. Murray NR, Jamieson L, Yu W, Zhang J, Gökmen-Polar Y, et al. (2004) Protein kinase Ciota is required for Ras transformation and colon carcinogenesis in vivo. J Cell Biol 164: 797–802.
47. Sun R, Gao P, Chen L, Ma D, Wang J, et al. (2005) Protein kinase C zeta is required for epidermal growth factor-induced chemotaxis of human breast cancer cells. Cancer Res 65: 1433–1441.
48. Frederick LA, Matthews JA, Jamieson L, Justilien V, Thompson EA, et al. (2008) Matrix metalloproteinase-10 is a critical effector of protein kinase Ciota-Par6alpha-mediated lung cancer. Oncogene 27: 4841–4853.
49. Kessenbrock K, Plaks V, Werb Z (2010) Matrix metalloproteinases: regulators of the tumor microenvironment. Cell 141: 52–67.
50. Brooks PC, Strömblad S, Sanders LC, von Schalscha TL, Aimes RT, et al. (1996) Localization of matrix metalloproteinase MMP-2 to the surface of invasive cells by interaction with integrin alpha v beta 3. Cell 85: 683–693.
51. Yu WH, Woessner JF, McNeish JD, Stamenkovic I (2002) CD44 anchors the assembly of matrilysin/MMP-7 with heparin-binding epidermal growth factor precursor and ErbB4 and regulates female reproductive organ remodeling. Genes Dev 16: 307–323.
52. Redondo-Muñoz J, Escobar-Díaz E, Samaniego R, Terol MJ, García-Marco JA, et al. (2006) MMP-9 in B-cell chronic lymphocytic leukemia is up-regulated by alpha4beta1 integrin or CXCR4 engagement via distinct signaling pathways, localizes to podosomes, and is involved in cell invasion and migration. Blood 108: 3143–3151.
53. Redondo-Muñoz J, Ugarte-Berzal E, García-Marco JA, del Cerro MH, Van den Steen PE, et al. (2008) Alpha4beta1 integrin and 190-kDa CD44v constitute a cell surface docking complex for gelatinase B/MMP-9 in chronic leukemic but not in normal B cells. Blood 112: 169–178.
54. Redondo-Muñoz J, Ugarte-Berzal E, Terol MJ, Van den Steen PE, Hernández del Cerro M, et al. (2010) Matrix metalloproteinase-9 promotes chronic lymphocytic leukemia b cell survival through its hemopexin domain. Cancer Cell 17: 160–172.

B7h Triggering Inhibits the Migration of Tumor Cell Lines

Chiara Dianzani,* Rosalba Minelli,* Casimiro Luca Gigliotti,† Sergio Occhipinti,‡ Mirella Giovarelli,‡ Laura Conti,‡ Elena Boggio,† Yogesh Shivakumar,† Gianluca Baldanzi,§ Valeria Malacarne,§ Elisabetta Orilieri,† Giuseppe Cappellano,† Roberto Fantozzi,* Daniele Sblattero,† Junji Yagi,¶ Josè Maria Rojo,‖ Annalisa Chiocchetti,† and Umberto Dianzani†

Vascular endothelial cells (ECs) and several cancer cells express B7h, which is the ligand of the ICOS T cell costimulatory molecule. We have previously shown that B7h triggering via a soluble form of ICOS (ICOS-Fc) inhibits the adhesion of polymorphonuclear and tumor cell lines to HUVECs; thus, we suggested that ICOS-Fc may act as an anti-inflammatory and antitumor agent. Because cancer cell migration and angiogenesis are crucial for metastasis dissemination, the aim of this work was to evaluate the effect of ICOS-Fc on the migration of cancer cells and ECs. ICOS-Fc specifically inhibited the migration of HUVECs, human dermal lymphatic ECs, and the HT29, HCT116, PC-3, HepG2, JR8, and M14 tumor cell lines expressing high levels of B7h, whereas it was ineffective in the RPMI7932, PCF-2, LM, and BHT-101 cell lines expressing low levels of B7h. Furthermore, ICOS-Fc downmodulated hepatocyte growth factor facilitated the epithelial-to-mesenchymal transition in HepG2 cells. Moreover, ICOS-Fc downmodulated the phosphorylation of focal adhesion kinase and the expression of β-Pix in both HUVECs and tumor cell lines. Finally, treatment with ICOS-Fc inhibited the development of lung metastases upon injection of NOD-SCID-IL2Rγnull mice with CF-PAC1 cells, as well as C57BL/6 mice with B16-F10 cells. Therefore, the B7h−ICOS interaction may modulate the spread of cancer metastases, which suggests the novel use of ICOS-Fc as an immunomodulatory drug. However, in the B16-F10–metastasized lungs, ICOS-Fc also increased IL-17A/RORc and decreased IL-10/Foxp3 expression, which indicates that it also exerts positive effects on the antitumor immune response. ***The Journal of Immunology*****, 2014, 192: 4921–4931.**

B7 homologoud protein (B7h, also known as B7H2, B7-RP1, ICOSL, GL50, and CD275) belongs to the B7 family of surface receptors and it binds ICOS (CD278), which belongs to the CD28 family (1–9). ICOS is selectively expressed by activated T cells, whereas B7h is expressed by a wide variety of cell types, including B cells, macrophages, dendritic cells (DCs), and a subset of T cells. However, B7h is also expressed by cells of a nonhemopoietic origin such as vascular endothelial cells (ECs), epithelial cells, and fibroblasts, as well as in many primary tumors and tumor cell lines (10–12).

The main known function of B7h is the triggering of ICOS, which functions as a costimulatory molecule for T cells by enhancing their cytokine secretion (3, 13, 14), and in particular, the secretion of IL-10, IL-17, IFN-γ (in humans), IL-4 (in mice), and IL-21 (in both species). The expression of B7h in nonlymphoid tissues, such as the brain, heart, kidney, liver, and intestine, suggests that it regulates the activation of Ag-experienced effector/memory T cells, which are recruited to or reside within these peripheral tissues (15). However, B7h expression also plays a role in secondary lymphoid tissue, particularly in the interaction between T and B cells; ICOS is expressed at high levels by Th follicular cells, and ICOS deficiency has been associated with the defective formation of lymphoid follicles in mice and common variable immunodeficiency in humans (16).

Recent reports have shown that the B7h–ICOS interaction may trigger bidirectional signals that can also modulate the response of the cells expressing B7h. This B7h-mediated "reverse signaling" can induce the partial maturation of immature mouse DCs with augmentation of IL-6 secretion (17). In humans, we have found that B7h triggering via ICOS-Fc, a recombinant soluble form of ICOS, substantially alters DC behavior by modulating the secreted cytokine pattern, which promotes the capacity to cross-present endocytosed Ags in class I MHC molecules and inhibits the adhesiveness to EC

*Department of Drug Science and Technology, University of Torino, 10125 Torino, Italy; †Interdisciplinary Research Center of Autoimmune Diseases, Department of Health Sciences, "A. Avogadro" University of Eastern Piedmont, 28100 Novara, Italy; ‡Department of Molecular Biotechnology and Health Sciences, University of Torino, 10126 Torino, Italy; §Department of Translational Medicine, "A. Avogadro" University of Eastern Piedmont, 28100 Novara, Italy; ¶Department of Microbiology and Immunology, Tokyo Women's Medical University, Tokyo 108-8639, Japan; and ‖Departamento de Medicina Celular y Molecular, Centro de Investigaciones Biologicas, Consejo Superior de Investigaciones Cientıficas, 28006 Madrid, Spain

Received for publication March 1, 2013. Accepted for publication March 11, 2014.

This work was supported by the Associazione Italiana Ricerca sul Cancro (Milan; Grant IG 14430), the Compagnia di San Paolo (Torino), the Fondazione Italiana Sclerosi Multipla (Genoa; Grant 2011/R/11), the Fondazione Amici di Jean (Torino), and the Fondazione Cassa di Risparmio di Cuneo (Cuneo).

C.D. and A.C. performed the functional experiments, analyzed the data, and contributed to writing the manuscript; E.B. and C.L.G. contributed to the cell and tissue preparation, flow cytometry assay, real-time PCR, and analysis; S.O. and L.C. performed the in vivo experiments; R.M., Y.S., and G.C. contributed to the adhesion, migration, and Western blot assays; G.B. performed the epithelial-to-mesenchymal transition and contributed to writing the manuscript; V.M. contributed to the epithelial-to-mesenchymal transition and confocal microscopy assay; D.S. and E.O. prepared the recombinant proteins; R.F., J.Y., M.G., and J.M.R. designed the study and wrote the manuscript; U.D. designed the study, supervised the research, and wrote the manuscript.

Address correspondence and reprint requests to Dr. Annalisa Chiocchetti, Interdisciplinary Research Center of Autoimmune Diseases and Department of Health Sciences, Via Solaroli 17 28100, Novara, Italy. E-mail address: annalisa.chiocchetti@med.unipmn.it

The online version of this article contains supplemental material.

Abbreviations used in this article: DC, dendritic cell; EC, endothelial cell; EMT, epithelial-to-mesenchymal transition; FAK, focal adhesion kinase; HDLEC, human dermal lymphatic endothelial cell; HGF, hepatocyte growth factor; Luc, luciferase; MFI-R, mean fluorescence intensity ratio; NSG, NOD-SCID-IL2Rγnull; Treg, regulatory T cell; VEGF-A, vascular endothelial growth factor-A.

www.jimmunol.org/cgi/doi/10.4049/jimmunol.1300587

and the migratory response to chemoattractants (18). Moreover, we showed that B7h stimulation inhibits the capacity of HUVECs to adhere to several tumor cell lines and granulocytes (11). This inhibitory effect was similarly detected when B7h was triggered on either HUVECs or the tumor cell lines and was accompanied by the decreased phosphorylation of ERK and p38 in HUVECs only. This indicated that the B7h–ICOS interaction modulates the recruitment of granulocytes in inflammatory sites and the spread of cancer metastases from the site of the primary tumor through the bloodstream (11).

The aim of the research reported in this article was to extend these observations by assessing the effect of B7h triggering on other key issues of tumor growth. Tumor growth depends on the proliferation and death rate of the tumor cells, metastasis dissemination depends on their capacity to migrate, and both tumor growth and dissemination are favored by neoangiogenesis within the tumor mass; thus, we assessed the effect of B7h triggering on the proliferation, apoptosis, and migration of tumor cells and vascular ECs. The results showed that B7h triggering strikingly inhibited the migration activity of both tumor and ECs in vitro, which was associated with the dephosphorylation of focal adhesion kinase (FAK) and decreased β-Pix expression. However, B7h triggering had no effect on their proliferation, apoptosis, or the ECs' capacity to form capillary-like structures. Moreover, B7h triggering hampered tumor cell metastasis in vivo.

Materials and Methods

Cells

HUVECs were isolated from human umbilical veins via trypsin treatment (1%) and cultured in M199 medium (Sigma-Aldrich, St. Louis, MO) with the addition of 20% FCS (Invitrogen, Burlington, ON, Canada) and 100 U/ml penicillin, 100 μg/ml streptomycin, 5 UI/ml heparin (Sigma-Aldrich), 12 μg/ml bovine brain extract, and 200 mM glutamine (Hyclone Laboratories, South Logan, UT). HUVECs were grown to confluence in flasks and used at the second to fifth passage. The purity of the ECs preparation was evaluated using morphologic criteria and positive immunofluorescence for factor VIII. Contamination with blood leukocytes was assessed via immunofluorescence with an anti-CD45 Ab. The use of HUVECs was approved by the Ethics Committee of the ''Presidio Ospedaliero Martini'' of Turin and conducted in accordance with the Declaration of Helsinki. Written informed consent was obtained from all donors. Human dermal lymphatic ECs (HDLECs) were purchased from Promo Cell and cultured with Endothelial Cell Growth Medium MV2 (Promo Cell GmbH, Heidelberg, Germany). The following human tumor cell lines were used: HT29, HCT116 (colon adenocarcinoma), PC-3 (prostate carcinoma), CF-PAC1 (human pancreas carcinoma), HepG2 (hepatic carcinoma), and B16-F10 (murine melanoma) from the American Type Culture Collection (ATCC; Manassas, VA); M14, JR8, RPMI7932, PCF-2, and LM (melanoma) from Dr. Pistoia (Gaslini Institute, Genoa, Italy); and BHT-101 (thyroid carcinoma) from Deutche Sammlung von Mikroorganismen and Zellculturen (Braunschweig, Germany). The human tumor cell lines were grown in culture dishes as a monolayer in RPMI 1640 medium (Invitrogen) and DMEM (Invitrogen) for HepG2, CF-PAC1, BHT-101, and B16-F10 plus 10% FCS, 100 U/ml penicillin, and 100 μg/ml streptomycin at 37°C in a 5% CO_2 humidified atmosphere.

The cells were treated or not treated with ICOS-Fc and ^{F119S}ICOS-Fc, in which the extracellular portion of human ICOS and its mutated form carrying a phenylalanine-to-serine substitution at position 119 (^{F119S}ICOS-Fc) were cloned as fusion proteins to the human IgG1 Fc region (11).

The cell-surface phenotypes were assessed via direct immunofluorescence and flow cytometry using the appropriate PE-conjugated anti-B7h mAb (R&D Systems, Minneapolis, MN) and the appropriate FITC-, PE-, and allophycocyanin-conjugated mAb to ICAM-1 (Biolegend, San Diego, CA), ICAM-2 (DiaClone Research, Manchester, U.K.), MadCAM (Abcam, Cambridge, MA), CD31, CD62L, CD62E, CD62P (Immunotools, Friesoythe, Germany), $CD44v_{6-7}$ (Bender Med-Systems, Vienna, Austria), Sialyl Lewis X (Santa Cruz Biotechnology, Dallas, TX), and VCAM-1 (eBiosciences, San Diego, CA). The expression of Sialyl Lewis A was assessed via indirect immunofluorescence using an appropriate mAb (Santa Cruz Biotechnology) and FITC-conjugated goat anti-mouse Ig (Caltag Laboratories, Burlingame, CA). The mean fluorescence intensity ratio (MFI-R) was calculated considering all of the alive cells according to the following formula: MFI of the B7h-stained sample histogram (arbitrary units)/MFI of the control histogram (arbitrary units). The B16-F10 cells were split into two cell lines expressing high or low levels of B7h ($B7h^{high}$ and $B7h^{low}$) via magnetic selection with PE-conjugated anti-B7h mAb and anti-PE microbeads (Miltenyi Biotec, Bergisch Gladbach, Germany).

Cell growth assays

In the MTT assay, the cells were normalized at 800 or 2500 cells/100 μl in 96-well plates for HT29 or HUVECs, respectively. After an overnight incubation, the medium was replaced with 100 μl culture medium with 0.5–4 μg/ml ICOS-Fc. In some experiments, the cells were refilled every 24 h with 4 μg/ml ICOS-Fc. After 24, 48, and 72 h of incubation, the viable cells were detected via MTT (Sigma-Aldrich) at 570 nm, as described by the manufacturer's protocol. The absorbance of the controls (i.e., the cells that received no drug) was normalized to 100%, and that of the ICOS-Fc–treated cells was expressed as the percentage of the controls. Eight replicate wells were used to determine each data point, and three different experiments were performed.

In the colony-forming assay, cells (800/well) were seeded into six-well plates and treated with the compounds. The medium was changed after 72 h, and the cells were cultured for another 10 d. Subsequently, the cells were fixed and stained with a solution of 80% crystal violet (Sigma-Aldrich) and 20% methanol (Sigma-Aldrich). The colonies were then photographed and counted with Gel Doc equipment (Bio-Rad Laboratories, Hercules, CA).

In the cell death assay, the cells were incubated with and without either etoposide (2 μg/ml; Sigma-Aldrich) or FCS for 18 h, and cell death was then evaluated by counting the live cells with the trypan blue exclusion test and detecting the dead cells upon cytofluorimetric analysis of the cells stained with FITC-conjugated Annexin V (BD Biosciences, San Jose, CA) and propidium iodide (Sigma-Aldrich).

Cell migration assays

In the Boyden chamber (BD Biosciences) migration assay, cells (8000) were plated onto the apical side of 50 μg/ml Matrigel-coated filters (8.2-mm diameter and 0.5-μm pore size; Neuro Probe; BIOMAP snc, Milan, Italy) in serum-free medium with or without 2 μg/ml ICOS-Fc or ^{F119S}ICOS-Fc. Medium containing either 20% FCS or 10 ng/ml vascular endothelial growth factor-A (VEGF-A; Sigma-Aldrich) or 50 ng/ml hepatocyte growth factor (HGF; PeproTech, Rocky Hill, CT) was placed in the basolateral chamber as a chemoattractant for the tumor, endothelial, or HepG2 cells, respectively. The chamber was incubated at 37°C under 5% CO_2. After 8 h, the cells on the apical side were wiped off with Q-tips. The cells on the bottom of the filter were stained with crystal violet and counted (five fields for each triplicate filter) with an inverted microscope (magnification ×100). The results are expressed as the number of migrated cells per high-power field.

In the wound-healing experiments, the cells were plated onto six-well plates (at a concentration of 10^6 cells/well) and grown to confluence. The cells were then left for 12 h with FCS-free medium (to prevent cell proliferation). The cell monolayers were carefully wounded by scratching with a sterile plastic pipette tip along the diameter of the well. The cells were washed twice with FCS-free medium and then incubated with culture medium in the absence or presence of 2 μg/ml ICOS-Fc. Five fields of each of the three wounds analyzed per condition were photographed immediately after the scratch had been made (0 h) and 24 h later to monitor cell movement into the wounded area.

In the cell scatter assay, the cells were plated on 24-well plates (2×10^4/well HepG2, 3×10^4/well BHT-101) in 10% FCS and stimulated with the indicated treatments. Phase-contrast images of random fields were acquired (after 48 h for HepG2 and 24 h for BHT-101) with an Axiovert 40 CFL microscope (Zeiss, Oberkochen, Germany) and analyzed with Image-Pro-Plus software. For each experimental point, the length of at least 100 cells and the percentage of disaggregated single cells were evaluated in 3 separate images. For confocal microscopy, the cells were washed with PBS and fixed in PBS containing 3% paraformaldehyde and 4% sucrose. The cells were permeabilized in cold HEPES-Triton buffer (20 mM HEPES, 300 mM sucrose, 50 mM NaCl, 3 mM MgCl2, 0.5% Triton X-100, pH 7.4). Intermediate washing was performed with PBS containing 0.2% BSA. PBS containing 2% BSA (Sigma-Aldrich) was used as a blocking reagent. Alexa Fluor 546 Phalloidin (Invitrogen) and TO-PRO3 (Invitrogen) were diluted in 2% PBS-BSA and added directly onto each glass coverslip in a humidified chamber for 30 min. Finally, each glass coverslip was washed briefly in water and mounted onto a glass microscope slide using Mowiol resin (Sigma-Aldrich, 20% Mowiol 4-88, 2.5% 1,4-diazabicyclo[2.2.2]octane in PBS, pH 7.4). Confocal images were acquired with a Leica confocal microscope TCS SP2 equipped with LCS Leica confocal software (63× objective for HepG2

or 40× objective for BHT-101; Leica Microsystems, Wetzlar, Germany). Basal planes are shown.

Angiogenesis assays

In the tube-formation assay, HUVEC cells were seeded onto 24-well plates (5×10^4/well) previously coated with 150 μl growth factor–reduced Matrigel (BD Biosciences) in the presence of ICOS-Fc (2–4 μg/ml) or control medium. The morphology of the capillary-like structures formed by the HUVECs was analyzed after 15 h of culture using an inverted microscope and was photographed with a digital camera. Tube formation was analyzed with an imaging system (Image-Pro).

In the spheroid sprouting assay, ECs were coated onto Cytodex microcarriers and embedded in a fibrin gel. Factor X, which was extracted from confluent fibroblasts medium, was added to the medium to promote ECs sprouting from the surface of the beads. After 4–5 d, numerous vessels could be observed with a phase-contrast microscope. The newly formed vessels were then treated or not treated with ICOS-Fc (4 μg/ml), and vessel morphology was analyzed 5 d later.

Western blot analysis

The cells were lysed in a buffer composed of 50 mM Tris-HCl pH 7.4, 150 mM NaCl, 5 mM EDTA, 1% nonyl phenoxypolyethoxylethanol 40, and phosphatase and protease inhibitor cocktails (P2850, P8340; Sigma-Aldrich). The tissues were lysed in a buffer composed of 160 mM NaCl, 20 mM Tris-HCl pH 7.4, 1 mM EDTA, 1 mM EGTA, 1% Triton X-100, 1% sodium deoxycholate, and 0.1% SDS. The lysates were then cleared of insoluble fractions through high-speed centrifugation, and the protein concentrations were determined with a commercially available kit (Bio-Rad Laboratories). Then 40 μg proteins were loaded on 10% SDS PAGE gels, and after electrophoresis, transferred onto Hybond-C extra nitrocellulose membranes (Ge Healthcare, Piscataway, NJ). These were blocked for 1 h at room temperature with 5% nonfat milk dissolved in TBST. The membranes were then probed overnight with Abs to β-Pix (SH3 domain; Millipore, Billerica, MA), phospho-FAK (Y397; Cell Signaling Technology, Danvers, MA), FAK (BD Biosciences), β-actin (A1978; Sigma-Aldrich), and after 3 washes, incubated for 1 h with HRP-conjugated secondary Abs (GE Healthcare, Piscataway, NJ). The bands were detected via chemiluminescence, and densitometric analysis was performed using Multi-Analyst software (version 1.1; Bio-Rad Laboratories).

In vivo experiments

Female 4- to 5-wk-old NOD-SCID-IL2Rγnull (NSG; The Jackson Laboratory, Bar Harbor, ME) mice were bred under pathogen-free conditions in the animal facility of the Molecular Biotechnology Center, University of Turin, and were treated in accordance with the University Ethical Committee and European guidelines. The mice were injected in the tail vein with stably expressing firefly luciferase (Luc) CF-PAC1 (human pancreas carcinoma) cells (0.5×10^6/mouse) and monitored for pulmonary metastases after 3 d via in vivo optical imaging. In each experiment, the mice were treated every day via the i.p. injection of either human ICOS-Fc plus mouse ICOS-Fc, human ICOS-Fc alone, mouse ICOS-Fc alone, human ^{F119S}ICOS-Fc alone (100 μg each), or the same volume of PBS as a control. Three days after tumor cell injection, the mice were injected i.p. with 150 mg/Kg luciferin (Perkin Elmer, Waltham, MA) in sterile PBS. They were then placed in the IVIS 200 (Perkin Elmer) induction chamber and subjected to inhalational isoflurane anesthesia (Abbott, Abbott Park, IL) at 2.5% with 1 l/min flow of oxygen. After 10 min, the mice were placed on the heated imaging platform of the IVIS 200 imaging station with inhalational isoflurane anesthesia during the imaging procedure. White light and Luc activity images were acquired with a 25-s exposure. The images

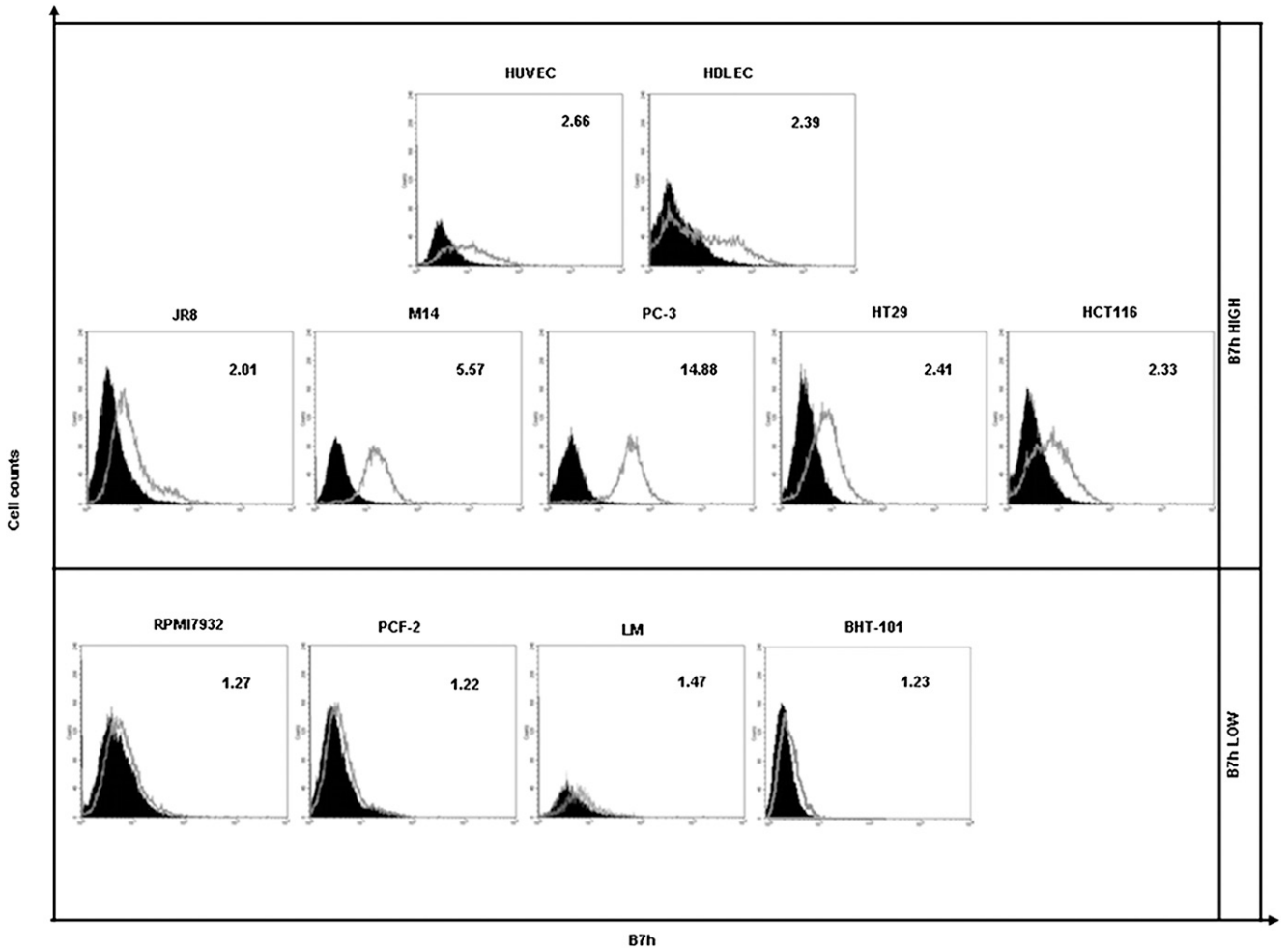

FIGURE 1. B7h expression in endothelial and tumor cell lines. B7h expression was assessed in the HUVEC, HDLEC, JR8, M14, PC-3, HT29, HCT116, RPMI7932, PCF-2, LM, and BHT-101 cell lines via flow cytometry using an anti-B7h mAb. The numbers in each panel indicate the MFI-R. The cutoff between the $B7h^{high}$ and $B7h^{low}$ cells was set at MFI-R = 2.

were analyzed with the Living Image software (PerkinElmer). The luminescent signal was quantified as the average radiance (p/s/cm^2/sr) measured in the regions of interest drawn in the lungs.

Female 5- to 7-wk-old C57BL/6 mice (Harlan Laboratories, Indianapolis, IN) were injected in the tail vein with B7h^{high} B16-F10 cells (10^6 cells/mouse) and then treated daily with an i.p. injection of either the mouse ICOS-Fc, the human ^{F119S}ICOS-Fc (100 μg each), or the same volume of PBS as a control. Two weeks after cell injection, the mice were euthanized, and the number of metastases detectable in the lung surfaces was evaluated by two blinded observers. In some experiments, the mice were euthanized 3 d after cell injection, and the metastases were counted in fixed sections of the lungs stained with H&E (Sigma-Aldrich).

The infiltrating cells were obtained by grinding the fresh lungs, obtained at day 3, through a 100-μm cell strainer mesh (BD Biosciences); the total RNA was then isolated using TRIzol reagent (Invitrogen). RNA (500 ng) was retrotranscribed using the ThermoScript RT PCR System (Invitrogen). IL-17A, IL-10, IL-21, RORc, Foxp3, and Bcl6 expression were evaluated with a gene expression assay (Assay-on Demand; Applied Biosystems, Foster City, CA). The β-glucuronidase gene was used to normalize the cDNA amounts. Real-time PCR was performed using the CFX96 System (Bio-Rad Laboratories) in duplicate for each sample in a 10 μl final volume containing 1 μl diluted cDNA, 5 μl TaqMan Universal PCR Master Mix (Applied Biosystems), and 0.5 μl Assay-on Demand mix. The results were analyzed with a Δ-Δ threshold cycle method.

In other experiments, the C57BL/6 mice were injected s.c. with 10^6B7h^{high} B16-F10 cells. When the tumor diameter reached 4 mm, the mice received an intratumoral injection of the mouse ICOS-Fc, human^{F119S}ICOS-Fc (100 μg each), or the same volume of PBS as a control. After 30 min, the tumors were excised and immediately frozen in liquid nitrogen for Western blot analyses.

Data analysis

The data are shown as the mean ± SEM. The statistical analyses were performed with GraphPad Prism 3.0 software using one-way ANOVA and Dunnett's test (GraphPad Software, San Diego, CA).

Results

B7h triggering has no effect on cell proliferation and apoptosis

To assess the effect of B7h triggering (via ICOS-Fc) on the proliferation, apoptosis, and migration of the tumor cells and vascular ECs, we used two primary EC lines (HUVECs and HDLECs) and nine continuous tumor cell lines (HT29 and HCT116 [colon carcinoma], PC-3 [prostate carcinoma], M14, JR8, RPMI7932, PCF-2, LM [melanoma], and BHT-101 cells [thyroid carcinoma]). The surface immunofluorescence and flow cytometry showed that B7h was expressed in all cell lines and at high levels (B7h^{high}) in HUVECs, HDLECs, JR8, M14, PC-3, HT29, and HCT116, but low levels (B7h^{low}) in BHT-101, RPMI7932, PCF-2, and LM (Fig. 1).

Initially, the effect of ICOS-Fc on cell proliferation and death was assessed in HUVECs, HT29, and PC-3, which expressed high levels of B7h. In the proliferation assay, the cells were cultured in the presence of various concentrations of ICOS-Fc (0.5–4 μg/ml) for 24–96 h, and cell proliferation was then assessed via the MTT and the clonogenic assays. The results showed that ICOS-Fc did not modulate cell proliferation in any cell line at any dose or time

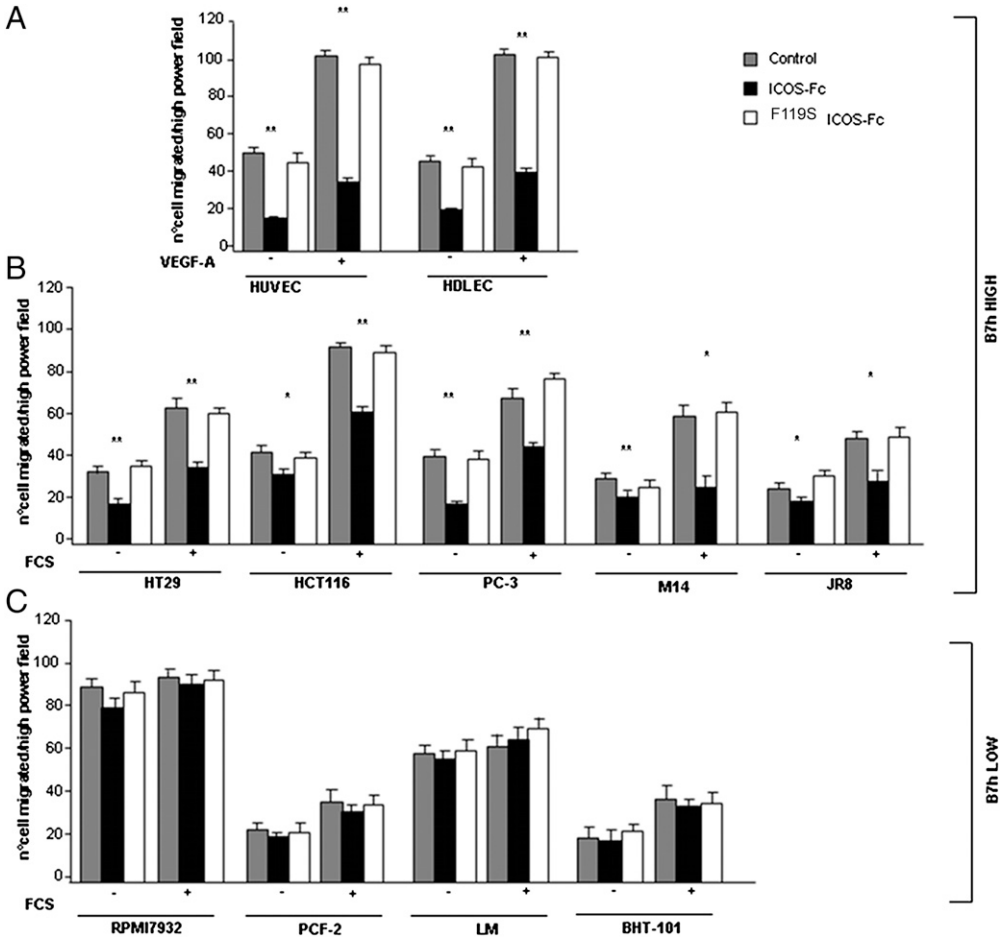

FIGURE 2. The effect of ICOS-Fc on the motility of the endothelial and tumor cell lines as assessed via a Boyden chamber assay. Cells: (**A**) HUVEC and HDLEC; (**B**) HT29, HCT116, PC-3, M14, and JR8; (**C**) RPMI7932, PCF-2, LM, and BHT-101 were plated onto the apical side of Matrigel-coated filters in 50 μl medium in the presence or absence of either 2 μg/ml ICOS-Fc or ^{F119S}ICOS-Fc; either VEGF-A (10 ng/ml) or 20% FCS was loaded in the basolateral chamber as chemotactic stimulus. The cells that migrated to the bottom of the filters were stained using crystal violet and counted (five fields for each triplicate filter) using an inverted microscope. The data are expressed as the mean ± SEM ($n = 5$) of the number of migrated cells per high-power field (*$p < 0.05$, **$p < 0.01$ versus the control).

(data not shown), even when the ICOS-Fc was refilled every 24 h. In the cell death assay, the cells were cultured for 18 h in the presence or absence of ICOS-Fc (2 μg/ml) either in the absence of FCS (to induce cell death by neglect) or in the presence of etoposide. Then cell survival was assessed after 18 h by counting the surviving cells with the trypan blue exclusion test, and the dead cells were evaluated by staining with propidium iodide and FITC-conjugated Annexin V followed by cytofluorimetric analysis. The results showed that ICOS-Fc did not induce cell death and did not modulate either cell death by neglect or that induced by etoposide in any cell line (data not shown).

B7h triggering inhibits cell migration and the epithelial-to-mesenchymal transition

To evaluate the effect of ICOS-Fc on cell migration, we seeded the endothelial and the tumor cell lines in the upper chamber of a Boyden chamber in serum-free medium in the presence or absence of ICOS-Fc (2 μg/ml) and allowed them to migrate for 8 h toward the lower chamber containing medium supplemented or not supplemented with either VEGF-A (10 ng/ml) or 20% FCS, which were used as chemoattractants for the endothelial and the tumor cells, respectively. As a control, the same experiments were performed in the presence of ^{F119S}ICOS-Fc, a mutated form of ICOS-Fc carrying a phenylalanine-to-serine amino acid substitution at position 119 that is unable to bind B7h. The results showed that ICOS-Fc significantly inhibited cell migration by ~50–70% in all of the B7h^{high} cell lines (i.e., HUVECs, HDLECs, HT29, HCT116, PC-3, M14, and JR8) in both the presence and the absence of the chemoattractants (Fig. 2A, 2B). This effect was specific because it was not exerted by ^{F119S}ICOS-Fc. In contrast, neither ICOS-Fc nor ^{F119S}ICOS-Fc exerted any effect on the B7h^{low} cell lines (i.e., RPMI7932, PCF-2, LM, and BHT-101), which indicated that the inhibitory effect was B7h mediated (Fig. 2C).

To confirm the effect of ICOS-Fc on directional cell migration, we performed the scratch assay, an in vitro "wound healing" assay, on PC-3, HT29, and HUVECs, because cell migration is highly efficient for PC-3, poor for HT29, and intermediate for HUVECs in this assay. A linear scratch was performed on a confluent monolayer of each cell line, and they were then cultured in FCS-free medium to minimize cell proliferation in the presence or absence of ICOS-Fc (2 μg/ml). A microscopic analysis evaluating cell capacity to migrate and fill the empty areas at different times showed that in the absence of ICOS-Fc, substantial cell migration was detectable in the wound area for PC-3 and HUVECs, and that it was substantially inhibited by ICOS-Fc (Fig. 3). This inhibition was also detectable for HT29 cells, which displayed a low migratory activity that was detectable as a fringing of the scratch edges after the 24-h incubation; this pattern was substantially inhibited by ICOS-Fc.

To assess the effect of ICOS-Fc on the epithelial-to-mesenchymal transition (EMT), we performed a scatter assay to treat the HepG2 cells (hepatic carcinoma) with HGF. In cultures, these cells grow as colonies that maintain an epithelial morphology; however, they break down cell junctions and acquire an elongated mesenchymal phenotype upon HGF/scatter factor treatment (19). A cytofluorimetric analysis showed that these cells express high levels of B7h (Fig. 4A). The cells were treated for 72 h in 10% FCS with or without HGF (50 ng/ml) and in the presence or absence of either ICOS-Fc (2 μg/ml) or ^{F119}ICOS-Fc (2 μg/ml). They were then directly analyzed via phase-contrast microscopy (Fig. 4B, *left panel*) or stained with Alexa Fluor 546 Phalloidin and imaged via confocal microscopy (Fig. 4B, *right panel*). The results showed that ICOS-Fc substantially inhibited the cell scatter induced by HGF by

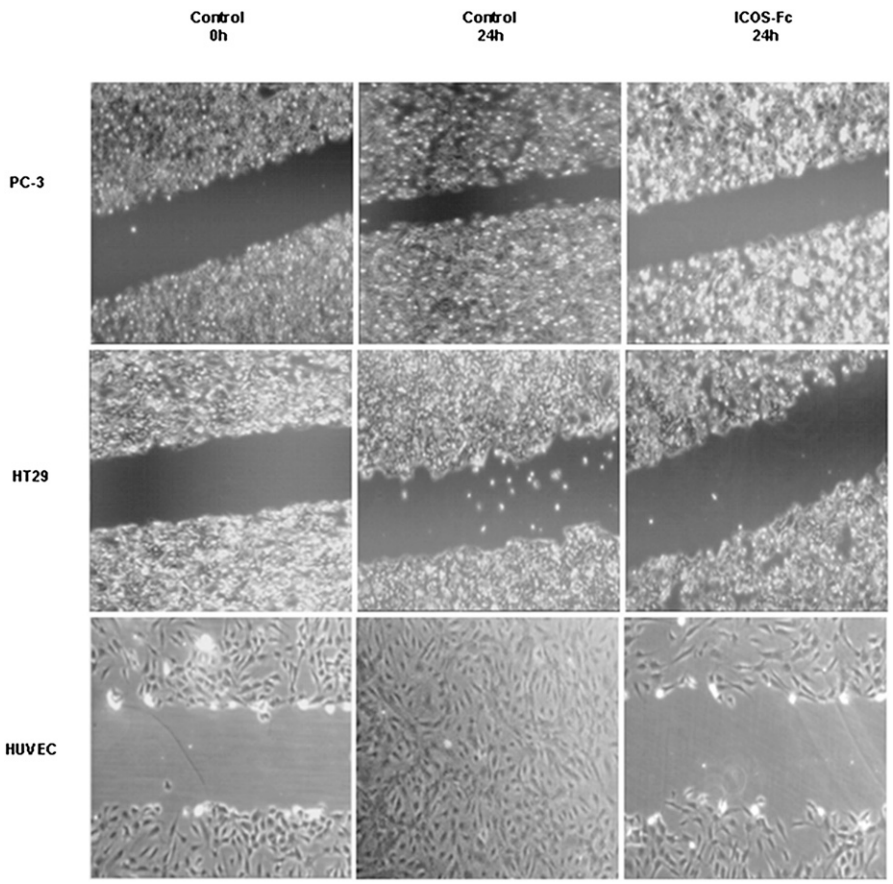

FIGURE 3. Effect of ICOS-Fc on the motility of the PC-3, HT29, and HUVECs as assessed using a "wound-healing" assay. The cells were grown to confluence on six-well plates. A scratch was made through the cell layer using a pipette tip; the cells were washed and then cultured in the presence or absence of 2 μg/ml ICOS-Fc for 24 h. Microphotographs of the wounded area were taken immediately after the scratch was made (0 h) and 24 h later to monitor cell migration into the wounded area (original magnification ×10). Panels show a representative experiment from three experiments.

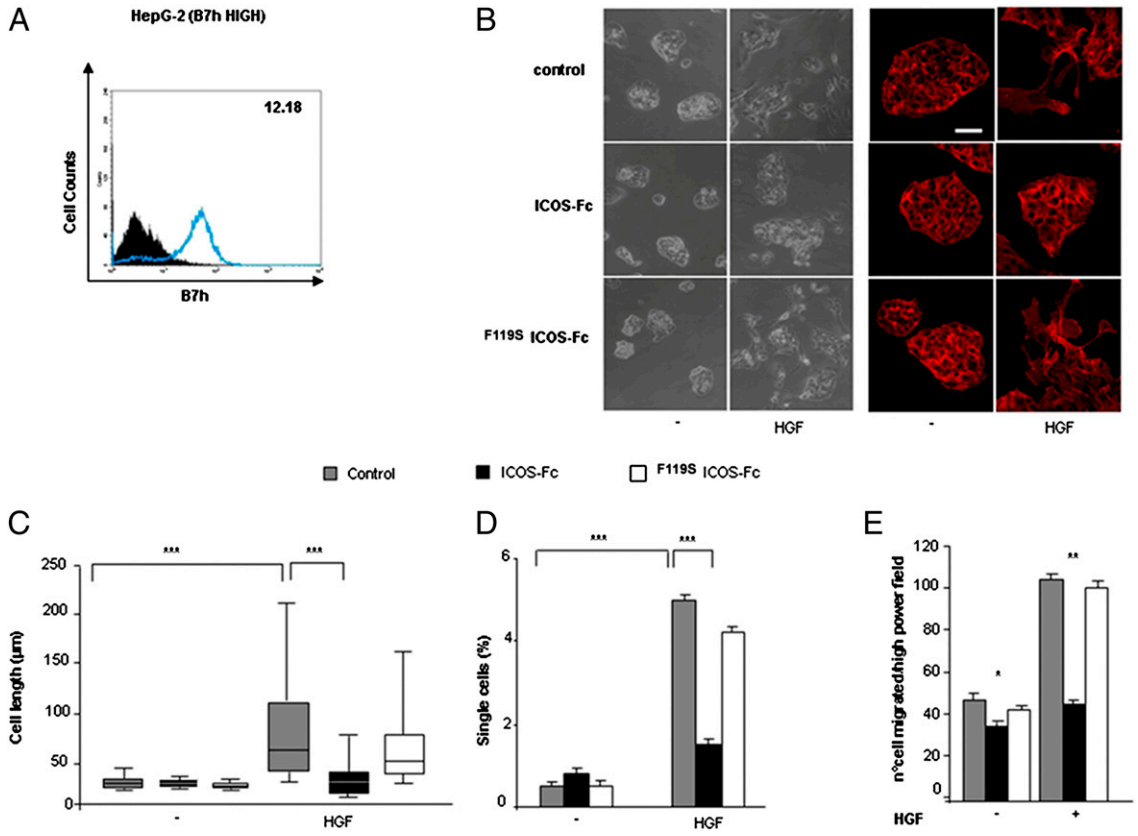

FIGURE 4. ICOS-Fc impairs HGF-induced cell scatter in HepG2 cells. (**A**) Cytofluorimetric analysis of the B7h expression in the HepG2 cells (performed as in Fig. 1). The HepG2 cells were treated for 48 h in 10% FCS with or without HGF (50 ng/ml), ICOS-Fc (2 μg/ml), or ^{F119S}ICOS-Fc (2 μg/ml). (**B**) The cells were photographed via phase contrast (*left panel*) or stained with Alexa Fluor 546 Phalloidin and imaged via confocal microscopy (*right panel*). Scale bar, 40 μm. (**C**) Whisker plot showing the cell length (excluding the outliers of a representative experiment). (**D**) Percentage of the disaggregated single cells (mean ± SEM of 4 experiments); at least 100 cells were counted for each point. (**E**) Effect of ICOS-Fc on the migration of HepG2 cells treated with HGF in the Boyden chamber assay (performed as in Fig. 2). $*p < 0.05$, $**p < 0.01$, $***p < 0.001$.

impairing the acquisition of the elongated mesenchymal morphology (median length of ICOS-Fc–untreated versus –treated cells: 60 mm versus 31 mm; Fig. 4C) and promoting the maintenance of colonies with cell-to-cell junctions and smooth borders with decreased numbers of disaggregated single cells (Fig. 4D). We also assessed the effect of ICOS-Fc on the migration of HepG2 cells induced by HGF (50 ng/ml) in the Boyden chamber assay. In accordance with the previous results, ICOS-Fc, but not ^{F119S}ICOS-Fc, inhibited the stimulated migration of HepG2 by ~50% (Fig. 4E). To assess whether these effects were dependent on B7h expression, we evaluated the effect of ICOS-Fc and ^{F119S}ICOS-Fc on the HGF-induced cell scattering of BHT-101, which was previously shown to express low levels of B7h (Fig. 1) and to display no ICOS-Fc–induced migration inhibition (Fig. 2). Because these cells showed modest elongation upon HGF treatment, their scattering was quantified only by counting the percentage of disaggregated single cells. The results showed that neither ICOS-Fc nor ^{F119S}ICOS-Fc inhibited BHT-101 cell scattering (Supplemental Fig. 1).

B7h triggering has no effect on angiogenesis

To assess the effect of B7h triggering on angiogenesis, we evaluated the effect of ICOS-Fc via the endothelial tube-formation assay and the spheroid sprouting assay. In the tube-formation assay, HUVECs were seeded onto 24-well plates (5×10^4/well) previously coated with 150 μl growth factor–reduced Matrigel in the presence of ICOS-Fc (2–4 μg/ml) or control medium. The morphology of capillary-like structures formed by HUVECs was analyzed 15 h after culturing. The results showed that ICOS-Fc did not significantly affect tube formation in HUVECs (data not shown).

In the spheroid sprouting assay, ECs were coated onto Cytodex microcarriers and embedded in a fibrin gel in the presence of factor X to promote EC sprouting from the surface of the beads. After 4–5 d, the newly formed vessels were treated or not treated with ICOS-Fc (4 μg/ml); vessel morphology was analyzed 5 d later. The results showed that ICOS-Fc did not significantly affect vessel caliper or length (data not shown).

B7h triggering inhibits β-Pix expression and FAK phosphorylation

To assess whether treatment with ICOS-Fc modulated the expression of adhesion molecules, we analyzed the surface expression of ICAM-1, ICAM-2, MadCAM, CD62P, CD31, CD44v_{6-7}, CD62E, Sialyl Lewis A, CD62L, VCAM-1, and Sialyl Lewis X via immunofluorescence and flow cytometry in JR8, M14, and HT-29 cells treated or untreated with ICOS-Fc for 30 min, 1, 4, and 24 h. The results showed that ICOS-Fc did not modulate the expression of any of these molecules (data not shown), which is in accordance with previous data obtained for HUVECs and DCs (11, 18).

In previous studies, we have shown that B7h triggering inhibits the phosphorylation of p38 and ERK induced by either E-selectin triggering or osteopontin in HUVECs (this occurred without affecting their basal phosphorylation), whereas no effect was detected in the tumor cell lines (11). Moreover, we showed that in

DCs, B7h inhibits the expression of the Rac-1 activator β-Pix, which is involved in cell motility (18). Therefore, we evaluated the effect of ICOS-Fc on the β-Pix expression in two B7h^{high} cell lines (PC-3, HUVECs) and two B7h^{low} cell lines (RPMI7932, BHT-101), and extended the analysis to the phosphorylation of FAK, involved in cell migration. The cells were either not treated or were treated with ICOS-Fc or ^{F119S}ICOS-Fc; β-Pix expression and FAK phosphorylation were then assessed via Western blot after 30 min. The results showed that ICOS-Fc substantially decreased β-Pix expression and FAK phosphorylation in the B7h^{high} cell lines (Fig. 5A, 5B), whereas no effect was detected in the B7h^{low} cell lines (Fig. 5C, 5D). The treatment with ^{F119S}ICOS-Fc showed no effect for any cell line.

B7h triggering inhibits tumor cell metastasis in vivo

The effect of B7h triggering on the metastasis capability in vivo was assessed by injecting NSG mice with CF-PAC1 Luc cells (human pancreas carcinoma). A previous in vitro analysis showed that this cell line expresses high levels of B7h (Fig. 6A) and that its treatment with ICOS-Fc, but not with ^{F119S}ICOS-Fc, inhibits migration in the Boyden chamber assay (Fig. 6B), as well as β-Pix expression and FAK phosphorylation (Fig. 6C); these findings are in accordance with the data obtained for the other B7h^{high} cell lines.

NSG mice were i.v. injected with 0.5×10^6 CF-PAC1 Luc cells and then i.p. treated with both the human and the mouse ICOS-Fc ($n = 7$) or PBS ($n = 7$) every day to trigger both the B7h expressed by the human tumor cell line and that expressed by the mouse vascular ECs; this treatment would mimic the putative effect of the human ICOS-Fc injected in humans. Three days after cell injection, the mice were i.p. injected with luciferin and analyzed via in vivo optical imaging to evaluate the tumor cell growth in the lung. Qualitative (Fig. 6D) and quantitative (Fig. 6E) analyses showed that a significantly higher luminescent signal was present in control mice than in those treated with ICOS-Fc. To determine whether this effect was due to the human or mouse ICOS-Fc, we repeated these experiments by treating the mice with either the human ICOS-Fc alone ($n = 3$), the mouse ICOS-Fc alone ($n = 3$), the human ^{F119S}ICOS-Fc alone ($n = 3$), or PBS ($n = 3$). The qualitative (Fig. 6F) and quantitative (Fig. 6G) analyses showed that a significantly higher luminescent signal was present in the control mice and those treated with ^{F119S}ICOS-Fc than in mice treated with either the human or mouse ICOS-Fc alone. In contrast, no significant differences were detected between the control mice and those treated with ^{F119S}ICOS-Fc.

To confirm these data, we assessed the ICOS-Fc effect on the metastasis of B16-F10 cells (mouse melanoma) in C57BL/6 mice. In a preliminary experiment, we separated the B7h^{high} and B7h^{low} B16-F10 cells using magnetic beads and found that these cell lines maintained their phenotype for several weeks in culture. Moreover, treatment with ICOS-Fc, but not with ^{F119S}ICOS-Fc, inhibited migration in Boyden chamber assay, as well as β-Pix expression and FAK phosphorylation in the B7h^{high} cell line, whereas no effects were detected in the B7h^{low} cell line (Supplementary Fig. 2).

The C57BL/6 mice were i.v. injected with 10^6 B7h^{high} B16-F10 cells and then i.p. treated with either the mouse ICOS-Fc ($n = 3$), human ^{F119S}ICOS-Fc ($n = 3$), or PBS ($n = 3$) every day. The lung metastases were analyzed either after 3 d (for the tissue sections stained with H&E) or after 2 wk by counting the tumor nodules

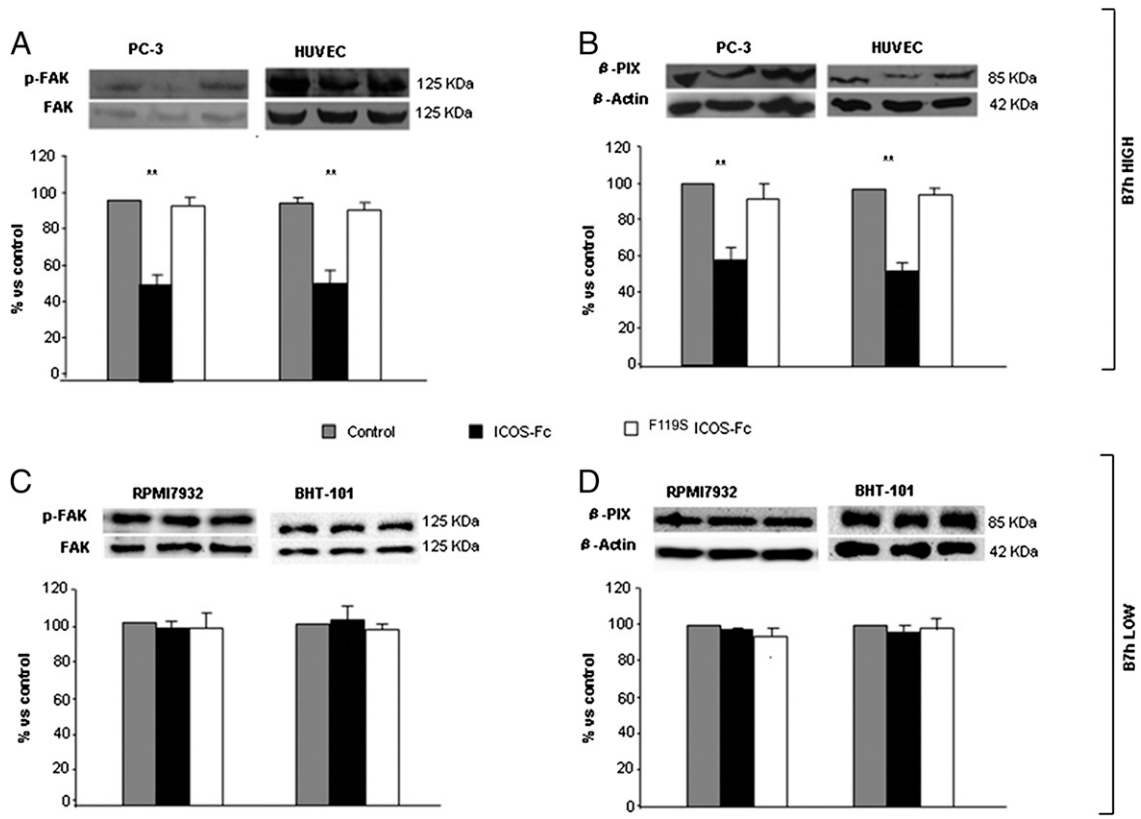

FIGURE 5. Effect of ICOS-Fc on FAK phosphorylation and β-Pix expression in the B7h^{high} (PC-3, HUVEC) and B7^{low} (RPMI7932, BHT-101) cell lines. The cell lines were treated with 4 μg/ml ICOS-Fc or ^{F119S}ICOS-Fc for 30 min; p-FAK (**A** and **C**) and β-Pix (**B** and **D**) expression were then evaluated via Western blot in the cell lysates. The same blots were also probed with anti-FAK or anti–β-actin Ab as a control. The bar graphs show the densitometric analysis of the gels expressed in arbitrary units; data are expressed as the mean ± SEM of the percentage of inhibition versus the control from three independent experiments (**$p < 0.01$ versus the control).

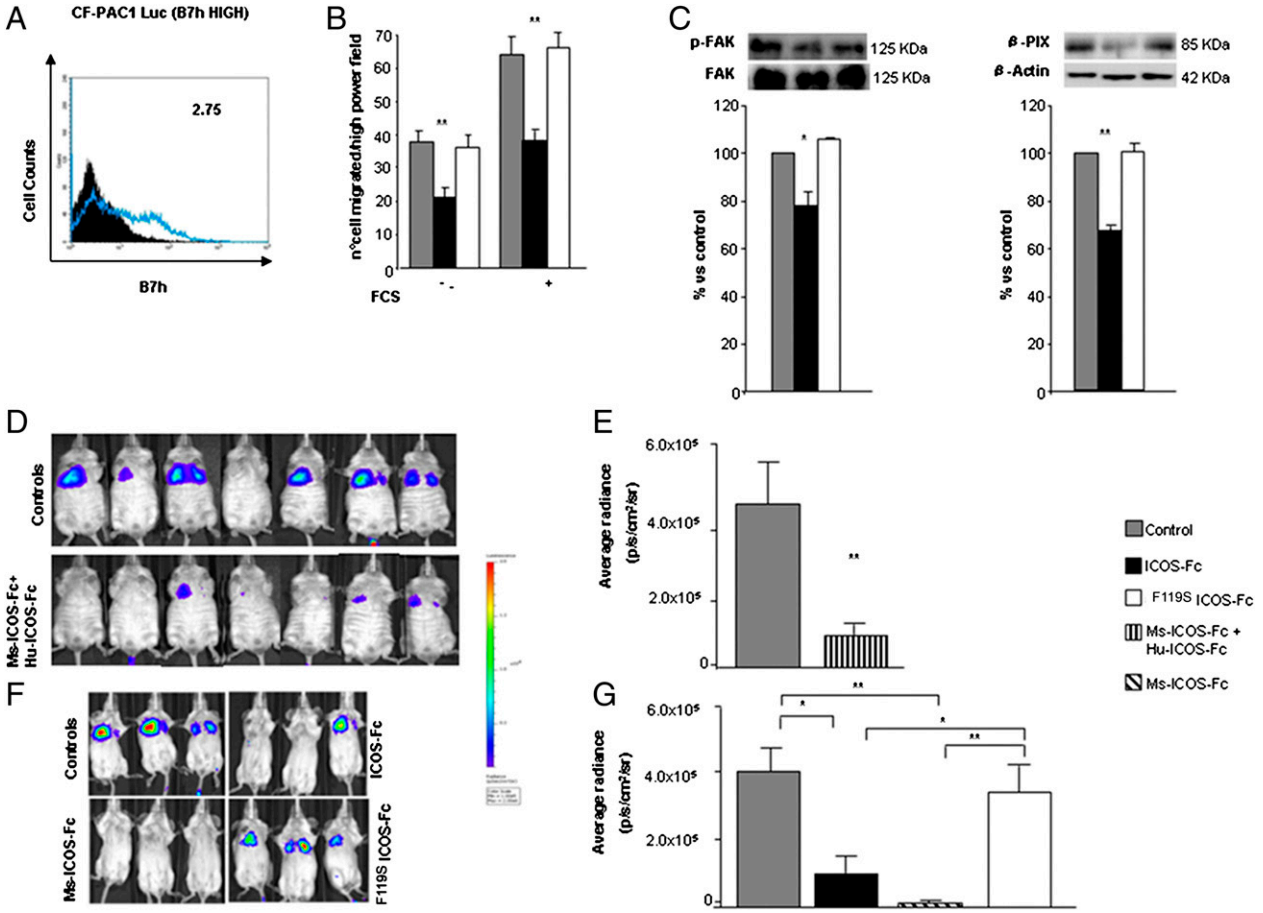

FIGURE 6. Effects of B7h triggering on CF-PAC1 tumor cell metastasis in vivo. (**A**) Cytofluorimetric analysis of B7h expression in the CF-PAC1 Luc cells (performed as in Fig. 1). (**B**) Effect of ICOS-Fc on the migration of the CF-PAC1 Luc cells in the Boyden chamber assay (performed as in Fig. 2). (**C**) Effect of ICOS-Fc on the expression of p-FAK and β-Pix (performed as in Fig. 5). (**D** and **E**) Mice were injected i.v. with 0.5×10^6 CF-PAC1 Luc cells and treated with the human ICOS-Fc plus mouse ICOS-Fc ($n = 7$) or PBS (control group, $n = 7$). (**F** and **G**) The mice injected with CF-PAC1 Luc were treated with either the human ICOS-Fc ($n = 3$), mouse ICOS-Fc ($n = 3$), human ^{F119S}ICOS-Fc ($n = 3$), or PBS (control group, $n = 3$). After 3 d, the mice were i.p. injected with luciferin, and pulmonary metastases were macroscopically detectable and documented via in vivo optical imaging. The luminescent signal was quantified as the average radiance (p/s/cm^2/sr), which was measured in regions of interest drawn in the lungs. Data are expressed as the mean ± SEM and were obtained in two independent experiments (*$p < 0.05$, **$p < 0.01$).

detectable on the lung surface. Both approaches showed that the mice treated with the mouse ICOS-Fc displayed significantly fewer metastases than those treated with either PBS or the human ^{F119S}ICOS-Fc (Fig. 7A, 7B). To determine whether the treatments modulated the immune response, we obtained infiltrating cells from the lungs, and we evaluated the mRNA levels of IL-17A and RORc (marking Th17 cells), IL-10 and Foxp3 (marking regulatory T cells [Tregs]), and IL-21 and Bcl6 (marking T follicular helper cells) via real-time PCR (because ICOS has a key role in Th17, Treg, and T follicular helper cell function) (3, 13–15). The results showed that treatment with the mouse ICOS-Fc significantly increased the expression of IL-17A and RORc, and decreased that of IL-10 and Foxp3 compared with the levels detected in control mice and those treated with the human ^{F119S}ICOS-Fc (Fig. 7C). In contrast, no differences were detected in the expression of Bcl6, whereas IL-21 was always undetectable (data not shown). Moreover, ICOS-Fc did not modulate the expression of these molecules in the control mice not injected with the B16-F10 cells; in these mice, Foxp3 and Bcl6 were expressed at low levels, whereas IL-17A, RORc, IL-10, and IL-21 were undetectable (data not shown).

To assess whether treatment with ICOS-Fc decreased β-Pix expression and FAK phosphorylation in vivo, the C57BL/6 mice were injected s.c. with 10^6 B7h^{high} B16-F10 cells. When the tumor diameter reached 4 mm, the mice received one intratumor injection of either the mouse ICOS-Fc, human ^{F119S}ICOS-Fc, or the same volume of PBS. After 30 min, the tumors were excised, and β-Pix expression and FAK phosphorylation were assessed in the tissue lysates via Western blot. The results showed that treatment with ICOS-Fc, but not with ^{F119S}ICOS-Fc, substantially decreased the expression of β-Pix compared with that detected in the control mice (Fig. 7D). The FAK expression was similar in all conditions, and the phospho-FAK expression was always undetectable (data not shown).

Discussion

Cancer progression involves a complex interplay between the tumor and the microenvironment that results in sustained proliferative signaling, resistance to cell death, as well as the promotion of angiogenesis, invasion, and metastasis (20–23). This work has shown that ICOS binding to B7h influences several of these events by acting on both ECs and tumor cells. These effects were specific; they were not displayed by a mutated form of ICOS-Fc that was incapable of binding B7h.

The most striking effect was that on tumor cells: ICOS-Fc inhibited EMT and migration in vitro, as well as metastasis in vivo. EMT is a transdifferentiation program required for tissue morphogenesis during the embryonic development; its induction is exploited by cancer cells to acquire invasive and metastatic properties. Recent

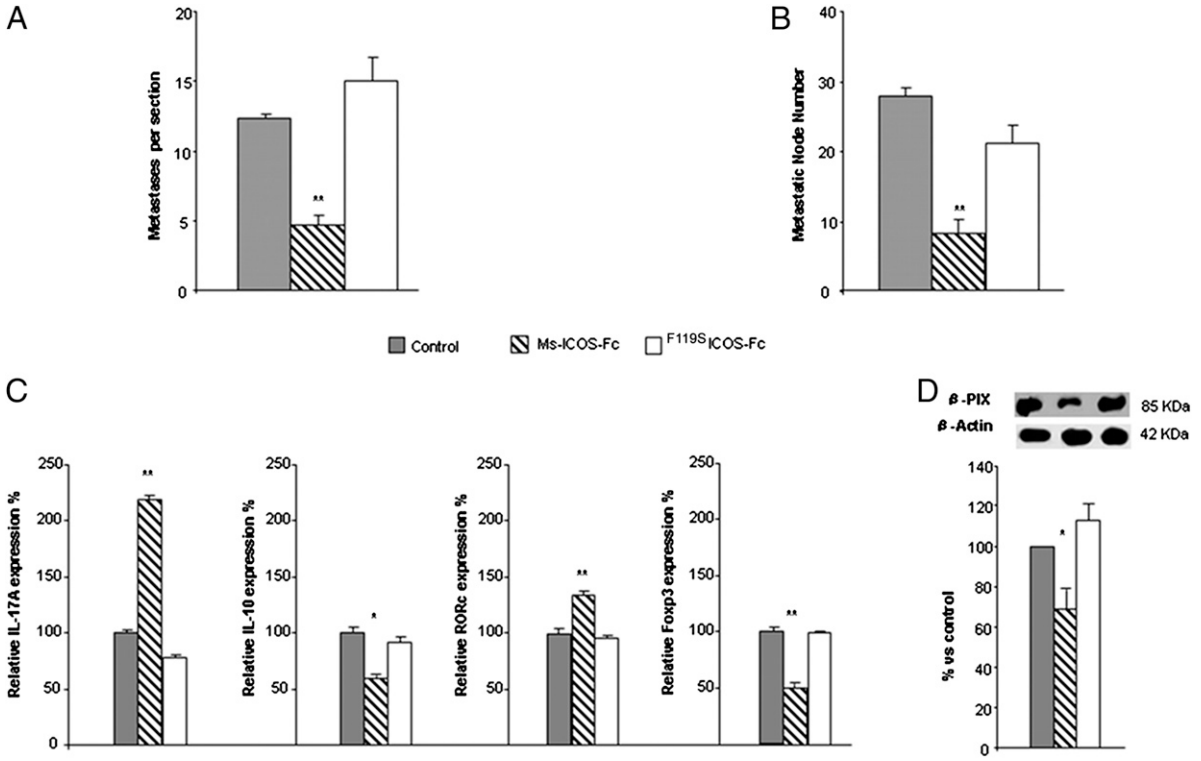

FIGURE 7. Effect of B7h triggering on B16-F10 cells in vivo. (**A** and **B**) Effect on metastasis in C57BL/6 mice injected in the tail vein with 10^6 B7h^{high} B16-F10 cells and treated daily with either the mouse ICOS-Fc ($n = 3$), human ^{F119S}ICOS-Fc ($n = 3$), or the same volume of PBS (control group, $n = 3$). The lung metastases were analyzed either after 3 d (on tissue sections stained with H&E) (A) or after 2 wk by counting the detectable tumor nodules on the lung surface (B); (**C**) infiltrating cells from the 3-d experiment were harvested and used for the real-time PCR analysis of IL-17A, IL-10, RORc, and Foxp3 expression; the data are normalized for the expression in the control mice (control expression set at 100%). (**D**) Effect on β-Pix expression in s.c. tumors treated with an intratumoral injection of either the mouse ICOS-Fc, human ^{F119S}ICOS-Fc, or the same volume of PBS. The C57BL/6 mice were s.c. injected with 10^6 B7h^{high} B16-F10 cells, and the tumors were treated when they reached 4 mm in diameter. The β-Pix expression was evaluated via Western blot in the lysates of the tumor tissue. The data are expressed as the mean ± SEM and were obtained from three experiments ($*p < 0.05$, $**p < 0.01$).

reports indicate that EMT is also involved in the emergence of cancer stem cells and contributes to drug resistance (24). A classical inducer of EMT is HGF (also known as scatter factor), which promotes an "invasive growth" of epithelial cells that is characterized by the disruption of intercellular contacts and the induction of cell motility, survival, and proliferation (19, 25). Our experiments on HepG2 cells show that ICOS-Fc effectively impairs their HGF-induced scattering by preserving the epithelial morphology and strongly reducing the HGF-induced migration. These findings suggest that ICOS-Fc could also affect EMT in vivo and decrease the metastatic potential of tumor cells.

To successfully metastasize (after the downregulation of cell-to-cell junctions and the acquisition of a migratory phenotype), tumor cells must invade the extracellular matrix and intravasate; they will then disseminate and become sites of origin for future metastases. Cell movement across the tissues plays a crucial role in several of these steps. Thus, a major aim in modern cancer therapy strategies is to counteract metastatic spreading by targeting the factors involved in the migratory activity of tumor cells. This has been mainly achieved using antagonists of the molecules involved in the adhesion of these cells to the extracellular matrix (26), as well as antagonists of proteases that facilitate cell migration by degrading the extracellular matrix (27–29). Unfortunately, none of these compounds has yet reached the market, primarily because of poor in vivo antitumor activity, unsuitable therapeutic index, or the rapid development of chemoresistance. This work suggests that B7h may be a novel target for these therapies because ICOS-Fc inhibits the migration of several tumor cell lines in vitro. This effect is not ascribable to drug toxicity because the proliferation and survival of tumor cells are not affected by ICOS-Fc. Moreover, this effect is specific; it is not detected in tumor cell lines expressing low levels of B7h.

This underlines a potential pharmacological limitation of ICOS-Fc, the efficacy of which is expected to be restricted to B7h^{high} tumors. It is intriguing that the migratory response to FCS appeared to be weaker in the B7h^{low} than in the B7h^{high} cell lines and that the B7h^{low} B16-F10 cells displayed lower migratory activity than their B7h^{high} counterparts, which suggests that B7h may play a direct role in cell migration. The antimetastatic effect of ICOS-Fc is supported by our in vivo experiments showing that treatment with ICOS-Fc inhibits the migration of both a human (CF-PAC1 Luc) and a mouse (B16-F10) tumor cell line into the lungs in mice. It is noteworthy that this effect was induced by both the human and the mouse ICOS-Fc in the CF-PAC1 Luc human/mouse model, which indicates that the effect was ascribable to the triggering of both varieties of B7h on the tumor cells, as well as the ECs. The human ICOS-Fc does not bind the mouse B7h, and the mouse ICOS-Fc weakly binds the human B7h (data not shown).

These data strengthen those obtained from previous research showing that ICOS-Fc inhibits tumor cell adhesion to ECs by acting on both the tumor cells and the ECs (11). Moreover, in the B16-F10 model, treatment with ICOS-Fc increased the expression of IL-17A and RORc, and decreased the expression of IL-10 and Foxp3; this suggests that ICOS-Fc may also exert positive effects on the antitumor immune response by increasing the Th17/Treg ratio. This observation is in accordance with reports showing that the triggering of B7h in immature mouse DCs induces partial maturation with the prominent augmentation of IL-6 secretion (17), as

well as reports indicating that IL-6 supports the conversion of $Foxp3^+CD4^+$ Tregs to Th17 cells (30). Moreover, we found that B7h triggering in human DCs increases the secretion of IL-23 (which is involved in Th17 expansion and survival) and supports Th17 cell activity (18). Finally, ICOS triggering in T cells (which is blocked by ICOS-Fc) is involved in the differentiation of both Tregs and Th17 cells (17, 31–33); however, its support of Treg differentiation prevails in the tumor environment (34, 35).

The possibility that ICOS-Fc may also affect tumor angiogenesis is suggested by the finding that it substantially inhibits the migration of vascular ECs. However, it does not inhibit EC proliferation or angiogenesis, as determined via the tubulogenesis and the sprouting assays, which indicates that the residual migratory potential of ECs is sufficient for these in vitro assays. However, this does not rule out the possibility that ICOS-Fc may be effective in limiting conditions in vivo. The antiangiogenic potential of ICOS-Fc is intriguing because the survival of the primary tumor beyond a certain size requires neovascularization of the tumor mass, and tumor-associated vessels represent a preferential pathway for metastasization to distant sites. Thus, controlling tumor-associated angiogenesis may limit cancer progression (21). However, clinical results from studies using individual antivascular agents have been unsatisfactory and have required the combinatorial use of conventional anticancer drugs and antivascular agents (22). Therefore, novel antivascular agents targeting B7h would be welcome in antitumor therapy.

In previous works, we demonstrated that B7h triggering inhibits the activation of the ERK and p38 axis induced in ECs via various proadhesive stimuli. This leads to cytoskeleton modifications with the disruption of the VE-cadherin/β-catenin complex and the formation of stress fibers involved in increasing the endothelial permeability and enabling the transendothelial migration of cancer cells (11). However, this is not a general effect because it was not detected in tumor cell lines (11) or DCs (18). In contrast, in DCs (18), ECs, and tumor cells (Fig. 6), ICOS-Fc downregulates the expression of β-Pix, which is a Rac-1 activator that is recruited by activated integrins and is required for rapid nascent adhesion turnover. Intriguingly, the downregulation of β-Pix expression is known to prevent cell spreading and lamellipodial formation, and to increase Rac1 activity (36, 37). Moreover, in ECs and tumor cells, B7h triggering inhibits the phosphorylation of FAK, which is a key mediator of signaling through integrins. The overexpression and activation of FAK have been found in a variety of human cancers and have been involved in cancer migration, invasion, EMT, and angiogenesis (38). FAK signaling has also been shown to promote angiogenesis in both embryonic development and tumor angiogenesis, and the increased phosphorylation and activation of FAK have been correlated with increased EC migration into wounded monolayers (39). The signaling pathways activated by B7h are presently unknown. In DCs, the engagement of B7.1 or B7.2 with CTLA4-Ig leads to the STAT-1–mediated production of IDO and decreased tryptophan levels (40, 41); however, it is unclear whether a similar signaling pathway is also activated by B7h.

Upon extrapolating these data to physiological conditions, it may be suggested that the physiological role of B7h-mediated signaling is based on its effect on invasion, which is involved not only in tumor progression (42), but also in tissue remodeling during embryonic development, wound healing, angiogenesis, and immune responses. In accordance with this possibility, the repair of excisional wounds was dramatically delayed in mice deficient in either ICOS or B7h; these mice showed decreased keratinocyte migration, angiogenesis, granulation tissue formation, and diminished infiltration of T cells, macrophages, and neutrophils (43). One possibility is that $B7h^+$ cells, which are recruited from the blood and the surrounding tissues for tissue defense and repair, are arrested in the injured tissue via B7h interacting with the ICOS that is expressed by the infiltrating T cells. Therefore, a defective B7h–ICOS interaction may eventually affect the accumulation of infiltrating cells in the injured tissue.

In conclusion, our data indicate that ICOS-Fc may be an effective antimetastasis drug acting on ECs and tumor cells both in vitro and in vivo. Therefore, ICOS-Fc (which affects cancer cell migration without severe toxic effects) may be a sound tool in cancer therapy that acts on several aspects of tumor progression.

Acknowledgments

We are grateful to the Obstetrics and Gynecology Unit, Martini Hospital, Torino, for providing human umbilical cords.

Disclosures

The authors have no financial conflicts of interest.

References

1. Greenwald, R. J., G. J. Freeman, and A. H. Sharpe. 2005. The B7 family revisited. *Annu. Rev. Immunol.* 23: 515–548.
2. Okazaki, T., Y. Iwai, and T. Honjo. 2002. New regulatory co-receptors: inducible co-stimulator and PD-1. *Curr. Opin. Immunol.* 14: 779–782.
3. Hutloff, A., A. M. Dittrich, K. C. Beier, B. Eljaschewitsch, R. Kraft, I. Anagnostopoulos, and R. A. Kroczek. 1999. ICOS is an inducible T-cell co-stimulator structurally and functionally related to CD28. *Nature* 397: 263–266.
4. Buonfiglio, D., M. Bragardo, S. Bonissoni, V. Redoglia, R. Cauda, S. Zupo, V. L. Burgio, H. Wolff, K. Franssila, G. Gaidano, et al. 1999. Characterization of a novel human surface molecule selectively expressed by mature thymocytes, activated T cells and subsets of T cell lymphomas. *Eur. J. Immunol.* 29: 2863–2874.
5. Buonfiglio, D., M. Bragardo, V. Redoglia, R. Vaschetto, F. Bottarel, S. Bonissoni, T. Bensi, C. Mezzatesta, C. A. Janeway, Jr., and U. Dianzani. 2000. The T cell activation molecule H4 and the CD28-like molecule ICOS are identical. *Eur. J. Immunol.* 30: 3463–3467.
6. Redoglia, V., U. Dianzani, J. M. Rojo, P. Portolés, M. Bragardo, H. Wolff, D. Buonfiglio, S. Bonissoni, and C. A. Janeway, Jr. 1996. Characterization of H4: a mouse T lymphocyte activation molecule functionally associated with the CD3/T cell receptor. *Eur. J. Immunol.* 26: 2781–2789.
7. Swallow, M. M., J. J. Wallin, and W. C. Sha. 1999. B7h, a novel costimulatory homolog of B7.1 and B7.2, is induced by TNFalpha. *Immunity* 11: 423–432.
8. Yoshinaga, S. K., J. S. Whoriskey, S. D. Khare, U. Sarmiento, J. Guo, T. Horan, G. Shih, M. Zhang, M. A. Coccia, T. Kohno, et al. 1999. T-cell co-stimulation through B7RP-1 and ICOS. *Nature* 402: 827–832.
9. Wang, S., G. Zhu, A. I. Chapoval, H. Dong, K. Tamada, J. Ni, and L. Chen. 2000. Costimulation of T cells by B7-H2, a B7-like molecule that binds ICOS. *Blood* 96: 2808–2813.
10. Xiao, J. X., P. S. Bai, B. C. Lai, L. Li, J. Zhu, and Y. L. Wang. 2005. B7 molecule mRNA expression in colorectal carcinoma. *World J. Gastroenterol.* 11: 5655–5658.
11. Dianzani, C., R. Minelli, R. Mesturini, A. Chiocchetti, G. Barrera, S. Boscolo, C. Sarasso, C. L. Gigliotti, D. Sblattero, J. Yagi, et al. 2010. B7h triggering inhibits umbilical vascular endothelial cell adhesiveness to tumor cell lines and polymorphonuclear cells. *J. Immunol.* 185: 3970–3979.
12. Minelli, R., L. Serpe, P. Pettazzoni, V. Minero, G. Barrera, C. L. Gigliotti, R. Mesturini, A. C. Rosa, P. Gasco, N. Vivenza, et al. 2012. Cholesteryl butyrate solid lipid nanoparticles inhibit the adhesion and migration of colon cancer cells. *Br. J. Pharmacol.* 166: 587–601.
13. Mesturini, R., S. Nicola, A. Chiocchetti, I. S. Bernardone, L. Castelli, T. Bensi, M. Ferretti, C. Comi, C. Dong, J. M. Rojo, et al. 2006. ICOS cooperates with CD28, IL-2, and IFN-gamma and modulates activation of human naïve CD4+ T cells. *Eur. J. Immunol.* 36: 2601–2612.
14. Mesturini, R., C. L. Gigliotti, E. Orilieri, G. Cappellano, M. F. Soluri, E. Boggio, A. Woldetsadik, C. Dianzani, D. Sblattero, A. Chiocchetti, et al. 2013. Differential induction of IL-17, IL-10, and IL-9 in human T helper cells by B7h and B7.1. *Cytokine* 64: 322–330.
15. Franko, J. L., and A. D. Levine. 2009. Antigen-independent adhesion and cell spreading by inducible costimulator engagement inhibits T cell migration in a PI-3K-dependent manner. *J. Leukoc. Biol.* 85: 526–538.
16. Yong, P. F., U. Salzer, and B. Grimbacher. 2009. The role of costimulation in antibody deficiencies: ICOS and common variable immunodeficiency. *Immunol. Rev.* 229: 101–113.
17. Tang, G., Q. Qin, P. Zhang, G. Wang, M. Liu, Q. Ding, Y. Qin, and Q. Shen. 2009. Reverse signaling using an inducible costimulator to enhance immunogenic function of dendritic cells. *Cell. Mol. Life Sci.* 66: 3067–3080.
18. Occhipinti, S., C. Dianzani, A. Chiocchetti, E. Boggio, N. Clemente, C. L. Gigliotti, M. F. Soluri, R. Minelli, R. Fantozzi, J. Yagi, et al. 2013. Triggering of B7h by the inducible costimulator modulates maturation and migration of monocyte-derived dendritic cells. *J. Immunol.* 190: 1125–1134.
19. Pan, F. Y., S. Z. Zhang, N. Xu, F. L. Meng, H. X. Zhang, B. Xue, X. Han, and C. J. Li. 2010. Beta-catenin signaling involves HGF-enhanced HepG2 scattering through activating MMP-7 transcription. *Histochem. Cell Biol.* 134: 285–295.

20. Hanahan, D., and R. A. Weinberg. 2011. Hallmarks of cancer: the next generation. *Cell* 144: 646–674.
21. Weis, S. M., and D. A. Cheresh. 2011. Tumor angiogenesis: molecular pathways and therapeutic targets. *Nat. Med.* 17: 1359–1370.
22. Mizukami, Y., J. Sasajima, T. Ashida, and Y. Kohgo. 2012. Abnormal tumor vasculatures and bone marrow-derived pro-angiogenic cells in cancer. *Int. J. Hematol.* 95: 125–130.
23. Hayot, C., O. Debeir, P. Van Ham, M. Van Damme, R. Kiss, and C. Decaestecker. 2006. Characterization of the activities of actin-affecting drugs on tumor cell migration. *Toxicol. Appl. Pharmacol.* 211: 30–40.
24. Singh, A., and J. Settleman. 2010. EMT, cancer stem cells and drug resistance: an emerging axis of evil in the war on cancer. *Oncogene* 29: 4741–4751.
25. Boccaccio, C., and P. M. Comoglio. 2006. Invasive growth: a MET-driven genetic programme for cancer and stem cells. *Nat. Rev. Cancer* 6: 637–645.
26. Sawyer, T. K. 2004. Cancer metastasis therapeutic targets and drug discovery: emerging small-molecule protein kinase inhibitors. *Expert Opin. Investig. Drugs* 13: 1–19.
27. Zucker, S., J. Cao, and W. T. Chen. 2000. Critical appraisal of the use of matrix metalloproteinase inhibitors in cancer treatment. *Oncogene* 19: 6642–6650.
28. Coussens, L. M., B. Fingleton, and L. M. Matrisian. 2002. Matrix metalloproteinase inhibitors and cancer: trials and tribulations. *Science* 295: 2387–2392.
29. Overall, C. M., and C. López-Otín. 2002. Strategies for MMP inhibition in cancer: innovations for the post-trial era. *Nat. Rev. Cancer* 2: 657–672.
30. Komatsu, N., K. Okamoto, S. Sawa, T. Nakashima, M. Oh-hora, T. Kodama, S. Tanaka, J. A. Bluestone, and H. Takayanagi. 2014. Pathogenic conversion of Foxp3+ T cells into TH17 cells in autoimmune arthritis. *Nat. Med.* 20: 62–68.
31. Park, H., Z. Li, X. O. Yang, S. H. Chang, R. Nurieva, Y. H. Wang, Y. Wang, L. Hood, Z. Zhu, Q. Tian, and C. Dong. 2005. A distinct lineage of CD4 T cells regulates tissue inflammation by producing interleukin 17. *Nat. Immunol.* 6: 1133–1141.
32. Paulos, C. M., C. Carpenito, G. Plesa, M. M. Suhoski, A. Varela-Rohena, T. N. Golovina, R. G. Carroll, J. L. Riley, and C. H. June. 2010. The inducible costimulator (ICOS) is critical for the development of human T(H)17 cells. *Sci. Transl. Med.* 2: 55ra78.
33. Ito, T., S. Hanabuchi, Y. H. Wang, W. R. Park, K. Arima, L. Bover, F. X. Qin, M. Gilliet, and Y. J. Liu. 2008. Two functional subsets of FOXP3+ regulatory T cells in human thymus and periphery. *Immunity* 28: 870–880.
34. Strauss, L., C. Bergmann, M. J. Szczepanski, S. Lang, J. M. Kirkwood, and T. L. Whiteside. 2008. Expression of ICOS on human melanoma-infiltrating CD4+CD25highFoxp3+ T regulatory cells: implications and impact on tumor-mediated immune suppression. *J. Immunol.* 180: 2967–2980.
35. Martin-Orozco, N., Y. Li, Y. Wang, S. Liu, P. Hwu, Y. J. Liu, C. Dong, and L. Radvanyi. 2010. Melanoma cells express ICOS ligand to promote the activation and expansion of T-regulatory cells. *Cancer Res.* 70: 9581–9590.
36. Schmidt, M. H., K. Husnjak, I. Szymkiewicz, K. Haglund, and I. Dikic. 2006. Cbl escapes Cdc42-mediated inhibition by downregulation of the adaptor molecule betaPix. *Oncogene* 25: 3071–3078.
37. Lee, J., I. D. Jung, W. K. Chang, C. G. Park, D. Y. Cho, E. Y. Shin, D. W. Seo, Y. K. Kim, H. W. Lee, J. W. Han, and H. Y. Lee. 2005. p85 beta-PIX is required for cell motility through phosphorylations of focal adhesion kinase and p38 MAP kinase. *Exp. Cell Res.* 307: 315–328.
38. Zhao, J., and J. L. Guan. 2009. Signal transduction by focal adhesion kinase in cancer. *Cancer Metastasis Rev.* 28: 35–49.
39. Romer, L. H., N. McLean, C. E. Turner, and K. Burridge. 1994. Tyrosine kinase activity, cytoskeletal organization, and motility in human vascular endothelial cells. *Mol. Biol. Cell* 5: 349–361.
40. Orabona, C., U. Grohmann, M. L. Belladonna, F. Fallarino, C. Vacca, R. Bianchi, S. Bozza, C. Volpi, B. L. Salomon, M. C. Fioretti, et al. 2004. CD28 induces immunostimulatory signals in dendritic cells via CD80 and CD86. *Nat. Immunol.* 5: 1134–1142.
41. Grohmann, U., C. Orabona, F. Fallarino, C. Vacca, F. Calcinaro, A. Falorni, P. Candeloro, M. L. Belladonna, R. Bianchi, M. C. Fioretti, and P. Puccetti. 2002. CTLA-4-Ig regulates tryptophan catabolism in vivo. *Nat. Immunol.* 3: 1097–1101.
42. Sliva, D. 2004. Signaling pathways responsible for cancer cell invasion as targets for cancer therapy. *Curr. Cancer Drug Targets* 4: 327–336.
43. Maeda, S., M. Fujimoto, T. Matsushita, Y. Hamaguchi, K. Takehara, and M. Hasegawa. 2011. Inducible costimulator (ICOS) and ICOS ligand signaling has pivotal roles in skin wound healing via cytokine production. *Am. J. Pathol.* 179: 2360–2369.

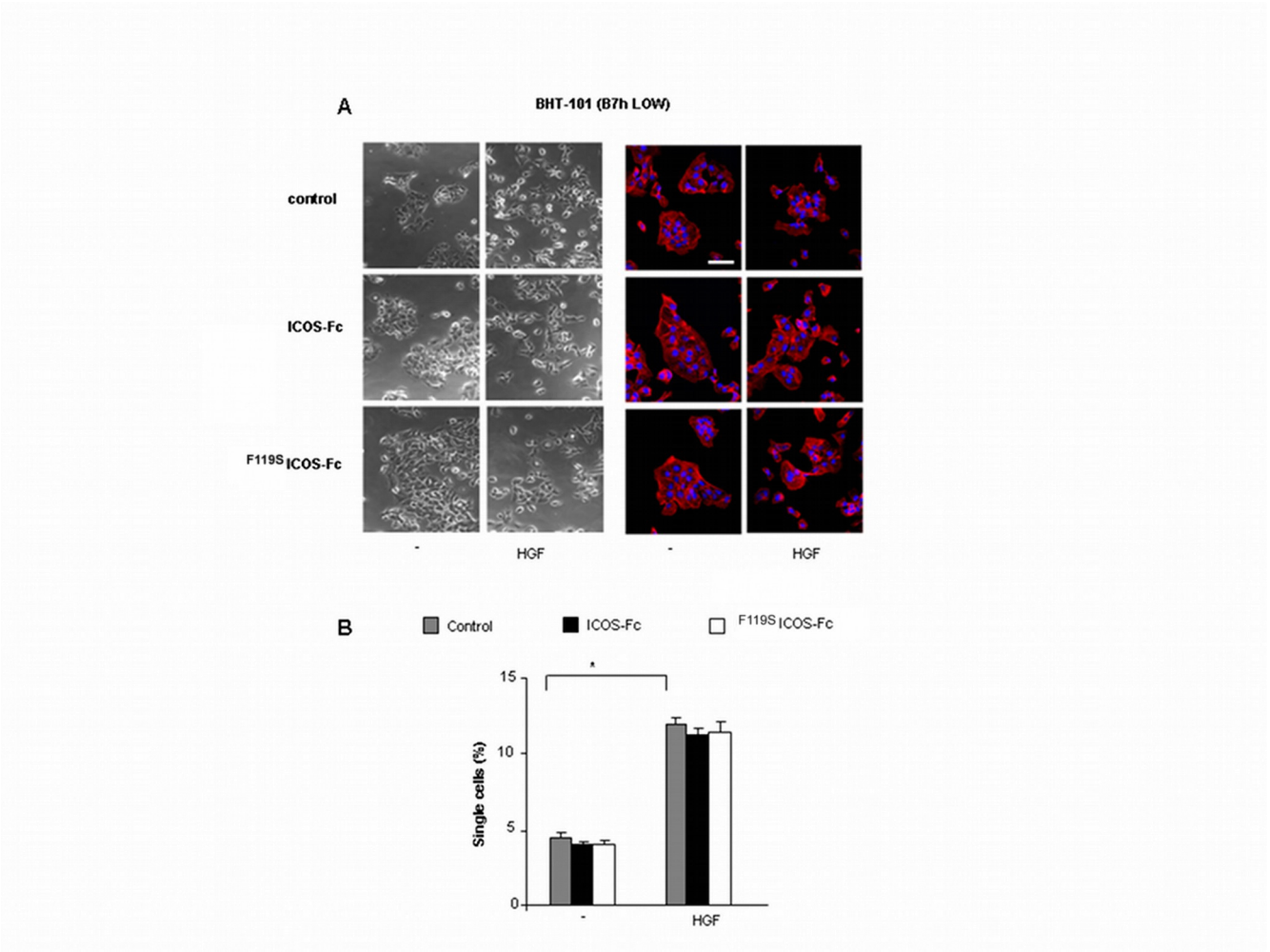

FIGURE S1: ICOS-Fc does not affect HGF induced cells scatter in BHT-101.Cells were treated for 24 h with or without HGF (50 ng/ml), ICOS-Fc (2 µg/ml) or ^{F119S}ICOS-Fc (2 µg/ml). (**A**) Cells were photographed by phase contrast (*left panel*) or stained with Phalloidin-Alexa-Fluor 546 (red) / TO-PRO 3 (blue) (*right panel*) and imaged by confocal microscopy. Scale bar 40 µm. (**B**) Percentage of disaggregated single cells (mean±SEM of 4 experiments); at least 100 cells were counted for each point (* $P < 0.01$).

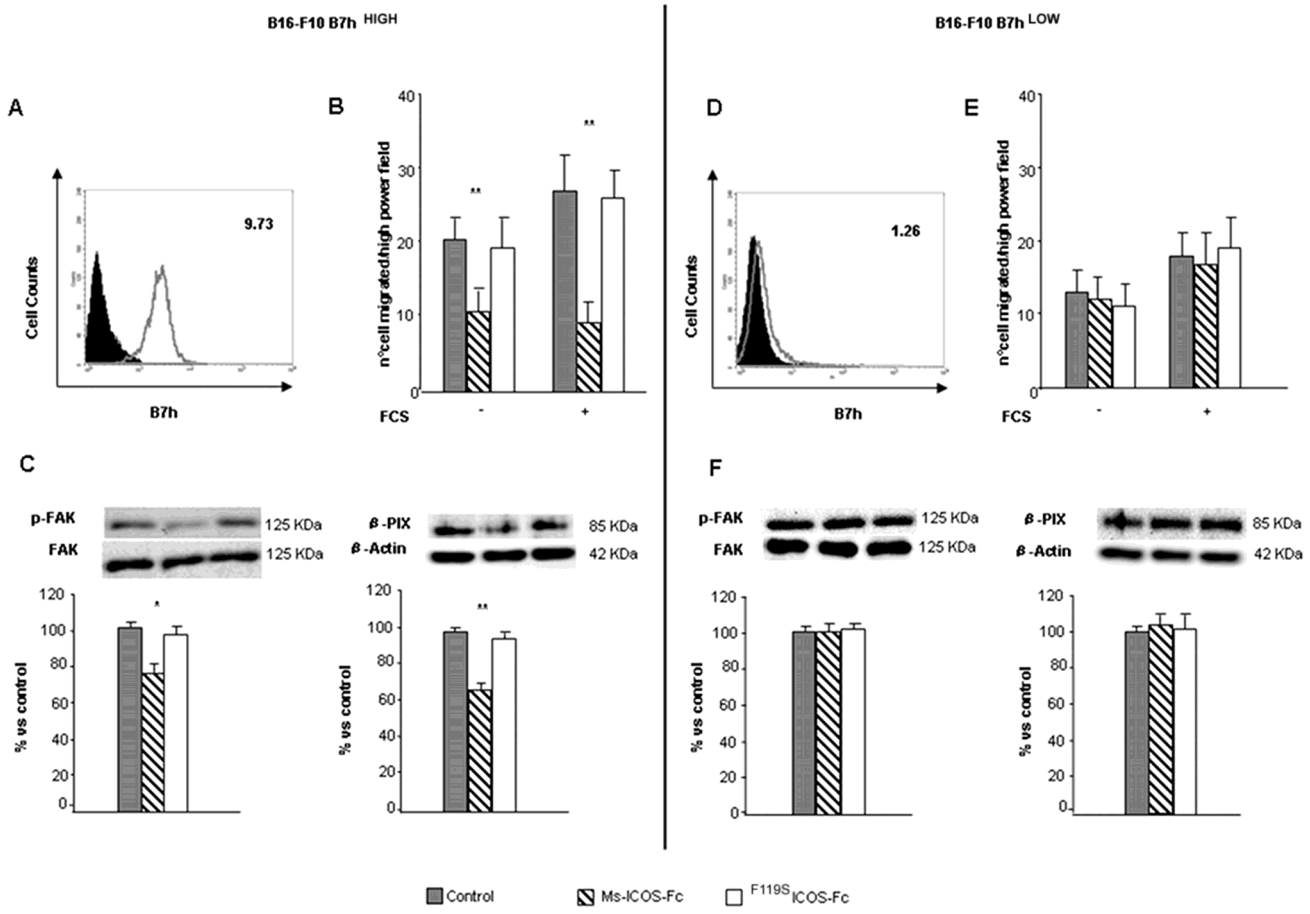

FIGURE S2: Effect of ICOS-Fc on B7h^{high} and B7h^{low} B16-F10 cells *in vitro*. (**A, D**) Cytofluorimetric analysis of B7h expression performed as in Fig. 1. (**B, E**) Effect of ICOS-Fc on cell migration in the Boyden chamber assay performed as in Fig. 2. (**C, F**) Effect of ICOS-Fc on FAK phosphorylation (*left panel*) and β-Pix expression (*right panel*) performed as in Fig. 5. Data are expressed as mean±SEM from 3 independent experiments (** P<0.01, * P<0.05 versus the control).

Acknowledgments

First and foremost, I would like to express my gratitude to Prof. Andrea Graziani, for giving me the opportunity to conduct my PhD in his laboratory. All I know about this amazing job comes from him. I also wish to thank my supervisor Dr. Gianluca Baldanzi for his unlimited patience, constant support and for being a “map” during my PhD. Without him I would have lost.

I would like to thank Prof. Andrew L. Snow and his PhD student, Sasha Larsen, for all the experiments conducted on XLP1 patients’ samples, and MD Kim E. Nichols with Das Rupali, for the *in vivo* experiments. Many thanks to all of them for helpful discussions, and for the intense and fundamental work they put in this project.

Many thanks to Dr. Ignacio Rubio, who was a terrific supervisor during the months I’ve spent in his wonderful lab in Germany, and Govind, Anne, Stephanie, Katha and Ute, who shared with me their precious advices in the lab, and wonderful time outside the lab. I want to extend this acknowledgment to all the third floor of the CMB Institute in Jena, especially to Govind, Jörg, Ben, Matthias, Odeta, Nderim, Dimitris, and Martina; they made every single day of my German experience so special. Many thanks to Christoph Biskup, who spent his nights and free time with me in preparing the algoritm, which is described in this thesis.

Finally, I would like to thank all the past and present members of the laboratory. A big, big thank you goes to Valentina for being always an amazing colleague and friend in the lab, and Elisa, for her helpful contribution in this project. Many thanks to Daniela and her group, Stefania and Pasquale, for always involving me in the scientific discussions and future projects.
I’m grateful to the ghrelin group, led by Nicoletta, particularly to “The Three Musketeers” Elia, Michele and Simone, for the constant scientific support and for being really good friends.

Most importantly, I thank my beloved parents and sister. Thank you for always being there, for guiding me and encouraging me through this journey.

Bibliography

1. Rainero, E., et al., *The diacylglycerol kinase alpha/atypical PKC/beta1 integrin pathway in SDF-1alpha mammary carcinoma invasiveness.* PLoS One, 2014. **9**(6): p. e97144.
2. Dianzani, C., et al., *B7h triggering inhibits the migration of tumor cell lines.* J Immunol, 2014. **192**(10): p. 4921-31.
3. Neefjes, J., et al., *Towards a systems understanding of MHC class I and MHC class II antigen presentation.* Nat Rev Immunol, 2011. **11**(12): p. 823-36.
4. Brownlie, R.J. and R. Zamoyska, *T cell receptor signalling networks: branched, diversified and bounded.* Nat Rev Immunol, 2013. **13**(4): p. 257-69.
5. Weiss, A. and D.R. Littman, *Signal transduction by lymphocyte antigen receptors.* Cell, 1994. **76**(2): p. 263-274.
6. Kroczek, R.A., H.W. Mages, and A. Hutloff, *Emerging paradigms of T-cell co-stimulation.* Curr Opin Immunol, 2004. **16**(3): p. 321-7.
7. Asada, A., et al., *The calcium-independent protein kinase C participates in an early process of CD3/CD28-mediated induction of thymocyte apoptosis.* Immunology, 2000. **101**: p. 309-315.
8. Zha, Y., et al., *T cell anergy is reversed by active Ras and is regulated by diacylglycerol kinase-alpha.* Nat Immunol, 2006. **7**(11): p. 1166-73.
9. Baniyash, M., *TCR zeta-chain downregulation: curtailing an excessive inflammatory immune response.* Nat Rev Immunol, 2004. **4**(9): p. 675-87.
10. Di Bartolo, V., et al., - *Tyrosine 319, a Newly Identified Phosphorylation Site of ZAP-70, Plays a Critical Role in T Cell Antigen Receptor Signaling.* - J Biol Chem, 1999. **274 (10)**(-0021-9258 (Print)): p. 6285-94.
11. Wang, H., et al., *ZAP-70: an essential kinase in T-cell signaling.* Cold Spring Harb Perspect Biol, 2010. **2**(5): p. a002279.
12. Finco, T., et al., *LAT Is Required for TCR-Mediated Activation of PLCgamma1 and the Ras Pathway.* Immunity, 1998. **Vol. 9**: p. 617–626.
13. Jackman, J., et al., *Molecular cloning of SLP-76, a 76-kDa tyrosine phosphoprotein associated with Grb2 in T cells*, in *J Biol Chem,* 1995.
14. Rossy, J., et al., *The integration of signaling and the spatial organization of the T cell synapse.* Front Immunol, 2012. **3**: p. 352.
15. Andreotti, A.H., et al., *T-cell signaling regulated by the Tec family kinase, Itk.* Cold Spring Harb Perspect Biol, 2010. **2**(7): p. a002287.
16. Huang, Y.H. and K. Sauer, *Lipid signaling in T-cell development and function.* Cold Spring Harb Perspect Biol, 2010. **2**(11): p. a002428.
17. Rao, A., L. Chun, and P. Hogan, *TRANSCRIPTION FACTORS OF THE NFAT FAMILY: Regulation and Function.* Annu. Rev. Immunol., 1997. **15**: p. 707-47.
18. Penninger, J.M. and G.R. Crabtree, *The Actin Cytoskeleton and Lymphocyte Activation.* Cell, 1999. **96**: p. 9-12.
19. Mellor, H. and P. Parker, *The extended protein kinase C superfamily.* Biochem. J., 1998. **332**: p. 281-292.
20. Monks, C., et al., *Selective modulation of protein kinase C-θ during T-cell activation.* Nature, 1997. **385**.
21. Altman, A. and M. Villaba, *Protein kinase C-y (PKCy): it's all about location, location, location.* Immunological Reviews, 2003. **192**: p. 53-63.
22. Ebinu, J., et al., *RasGRP links T-cell receptor signaling to Ras.* Blood, 2000. **95**(10): p. 3199-3203.

23. Quann, E.J., et al., *A cascade of protein kinase C isozymes promotes cytoskeletal polarization in T cells.* Nat Immunol, 2011. **12**(7): p. 647-54.
24. Jun, J.E., I. Rubio, and J.P. Roose, *Regulation of ras exchange factors and cellular localization of ras activation by lipid messengers in T cells.* Front Immunol, 2013. **4**: p. 239.
25. Ebinu, J., et al., *RasGRP, a Ras guanyl nucleotide- releasing protein with calcium- and diacylglycerol-binding motifs.* Science, 1998. **280**(5366): p. 1082-6.
26. Roose, J.P., et al., *A diacylglycerol-protein kinase C-RasGRP1 pathway directs Ras activation upon antigen receptor stimulation of T cells.* Mol Cell Biol, 2005. **25**(11): p. 4426-41.
27. Roose, J.P., et al., *Unusual interplay of two types of Ras activators, RasGRP and SOS, establishes sensitive and robust Ras activation in lymphocytes.* Mol Cell Biol, 2007. **27**(7): p. 2732-45.
28. Genot, E., et al., *Multiple p2lras effector pathways regulate nuclear factor of activated T cells.* EMBO J, 1996. **15**(15): p. 3923-3933.
29. Gupta, S. and R.J. Davis, *MAP kinase binds to the NH2-terminal activation domain of c-Myc.* FEBS Letters, 1994. **353**: p. 281-285.
30. Rincon, M., R. Flavell, and R. Davis, *Signal transduction by MAP kinases in T lymphocytes.* Oncogene, 2001. **20**: p. 2490-2497.
31. Bommhardt, U., et al., *MEK Activity Regulates Negative Selection of Immature CD4+CD8+ Thymocytes.* The Journal of Immunology, 2000. **164**(5): p. 2326-2337.
32. Slagsvold, H.H., et al., *Nuclear receptor and apoptosis initiator NGFI-B is a substrate for kinase ERK2.* Biochem Biophys Res Commun, 2002. **291**(5): p. 1146-50.
33. Wingate, A.D., et al., *Nur77 is phosphorylated in cells by RSK in response to mitogenic stimulation.* Biochem J, 2006. **393**(Pt 3): p. 715-24.
34. Wang, A., et al., *Phosphorylation of Nur77 by the MEK-ERK-RSK cascade induces mitochondrial translocation and apoptosis in T cells.* J Immunol, 2009. **183**(5): p. 3268-77.
35. Lin, B., et al., *Conversion of Bcl-2 from Protector to Killer by Interaction with Nuclear Orphan Receptor Nur77/TR3.* Cell, 2004. **116**: p. 527–540.
36. Thompson, J., et al., *Protein kinase C regulates mitochondrial targeting of Nur77 and its family member Nor-1 in thymocytes undergoing apoptosis.* Eur J Immunol, 2010. **40**(7): p. 2041-9.
37. Grakoui, A., et al., *The immunological synapse: a molecular machine controlling T cell activation.* Science, 1999. **285**(5425): p. 221-227.
38. Monks, C., et al., *Three-dimensional segregation of supramolecular activation clusters in T cells.* Nature, 1998. **395**: p. 82-86.
39. Dustin, M.L. and T.A. Springer, *T-cell receptor cross-linking transiently stimulates adhesiveness through LFA-1* Nature, 1989. **341**: p. 619-624.
40. Mittelbrunn, M., et al., *VLA-4 integrin concentrates at the peripheral supramolecular activation complex of the immune synapse and drives T helper 1 responses.* Proc Natl Acad Sci U S A, 2004. **101**(30): p. 11058-63.
41. Dustin, M.L., A.K. Chakraborty, and A.S. Shaw, *Understanding the structure and function of the immunological synapse.* Cold Spring Harb Perspect Biol, 2010. **2**(10): p. a002311.
42. Cemerski, S., et al., *The balance between T cell receptor signaling and degradation at the center of the immunological synapse is determined by antigen quality.* Immunity, 2008. **29**(3): p. 414-22.
43. Varma, R., et al., *T Cell Receptor-Proximal Signals Are Sustained in Peripheral Microclusters and Terminated in the Central Supramolecular Activation Cluster.* Immunity, 2006. **25**(1): p. 117-127.

44. Lee, K., et al., *T cell receptor signaling precedes immunological synapse formation.* Science, 2002. **295**(5559): p. 1539-42.
45. Lee, K., et al., *The immunological synapse balances T cell receptor signaling and degradation.* Science, 2003. **302**(5648): p. 1218-22.
46. Stinchcombe, J.C., et al., *Centrosome polarization delivers secretory granules to the immunological synapse.* Nature, 2006. **443**(7110): p. 462-5.
47. Huse, M., *Microtubule-organizing center polarity and the immunological synapse: protein kinase C and beyond.* Front Immunol, 2012. **3**: p. 235.
48. Spitaler, M., et al., *Diacylglycerol and protein kinase D localization during T lymphocyte activation.* Immunity, 2006. **24**(5): p. 535-46.
49. Basu, R., et al., *The variable hinge region of novel PKCs determines localization to distinct regions of the immunological synapse.* PLoS One, 2014. **9**(4): p. e95531.
50. Billadeau, D.D., J.C. Nolz, and T.S. Gomez, *Regulation of T-cell activation by the cytoskeleton.* Nat Rev Immunol, 2007. **7**(2): p. 131-43.
51. de Saint Basile, G., G. Menasche, and A. Fischer, *Molecular mechanisms of biogenesis and exocytosis of cytotoxic granules.* Nat Rev Immunol, 2010. **10**(8): p. 568-79.
52. Chauveau, A., et al., *Diacylglycerol kinase alpha establishes T cell polarity by shaping diacylglycerol accumulation at the immunological synapse.* Sci Signal, 2014. **7**(340): p. ra82.
53. Veillette, A., *SLAM-family receptors: immune regulators with or without SAP-family adaptors.* Cold Spring Harb Perspect Biol, 2010. **2**(3): p. a002469.
54. Cannons, J.L., S.G. Tangye, and P.L. Schwartzberg, *SLAM family receptors and SAP adaptors in immunity.* Annu Rev Immunol, 2011. **29**: p. 665-705.
55. Schwartzberg, P.L., et al., *SLAM receptors and SAP influence lymphocyte interactions, development and function.* Nat Rev Immunol, 2009. **9**(1): p. 39-46.
56. Ma, C.S., K.E. Nichols, and S.G. Tangye, *Regulation of cellular and humoral immune responses by the SLAM and SAP families of molecules.* Annu Rev Immunol, 2007. **25**: p. 337-79.
57. Veillette, A., *NK cell regulation by SLAM family receptors and SAP-related adapters.* Immunological Reviews, 2006. **214**: p. 22-34.
58. Veillette, A., *Immune regulation by SLAM family receptors and SAP-related adaptors.* Nat Rev Immunol, 2006. **6**(1): p. 56-66.
59. Sayos, J., et al., *The X-linked lymphoproliferative- disease gene product SAP regulates signals induced through the co-receptor SLAM.* Nature, 1998. **395**: p. 462-469.
60. Latour, S., et al., *Binding of SAP SH2 domain to FynT SH3 domain reveals a novel mechanism of receptor signalling in immune regulation.* Nat Cell Biol, 2003. **5**(2): p. 149-54.
61. Latour, S. and A. Veillette, *Molecular and immunological basis of X-linked lymphoproliferative disease.* Immunological Reviews, 2003. **192**: p. 212–224.
62. Chan, B., et al., *SAP couples Fyn to SLAM immune receptors.* Nat Cell Biol, 2003. **5**(2): p. 155-60.
63. Li, C., et al., *Dual functional roles for the X-linked lymphoproliferative syndrome gene product SAP/SH2D1A in signaling through the signaling lymphocyte activation molecule (SLAM) family of immune receptors.* J Biol Chem, 2003. **278**(6): p. 3852-9.
64. Cannons, J.L., et al., *SAP regulates T(H)2 differentiation and PKC-theta-mediated activation of NF-kappaB1.* Immunity, 2004. **21**(5): p. 693-706.
65. Gu, C., et al., *The X-linked lymphoproliferative disease gene product SAP associates with PAK-interacting exchange factor and participates in T cell activation.* Proc Natl Acad Sci U S A, 2006. **103**(39): p. 14447-52.

66. Li, C., D. Schibli, and S.S. Li, *The XLP syndrome protein SAP interacts with SH3 proteins to regulate T cell signaling and proliferation.* Cell Signal, 2009. **21**(1): p. 111-9.
67. Cannons, J.L., et al., *Biochemical and genetic evidence for a SAP-PKC-theta interaction contributing to IL-4 regulation.* J Immunol, 2010. **185**(5): p. 2819-27.
68. Proust, R., J. Bertoglio, and F. Gesbert, *The adaptor protein SAP directly associates with CD3zeta chain and regulates T cell receptor signaling.* PLoS One, 2012. **7**(8): p. e43200.
69. Purtilo, D., et al., *X-linked recessive progressive combined variable immunodeficiency (Duncan's disease).* Lancet, 1975. **1**(7913): p. 935-940.
70. Filipovich, A.H., et al., *X-linked lymphoproliferative syndromes: brothers or distant cousins?* Blood, 2010. **116**(18): p. 3398-408.
71. Nichols, K.E., et al., *Molecular and cellular pathogenesis of X-linked lymphoproliferative disease.* Immunological Rewievs, 2005. **203**: p. 180-199.
72. Booth, C., et al., *X-linked lymphoproliferative disease due to SAP/SH2D1A deficiency: a multicenter study on the manifestations, management and outcome of the disease.* Blood, 2011. **117**(1): p. 53-62.
73. Morra, M., et al., *X-LINKED LYMPHOPROLIFERATIVE DISEASE: A Progressive Immunodeficiency.* Annu. Rev. Immunol., 2001. **19**: p. 657–82.
74. Filipovich, A.H., *Gene therapy targets XLP.* Blood, 2013. **121**(7): p. 1066-7.
75. Rivat, C., et al., *SAP gene transfer restores cellular and humoral immune function in a murine model of X-linked lymphoproliferative disease.* Blood, 2013. **121**(7): p. 1073-6.
76. Dupré, L., et al., *SAP controls the cytolytic activity of CD8+ T cells against EBV-infected cells.* Blood, 2005. **105**: p. 4383-4389.
77. Sharifi, R., et al., *SAP mediates specific cytotoxic T-cell functions in X-linked lymphoproliferative disease.* Blood, 2004. **103**(10): p. 3821-7.
78. Hislop, A.D., et al., *Impaired Epstein-Barr virus-specific CD8+ T-cell function in X-linked lymphoproliferative disease is restricted to SLAM family-positive B-cell targets.* Blood, 2010. **116**(17): p. 3249-57.
79. Bottino, C., et al., *NTB-A, a Novel SH2D1A-associated Surface Molecule Contributing to the Inability of Natural Killer Cells to Kill Epstein-Barr Virus–infected B Cells in X-linked Lymphoproliferative Disease.* J. Exp. Med., 2001. **194**(3): p. 235–246.
80. Parolini, S., et al., *X-linked Lymphoproliferative Disease: 2B4 Molecules Displaying Inhibitory Rather Than Activating Function Are Responsible for the Inability of Natural Killer Cells to Kill Epstein-Barr Virus–infected Cells.* J. Exp. Med., 2000. **192**(3): p. 337–346.
81. Bendelac, A., L. Savage Pb Fau - Teyton, and L. Teyton, *The biology of NKT cells.* (0732-0582 (Print)).
82. Chung, B., et al., *Cutting Edge: Signaling Lymphocytic Activation Molecule-Associated Protein Controls NKT Cell Functions.* The Journal of Immunology, 2005. **174**(6): p. 3153-3157.
83. Pasquier, B., et al., *Defective NKT cell development in mice and humans lacking the adapter SAP, the X-linked lymphoproliferative syndrome gene product.* J Exp Med, 2005. **201**(5): p. 695-701.
84. Ma, C.S. and E.K. Deenick, *The role of SAP and SLAM family molecules in the humoral immune response.* Ann N Y Acad Sci, 2011. **1217**: p. 32-44.
85. Ma, C.S., et al., *Impaired humoral immunity in X-linked lymphoproliferative disease is associated with defective IL-10 production by CD4+ T cells.* Journal of Clinical Investigation, 2005. **115**(4): p. 1049-1059.
86. Qi, H., et al., *SAP-controlled T-B cell interactions underlie germinal centre formation.* Nature, 2008. **455**(7214): p. 764-9.

87. Lenardo, M.J., *Molecular Regulation of T Lymphocyte Homeostasis in the Healthy and Diseased.* Immunol Res, 2003. **27**(2–3): p. 387–397.
88. Brenner, D., P.H. Krammer, and R. Arnold, *Concepts of activated T cell death.* Crit Rev Oncol Hematol, 2008. **66**(1): p. 52-64.
89. Snow, A.L., et al., *Critical role for BIM in T cell receptor restimulation-induced death.* Biol Direct, 2008. **3**: p. 34.
90. Snow, A.L., et al., *Restimulation-induced apoptosis of T cells is impaired in patients with X-linked lymphoproliferative disease caused by SAP deficiency.* JCI, 2009. **119**: p. 2976–2989.
91. Nagy, N., et al., *The proapoptotic function of SAP provides a clue to the clinical picture of X-linked lymphoproliferative disease.* Proc Natl Acad Sci U S A, 2009. **106**(29): p. 11966-71.
92. Chen, G., et al., *Increased proliferation of CD8+ T cells in SAP-deficient mice is associated with impaired activation-induced cell death.* Eur J Immunol, 2007. **37**(3): p. 663-74.
93. Boehme, S. and M. Lenardo, *Propriocidal apoptosis of mature T lymphocytes occurs at S phase of the cell.* Eur J Immunol. , 1993. **23**(7): p. 1552-1560.
94. Lenardo, M., et al., *Mature T lymphocyte apoptosis--immune regulation in a dynamic and unpredictable antigenic environment.* Annu Rev Immunol., 1999. **17**: p. 221-253.
95. Lenardo, M., *Interleukin-2 programs mouse alpha beta T lymphocytes for apoptosis.* Nature. , 1991. **353**(6347): p. 858-61.
96. Katz, G., et al., *SAP facilitates recruitment and activation of LCK at NTB-A receptors during restimulation-induced cell death.* J Immunol, 2014. **192**(9): p. 4202-9.
97. Luo, B., et al., *Diacylglycerol kinases.* Cell Signal, 2004. **16**(9): p. 983-9.
98. Sakane, F., et al., *The C-terminal part of diacylglycerol kinase α lacking zinc fingers serves as a catalytic domain.* Biochem. J. , 1996. **381**: p. 583-590.
99. Merino, E., et al., *Role of the diacylglycerol kinase alpha-conserved domains in membrane targeting in intact T cells.* J Biol Chem, 2007. **282**(48): p. 35396-404.
100. Santos, T., et al., *Dynamics of diacylglycerol kinase zeta translocation in living T-cells. Study of the structural domain requirements for translocation and activity.* J Biol Chem, 2002. **277**(33): p. 30300-9.
101. van Baal, J., et al., *Translocation of diacylglycerol kinase theta from cytosol to plasma membrane in response to activation of G protein-coupled receptors and protein kinase C.* J Biol Chem, 2005. **280**(11): p. 9870-8.
102. Cipres, A., et al., *Regulation of diacylglycerol kinase alpha by phosphoinositide 3-kinase lipid products.* J Biol Chem, 2003. **278**(37): p. 35629-35.
103. Joshi, R.P. and G.A. Koretzky, *Diacylglycerol kinases: regulated controllers of T cell activation, function, and development.* Int J Mol Sci, 2013. **14**(4): p. 6649-73.
104. Merida, I., A. Avila-Flores, and E. Merino, *Diacylglycerol kinases: at the hub of cell signalling.* Biochem J, 2008. **409**(1): p. 1-18.
105. Jiang, Y., et al., *A domain with homology to neuronal calcium sensors is required for calcium-dependent activation of diacylglycerol kinase alpha.* J Biol Chem, 2000. **275**(44): p. 34092-9.
106. Jiang, Y., et al., *A domain with homology to neuronal calcium sensors is required for calcium-dependent activation of diacylglycerol kinase alpha.* J Biol Chem. , 2000. **275**(44): p. 34092-9.
107. Topham, M., et al., *Protein kinase C regulates the nuclear localization of diacylglycerol.* Nature, 1998. **394**(6694): p. 697-700.
108. Hogan, A., et al., *Interaction of gamma 1-syntrophin with diacylglycerol kinase-zeta. Regulation of nuclear localization by PDZ interactions.* J Biol Chem. , 2001. **276**(28): p. 26526-33.

109. Sakane, F., et al., *Porcine 80-kDa Diacylglycerol Kinase Is a Calcium-binding and Calcium/Phospholipid-dependent Enzyme and Undergoes Calcium- dependent Translocation.* the journal of biologycal chemestry, 1991. **266**(11): p. 7096-7100.
110. Flores, I., et al., *Phosphatidic Acid Generation through Interleukin 2 (IL-2)-induced α-Diacylglycerol Kinase Activation Is an Essential Step in IL-2-mediated Lymphocyte Proliferation.* JBC, 1996. **271**(17): p. 10334-10340.
111. Flores, I., et al., *Diacylglycerol Kinase Inhibition Prevents IL-2-Induced G1 to S Transition Through a Phosphatidylinositol-3 Kinase-Independent Mechanism.* The Journal of Immunology, 1999. **163**: p. 708-714.
112. Mills, G., et al., *Interleukin 2-induced lymphocyte proliferation is independent of increases in cytosolic-free calcium concentrations.* J Immunol., 1985. **134**(4): p. 2431-5.
113. Baldanzi, G., et al., *Diacylglycerol kinase-alpha phosphorylation by Src on Y335 is required for activation, membrane recruitment and Hgf-induced cell motility.* Oncogene, 2008. **27**(7): p. 942-56.
114. Cutupri, S., et al., *Src-mediated activation of alpha-diacylglycerol kinase is required for hepatocytes growth factor-induced cell motility.* The EMBO Journal, 2000. **19**(17): p. 4614-4622.
115. Merino, E., et al., *Lck-Dependent Tyrosine Phosphorylation of Diacylglycerol Kinase Regulates Its Membrane Association in T Cells.* The Journal of Immunology, 2008. **180**(9): p. 5805-5815.
116. Baldanzi, G., et al., *SAP-mediated inhibition of diacylglycerol kinase alpha regulates TCR-induced diacylglycerol signaling.* J Immunol, 2011. **187**(11): p. 5941-51.
117. Sanjuan, M.A., et al., *Role of Diacylglycerol Kinase alpha in the Attenuation of Receptor Signaling.* J Cell Biol, 2001. **153**(1): p. 207–219.
118. Sanjuan, M.A., et al., *T Cell Activation In Vivo Targets Diacylglycerol Kinase alpha to the Membrane: A Novel Mechanism for Ras Attenuation.* J Immunol, 2003. **170**: p. 2877–2883.
119. Jones, D.R., *Expression of a catalytically inactive form of diacylglycerol kinase a induces sustained signaling through RasGRP.* The FASEB Journal, 2002.
120. Olenchock, B.A., et al., *Disruption of diacylglycerol metabolism impairs the induction of T cell anergy.* Nat Immunol, 2006. **7**(11): p. 1174-81.
121. Zhong, X.P., et al., *Enhanced T cell responses due to diacylglycerol kinase zeta deficiency.* Nat Immunol, 2003. **4**(9): p. 882-90.
122. Riese, M.J., et al., *Decreased diacylglycerol metabolism enhances ERK activation and augments CD8+ T cell functional responses.* J Biol Chem, 2011. **286**(7): p. 5254-65.
123. Olenchock, B.A., et al., *Disruption of diacylglycerol metabolism impairs the induction of T cell anergy.* Nat Immunol, 2006. **7**(11): p. 1174-81.
124. Quann, E.J., et al., *Localized diacylglycerol drives the polarization of the microtubule-organizing center in T cells.* Nat Immunol, 2009. **10**(6): p. 627-35.
125. Gharbi, S.I., et al., *Diacylglycerol kinase zeta controls diacylglycerol metabolism at the immunological synapse.* Mol Biol Cell, 2011. **22**(22): p. 4406-14.
126. Biskup, C. and I. Rubio, *Real-time visualization and quantification of native Ras activation in single living cells.* Methods Mol Biol, 2014. **1120**: p. 285-305.
127. Czar, M.J., et al., *Altered lymphocyte responses and cytokine production in mice deficient in the X-linked lymphoproliferative disease gene SH2D1A/DSHP/SAP.* Proc Natl Acad Sci U S A, 2001. **98**(13): p. 7449-54.
128. Zhao, F., et al., *Positive and negative signaling through SLAM receptors regulate synapse organization and thresholds of cytolysis.* Immunity, 2012. **36**(6): p. 1003-16.
129. Altman, A. and M. Villalba, *Protein kinase C-theta (PKCtheta): it's all about location, location, location.* Immunol Rev, 2003. **192**: p. 53-63.

130. Ebinu, J.O., et al., *RasGRP links T-cell receptor signaling to Ras.* Blood, 2000. **95**(10): p. 3199-203.
131. Sanjuán, M.A., et al., *T cell activation in vivo targets diacylglycerol kinase alpha to the membrane: a novel mechanism for Ras attenuation.* J Immunol, 2003. **170**(6): p. 2877-83.
132. Jones, D.R., et al., *Expression of a catalytically inactive form of diacylglycerol kinase alpha induces sustained signaling through RasGRP.* FASEB J, 2002. **16**(6): p. 595-7.
133. Sanjuán, M.A., et al., *Role of diacylglycerol kinase alpha in the attenuation of receptor signaling.* J Cell Biol, 2001. **153**(1): p. 207-20.
134. Joshi, R.P., et al., *The zeta isoform of diacylglycerol kinase plays a predominant role in regulatory T cell development and TCR-mediated ras signaling.* Sci Signal, 2013. **6**(303): p. ra102.
135. Sanzone, S., et al., *SLAM-associated protein deficiency causes imbalanced early signal transduction and blocks downstream activation in T cells from X-linked lymphoproliferative disease patients.* J Biol Chem, 2003. **278**(32): p. 29593-9.
136. Lenardo, M.J., et al., *MATURE T LYMPHOCYTE APOPTOSIS—Immune Regulation in a Dynamic and Unpredictable Antigenic Environment.* Annu. Rev. Immunol. , 1999. **17**: p. 221-53.
137. Bouillet, P. and L.A. O'Reilly, *CD95, BIM and T cell homeostasis.* Nat Rev Immunol, 2009. **9**(7): p. 514-9.
138. Moran, A.E., et al., *T cell receptor signal strength in Treg and iNKT cell development demonstrated by a novel fluorescent reporter mouse.* J Exp Med, 2011. **208**(6): p. 1279-89.
139. Cheng, L., et al., *Functional redundancy of the Nur77 and Nor-1 orphan steroid receptors in T-cell apoptosis.* EMBO J., 1997. **16**(8): p. 1865–1875.
140. Manicassamy, S. and Z. Sun, *The Critical Role of Protein Kinase C- in Fas/Fas Ligand-Mediated Apoptosis.* The Journal of Immunology, 2006. **178**(1): p. 312-319.
141. Layer, K., et al., *Autoimmunity as the consequence of a spontaneous mutation in Rasgrp1.* Immunity, 2003. **2**(1074-7613): p. 243-55.
142. Springael, C., et al., *Rottlerin inhibits human T cell responses.* Biochem Pharmacol, 2007. **73**(4): p. 515-25.
143. Favata, M.F., et al., *Identification of a novel inhibitor of mitogen-activated protein kinase kinase.* THE JOURNAL OF BIOLOGICAL CHEMISTRY, 1998. **273**(29): p. 18623–18632.
144. Ohori, M., et al., *Identification of a selective ERK inhibitor and structural determination of the inhibitor-ERK2 complex.* Biochem Biophys Res Commun, 2005. **336**(1): p. 357-63.
145. Crotty, S., et al., *Hypogammaglobulinemia and exacerbated CD8 T-cell-mediated immunopathology in SAP-deficient mice with chronic LCMV infection mimics human XLP disease.* Blood, 2006. **108**(9): p. 3085-93.
146. Hurttia, H. and L. Leino, *Subcellular localization of diacylglycerol kinase activity in stimulated and unstimulated human peripheral blood lymphocytes and neutrophils.* Biochem Mol Biol Int. 1996 Oct;40(3):579-85., (1039-9712 (Print)).
147. Das, R. and P.G. Hamid Bassiri, 1 Susan Wiener,1 Pinaki P. Banerjee,3 Ming-Chao Zhong,4 Andre´ Veillette,4,5 Jordan S. Orange,3 and Kim E. Nichols1, *The adaptor molecule SAP plays essential roles during invariant NKT cell cytotoxicity and lytic synapse formation.* Blood, 2013.
148. Thompson, J. and A. Winoto, *During negative selection, Nur77 family proteins translocate to mitochondria where they associate with Bcl-2 and expose its proapoptotic BH3 domain.* J Exp Med, 2008. **205**(5): p. 1029-36.
149. Wu., C., et al., *SAP controls T cell responses to virus and terminal differentiation of TH2 cells.* Nature Immunology, 2001. **2**(5): p. 410-414.

150. Dominguez, C.L., et al., *Diacylglycerol kinase α is a critical signaling node and novel therapeutic target in glioblastoma and other cancers.* Cancer Discov, 2013. **3**(7): p. 782-97.
151. Shin, J., et al., *Differential regulation of primary and memory CD8 T cell immune responses by diacylglycerol kinases.* J Immunol, 2012. **188**(5): p. 2111-7.
152. Ghosh, S., et al., *Interleukin-2-inducible T-cell kinase (ITK) deficiency - clinical and molecular aspects.* J Clin Immunol, 2014. **34**(8): p. 892-9.
153. Huck, K., et al., *Girls homozygous for an IL-2–inducible T cell kinase mutation that leads to protein deficiency develop fatal EBV-associated lymphoproliferation.* Journal of Clinical Investigation, 2009. **119**(5): p. 1350-1358.
154. Chianale, F., et al., *Diacylglycerol kinase alpha mediates HGF-induced Rac activation and membrane ruffling by regulating atypical PKC and RhoGDI.* Proc Natl Acad Sci U S A, 2010. **107**(9): p. 4182-7.
155. Rainero, E., et al., *Diacylglycerol kinase alpha controls RCP-dependent integrin trafficking to promote invasive migration.* J Cell Biol, 2012. **196**(2): p. 277-95.